PICES Scientific Report No. 10
1999

PROCEEDINGS OF THE 1998 SCIENCE BOARD SYMPOSIUM ON THE IMPACTS OF THE 1997/98 EL NIÑO EVENT ON THE NORTH PACIFIC OCEAN AND ITS MARGINAL SEAS

Symposium Co-convenors:
Howard J. Freeland (Canada), William T. Peterson (U.S.A.) and Al Tyler (U.S.A.)

March 1999
Secretariat / Publisher
North Pacific Marine Science Organization (PICES)
c/o Institute of Ocean Sciences, P.O. Box 6000, Sidney, B.C. Canada. V8L 4B2
pices@ios.bc.ca
http://pices.ios.bc.ca

TABLE OF CONTENTS

PREFACE

The experience of the 1982 El Niño was an event that caught the scientific community off guard, leaving many oceanographers feeling somewhat chagrined. At that time there were no large ocean current programs operating in the Pacific coastal regions adjacent to the North and South American continents. In both Canada and the United States, some major projects designed to survey currents over several years ended just before the 1982/83 El Niño started!

The experience of 1982/83 was not to recur this time. As the El Niño built in 1997, several emergency proposals were developed to monitor its evolution and impact. The result was that the 1997/98 El Niño is probably the best observed climate event in history.

However, climatologists and oceanographers around the world were still taken aback by the development of the 1997/98 El Niño event during the spring of 1997, because the unusual timing and dramatic rise in intensity very much earlier than normal was so extraordinary. The media quickly tagged this as "the mother of all El Niños". Such an amusing description aside, this was, by any standards, a very large event, having a world-wide impact.

This one-day symposium reviewed the effects of the 1997/98 El Niño on the physical, chemical and biological state of the northern North Pacific Ocean. The object was to establish a list of impacts that the climate anomaly had on the ocean, extending all of the way from the physics through the ecological system, to plankton biology and onwards to the fisheries. The symposium organizers wanted to provide a forum for discussion from all regions of interest to the PICES family of nations on the impacts of the El Niño. The symposium took place in October 1998, when the El Niño was barely over. Of necessity, the descriptions are, therefore, preliminary in nature. The unwritten hope was that substantial areas of overlap would be discovered as scientists presented their favourite observations. This would prompt others to revisit their observations, and encourage co-operation among investigators from different regions.

As the presentations occurred, it quickly became apparent that stories being related from California, Oregon, British Columbia, Alaska, the Bering Sea and so on, had an enormous overlap. All regions were reporting temperature changes, alterations in the stratification, and reduced nutrients and plankton. To that degree the symposium was successful — a consistent story *had* been developed.

We present that symposium material here. Contributors from both oral and poster sessions were invited to generate extended abstracts for this volume of proceedings. Most of them accepted this offer enthusiastically. Four talks scheduled for either oral or poster sessions were not, in fact, presented at the symposium. For those, at the end of the volume, we simply publish the abstracts as they were submitted. The entire package will be available electronically via the PICES web page at http://pices.ios.bc.ca and as a limited number of printed copies. This is the first report in the PICES Scientific Report Series with colour figures!

The results are preliminary, but we believe this volume represents a useful first look at the impacts of the 1997/98 El Niño on the North Pacific Ocean. The next step is taking place. PICES, in cooperation with the Inter-American Tropical Tuna Commission (IATTC), the International Pacific Halibut Commission (IPHC), the Interim Scientific Committee for Tuna and Tuna-Like Species in the North Pacific Ocean (ISC), the North Pacific Anadromous Fish Commission (NPAFC) and the Scientific Committee on Oceanic Research (SCOR), is organizing a four-day *Beyond El Niño Conference* to

discuss evidence, consequences, mechanisms and implications of such events. This conference will be held March 23–26, 2000 in La Jolla, California.

Howard Freeland

The Big Picture – The ENSO of 1997–98

James J. O'Brien
Center for Ocean-Atmospheric Prediction Studies
The Florida State University
Tallahassee, FL 32306-2840
U.S.A.
e-mail: obrien@coaps.fsu.edu

The largest warm phase of the ENSO cycle occurred in 1997–1998. It was anticipated by some modelling efforts and tracked by the TOGA-TAO Array and TOPEX/Poseidon.

A post analysis of the low frequency surface winds and sea surface temperature anomalies has been done using the National Centers for Environmental Prediction (NCEP) reanalysis and Florida State University tropical winds and the NOAA so-called Reynolds sea surface temperature (SST) anomalies. An animation of the low-passed data shows the evolution of the surface winds and SST anomalies for 40 years. Briefly, one can realize that the Aleutian Low tends to be strong during the warm phase and *vice versa*. There is an obvious connection between the Gulf of Alaska and the equatorial Pacific.

The big event of 1997–98 was quite different than previous events including the previous monster warm phase event in 1982–87. In 1997 anomalously warm water appeared along the west coast of North America months before it could be forced by Kelvin wave advection from the south.

In the talk we emphasize some of the myths about El Niño. In particular the "Biggest Lie about El Niño" is that the warm water in the western Pacific gets advected to Equador. This is not true. Instead the intraseasonal Kelvin waves lower the thermocline by about 100–150m. This destoys the local heat balance and warming ensues by not mixing up the deeper cold water.

A free video has been prepared of the animation with the author's voice over. Please email for a copy to obrien@coaps.fsu.edu.

Atmospheric Anomalies in 1997: Links to ENSO?

James E. Overland,[1] Nicholas A. Bond[2] and Jennifer Miletta Adams[2]

[1] *NOAA, Pacific Marine Environmental Laboratory*
Seattle, WA 98115-0070, U.S.A.
e-mail: overland@pmel.noaa.gov

[2] *University of Washington, JISAO*
Seattle, WA 98195, U.S.A.

Abstract

In the summer of 1997, positive sea surface temperature anomalies (SSTA) of greater than 2°C extended across the Gulf of Alaska (GOA) and into the eastern Bering Sea (EBS). The SSTA in the EBS are at least in part due to atmospheric causes. Anomalously high 700-mb geopotential heights occurred over the region during April through August. This resulted in enhanced warming of the GOA and EBS due to increased insolation. The pattern of positive 700 mb height anomalies for April through August 1997 is similar to its counterpart formed by compositing the April through August anomalies that occurred during previous El Niños. The warming in the Bering Sea and North Pacific during summer 1997 appears to be due to the confluence of three factors: a decadal trend toward higher 700-mb heights, the El Niño, and a particularly strong blocking ridge weather pattern in May. As fall 1997 progressed, the SSTA in the EBS and non-coastal GOA dissipated due to increased storm activity, a winter signature of El Niño. More complete documentation is found at http://www.pmel.noaa.gov/~miletta/npac1997.html.

Introduction

The intent of this abstract is to investigate whether the observed anomalies in the Eastern Bering Sea (EBS) occurred over a larger region and to investigate the relationship of the sea surface temperature anomalies (SSTA) to concurrent meteorological anomalies. The EBS is remote from tropical influences by direct oceanographic connection; however, indirect connections exist through the atmosphere. Recent studies suggest that there can be a midlatitude response to tropical SSTA in all seasons (Livezey et al., 1997; Trenberth et al., 1998). Because the midlatitude background circulation differs between winter and summer, the nature of the midlatitude response to the El Niño–Southern Oscillation (ENSO) also varies seasonally. The influence of ENSO at midlatitudes is believed to be related to an equatorward extension of the midlatitude Pacific jet stream and changes in mean flow/eddy feedback (Higgins and Mo, 1997; Straus and Shukla, 1997).

Anomaly Fields in 1997

Sea surface temperature

Monthly SSTA fields in the North Pacific for March through August 1997 are shown in Figure 1. The fields are taken from the National Centers for Environmental Prediction (NCEP) Reynolds analyses, which are based on a blending of satellite observations and *in situ* data (Reynolds and Smith, 1995). Positive (negative) anomalies equal to or greater than 1°C are drawn in shades of red (blue), with a contour interval of 1°C. The onset and intensification of the warm equatorial SSTA associated with El Niño are recognizable, with a 1°C positive anomaly near 180° in April and a large warm signal from May onward. In the EBS in March, the cold SSTA are –2°C. In April and May, the cold SSTA gradually give way to the warm anomalies extending westward from the GOA. May also shows the strongest warm SSTA off the west coast of North

America at subtropical latitudes. By June, strong warm SSTA stretch from the equator along the west coast, across the GOA, and into the Bering Sea. The extreme warm SSTA persist through August. The warm SSTA in the EBS in July and August are greater than 2°C. Local buoy observations (mooring site 2) showed SST anomalies greater than 2°C (Stabeno, personal communication). Based on the Reynolds analyses, the EBS showed remarkable SST warming of more than 12°C in a 5-month period, compared to a more typical value of 8°C. By November (not shown) the warm SSTA in the Bering Sea and non-coastal North Pacific had dissipated.

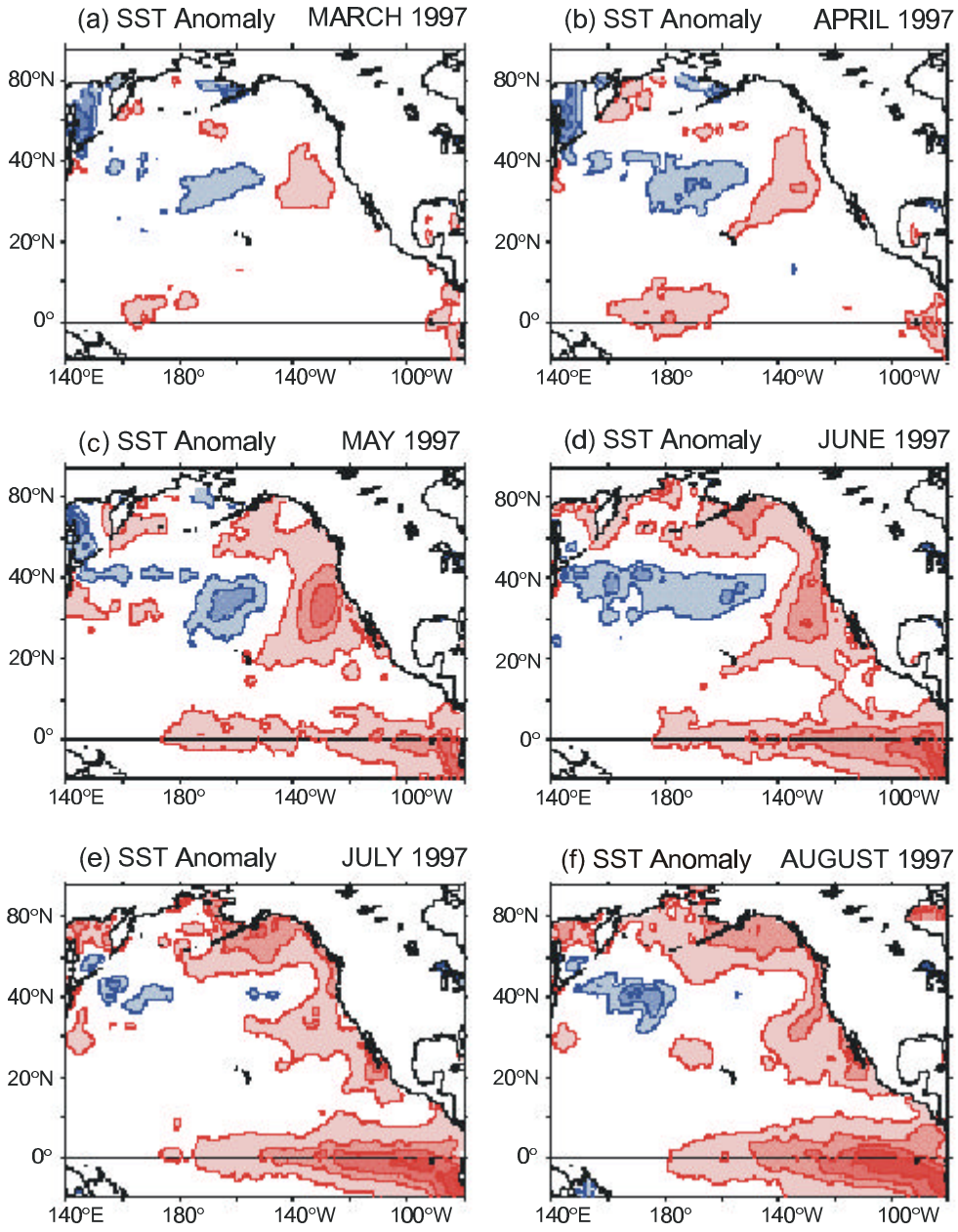

Figure 1. *Monthly SST anomalies (SSTA) for the North Pacific for 1997. Positive (negative) anomalies equal to or greater than 1°C are drawn in shades of red (blue) with a contour interval of 1°C. Data are from NCEP analysis (Reynolds and Smith, 1995) and are a blend of satellite and in situ observations. Note the increase of the equatorial SST anomaly after April. Subarctic SSTA increase after May, first in the Gulf of Alaska and then in the Bering Sea.*

700-mb geopotential height

The 700-mb geopotential height anomalies for April–August are shown in Figure 2a. The 5-month mean anomaly pattern shows positive heights over the western Alaska and the EBS and negative heights across the Pacific centered at about 45°N. Time series of the 700-mb height (Figure 2b) at Mooring 2 site (cross location in Figure 2a) also shows the strong tendency for higher geopotential heights in the EBS; particularly prominent positive anomalies occurred in late May, late June, and mid-late August.

Solar radiation

The net short wave anomalies from the NCEP reanalyses at the surface for April–August 1997 are shown in Figure 3. In the 5-month mean, an extra 5–10 W m^{-2} was available to warm the ocean in the central and eastern Bering Sea with the greatest anomalous heating over Bristol Bay. The time series in Figure 3b shows that the positive flux anomalies at the Mooring 2 site were about 30 W m^{-2} from mid-May through mid-July. Assuming a typical mixed layer depth of 20 m, this amount of anomalous heat would increase the SST by 2°C.

Link to the Tropical Pacific?

Historical composites

In this section we examine covariability between equatorial SSTA and midlatitude atmospheric circulation in all spring/summer months with a strong El Niño signal. This is reasonable because the midlatitude atmospheric circulation responds relatively quickly, on time scales of a few weeks or less, to tropical Pacific anomalies. As a measure of equatorial SSTA we use the NINO3 index greater than 1.3 for SSTA between 5°N–5°S and 150°–90°W, available from NCEP. The range of years considered is 1958–1996, limited by the NCEP reanalyses data set.

The atmospheric circulation for the North Pacific during the months of May and August 1997 best resembled that which occurred for previous El Niños. The overall similarity on a seasonal basis is shown in Figure 4 which compares the April–August mean 700-mb height field for 1997 and El Niño composites. The 700-mb height anomaly pattern is an amplified version of the ENSO composite. The influence of the ENSO on northern hemisphere atmospheric conditions is most apparent

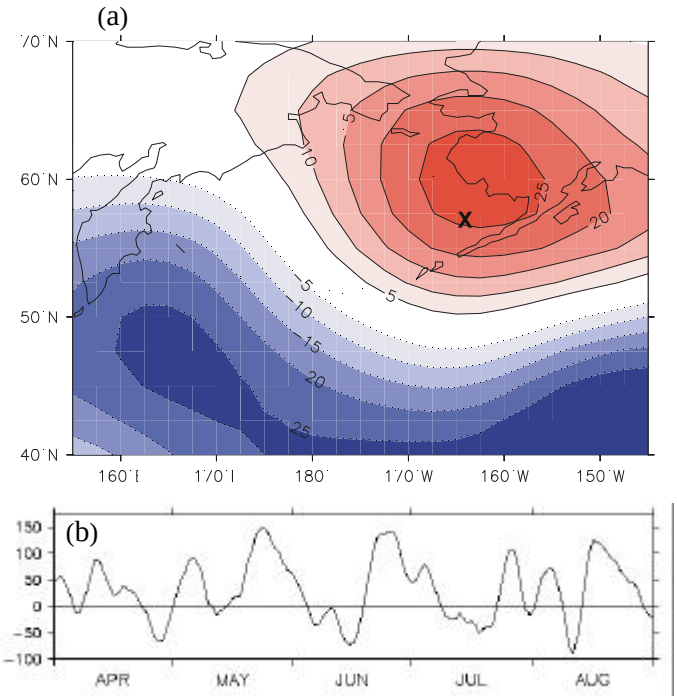

Figure 2. *Geopotential height anomalies in meters at 700 mb for spring and summer of 1997. (a) Five-month (April–August) mean anomaly. (b) Time series of daily anomalies at 57°N, 164°W (mooring site 2, x on Figure 2a) for the same 5-month period, smoothed with a 5-day running mean. There are seven peaks of high geopotential height.*

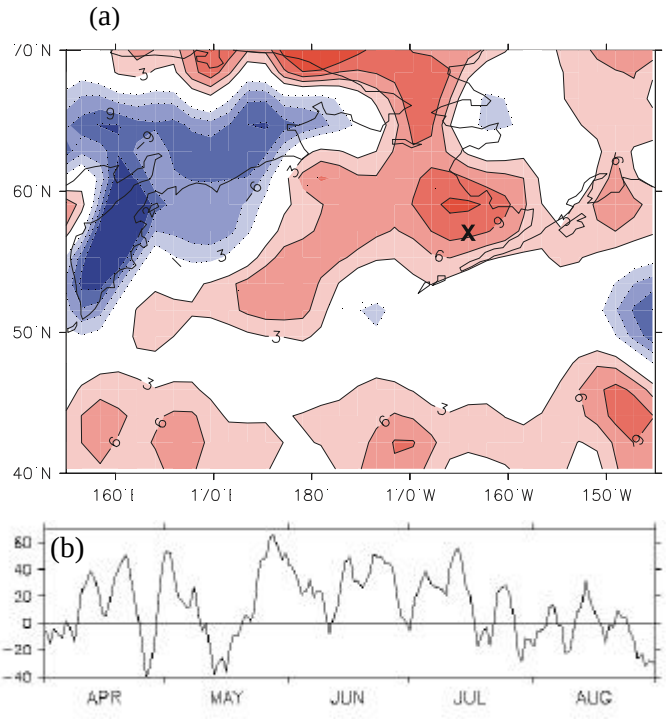

Figure 3. *Net shortwave radiative flux anomalies at the surface in W m^{-2} for spring and summer of 1997. Positive values are downward, implying a surface warming. (a) Five-month (April–August) mean anomaly. (b) Time series of daily anomalies at 57°N, 164°W for the same 5-month period, smoothed with a 5-day running mean. There is anomalous heating centered on the EBS from late May through early June.*

on a seasonal time scale. As suggested by Figure 4, the El Niño of 1997 during April and May had an effect on the North Pacific, yet the tropical SSTA were only ~1°C. These modest anomalies must be considered in light of the seasonal cycle of the tropical Pacific. Since central and eastern tropical Pacific SSTs are warmest during the boreal spring, relatively minor warming can cause the SST to exceed the 27°C threshold for deep cumulus convection. It is these anomalies in deep convection and the associated upper-tropospheric zonal wind anomalies that have repercussions on the global atmospheric circulation.

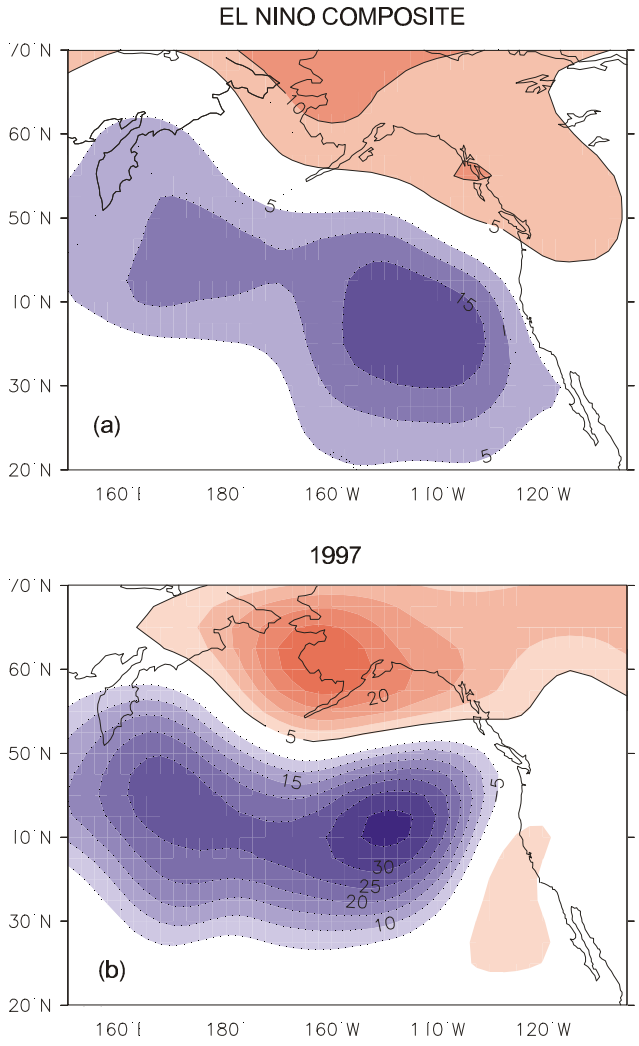

Figure 4. *April–August 700 mb geopotential height fields. (a) Composite for months with a strong El Niño signal and (b) April–August 1997.*

Summary

The warm SSTA in the EBS and GOA during the spring and summer of 1997 were partly related to concurrent large-scale atmospheric anomalies. The principal processes involved in producing the warm SSTA were enhanced warm-air advection and insolation as revealed by the anomalous distributions of low-level temperature, geopotential height, relative humidity, and cloud cover.

The atmospheric circulation anomalies for the EBS and GOA during spring and summer of 1997 appear to represent a particularly strong manifestation of the effect of ENSO. Support for a connection to the tropical Pacific during this time of year is provided by the GCM results of Livezey et al. (1997). A particularly prominent role for the tropical Pacific should be expected because local ENSO forcing, i.e., tropical Pacific SST, Outward Longwave Radiation (OLR), and 200-mb zonal wind anomalies during the spring and summer of 1997, were exceptionally large by historical standards.

The warming in the Bering Sea and North Pacific during summer 1997 appears to be due to the confluence of three factors: a decadal trend toward higher 700-mb geopotential heights as noted in the time series of the spring teleconnection or NP pattern (Figure 5), the atmospheric ENSO connection (Figure 4), and a particularly strong blocking ridge weather pattern in May. Thus natural within-year variability coincided with interannual and decadal variability to produce extremely anomalous sea temperature conditions in the Bering Sea.

Acknowledgments We appreciate the support from NASA Polar Programs, ONR Polar Programs, and the International Arctic Research Center.

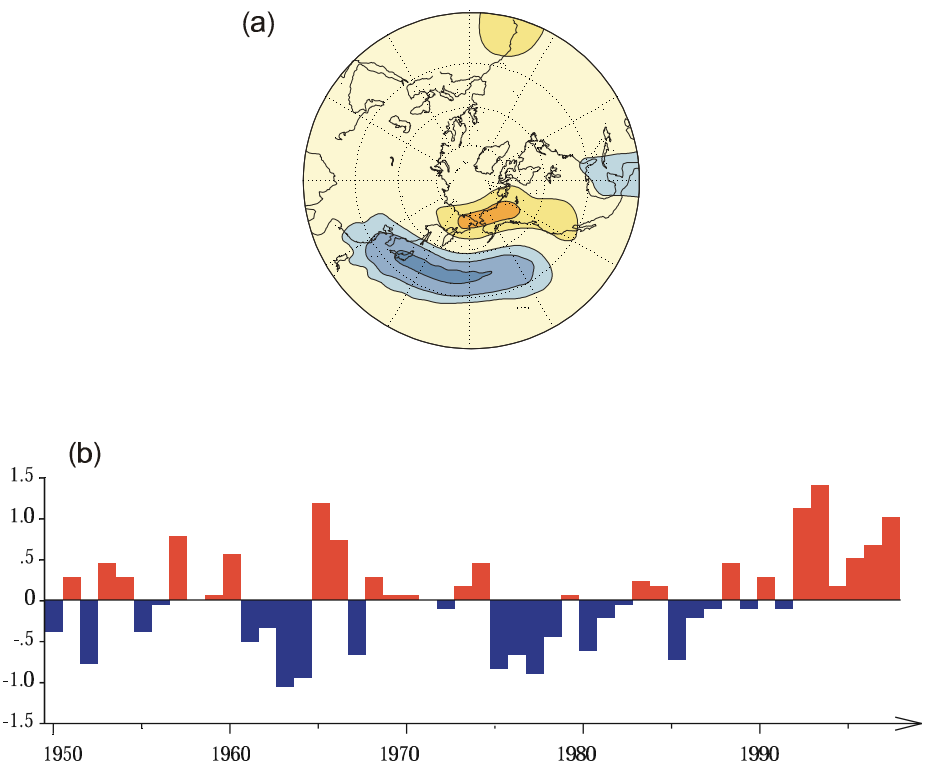

Figure 5. *The prominent teleconnection for spring/summer in the North Pacific is (a) the "North Pacific" (NP) pattern. It has a north/south out of phase relationship for 700-mb heights (Bell and Halpert, 1995). There has been a regime of higher 700-mb heights over the Bering Sea and Alaska since 1989, a positive NP signal. (b) Time series of March–July mean NP amplitudes.*

References

Bell, G.D., and Halpert, M.S. 1995. Atlas of intraseasonal and interannual variability 1986–1993. NOAA Atlas No. 12 CPC, NOAA/NWS/NMC, Washington, D.C., 256 pp.

Higgins, R.W., and Mo, K.C. 1997. Persistent North Pacific Circulation anomalies and the tropical intraseasonal oscillation. *J. Clim., 10*, 223–244.

Livezey, R.E., Masutani, M., Leetmaa, A., Rui, H., Ji, M., and Kumar, A. 1997. Teleconnective response of the Pacific–North American region atmosphere to large central Equatorial Pacific SST anomalies. *J. Clim., 10*, 1787–1819.

Reynolds, R.W., and Smith, T.M. 1995. A high-resolution global sea surface temperature climatology. *J. Clim., 8*, 1571–1583.

Straus, D.M., and Shukla, J. 1997. Variations of mid-latitude transient dynamics associated with ENSO. *J. Atmos. Sci., 54*, 777–790.

Trenberth, K.E., Branstator, G.W., Karoly, D., Kumar, A., Lau, N., and Ropelewski, C. 1998. Progress during TOGA in understanding and modeling global teleconnections associated with tropical sea surface temperature. *J. Geophys. Res., 103*, 14,291–14,324.

The ENSO Signal in the Northwest Pacific

Vladimir Ponomarev, Olga Trusenkova, Serge Trousenkov,
Dmitry Kaplunenko, Elena Ustinova, and Antonina Polyakova
Pacific Oceanological Institute Russian Academy of Sciences
pacific@online.marine.su

Abstract

The oscillations of the El Niño–Southern Oscillation (ENSO) scale (3–7 years) in oceanographic and meteorological characteristics in the Northwest Pacific are studied. Monthly mean sea surface temperature (SST) for the period of 1947–1978 was subjected to the Complex Empirical Orthogonal Functions (CEOF) analysis in time domain to study moving features in SST anomaly patterns in the North Pacific. Both unlagged and lagged correlations were found between air temperature at the Northwest Pacific Margin coastal meteorological stations for the 20th century or ice extent in the Sea of Okhotsk for the second part of the 20th century with SOI. Meteorological situations were also considered over the North Pacific based on the classification developed by Polyakova (1992, 1997). Six principal types of synoptic situations represented by characteristic sea level pressure (SLP) fields are associated mainly with different locations of cyclone tracks and of high/low pressure over the North Pacific. It was shown that the ENSO signal with a lag of about half a year may be associated with the Northwest Pacific Ocean memory in a seasonal cycle. The ENSO signal with a lag of about one year is probably conditioned by both oceanic SST anomalies propagating from the tropic–equatorial Pacific to the extratropic areas and by theatmosphere circulation response to these anomalies.

1. Introduction

The El-Niño - Southern Oscillation (ENSO) is an oscillation of a 3–7 year period in the atmosphere–ocean system (Bjerknes, 1969) observed mainly in the equatorial/tropical Pacific as an alternation of El Niño/La Niña events in the ocean (Wyrtki, 1975) and Southern Oscillation in the atmosphere studied by numerous researchers started from the pioneer work of Walker (1924).

El Niño, or warm phase of ENSO, is an oceanographic phenomenon of warm surface water pool formation offshore of the coasts of Ecuador and Peru, accompanied by the following events:

- Subtropic High Pressure weakens in the Southeast Pacific while sea level pressure (SLP) rises over Australia–Indonesian area that corresponds to negative phase of Southern Oscillation (negative values of Southern Oscillation Index – SOI);
- typical Walker circulation and southern/northern hemisphere trade winds weaken;
- atmospheric convection area of Walker circulation shifts eastward from the western (Australian–Indonesian area) to the central tropical/equatorial Pacific and South America maritime area;
- westerly winds originate over the area of the western and central equatorial Pacific;
- a warm sea surface temperature (SST) anomaly moves east to the central eastern equatorial Pacific while a cold anomaly forms in the western area;
- heating decreases in the western tropical Pacific and South Asian winter monsoon weakens;
- meridional winds and Hadley circulation weaken in the western area and shift eastward;
- low winter and spring rainfall in the Australia–Indonesian area with Australian summer monsoon onset late and generally poor.

The modern state of the problem is described as achievements of the TOGA Program (Learning to Predict Climate Variations Associated with El Niño and Southern Oscillation, Accomplishments and Legacies of the TOGA Program, 1996) where most of the important recent scientific results related to ENSO, including the extratropic response to ENSO and its relationship with the Asian–Australian monsoon (Yang and Webster, 1990), are also outlined.

To explain the reason and physical mechanism of ENSO, the basic idea of coupled atmosphere–ocean instability in tropics was suggested in early 80s (Philander et al., 1984). The unstable coupled atmosphere–ocean mode was found using shallow water atmosphere–ocean models (Philander et al., 1984; Hirst, 1986).

At the same time, a lot of meteorological and oceanographic data, observed in both the tropics and extratropics during ENSO events were collected and analyzed particularly on the basis of the TOGA project. As suggested, irregularity of ENSO may be caused by nonlinearity in the ocean–atmosphere system and interactions between ENSO and anomalies of the annual cycle in the tropics and extratropics. Substantial anomalies of ENSO cycles and changes of El Niño and La Niña occurrences during winters from 1950 to 1995 were shown by Zhang and Wallace (1996) and many others. In particular, La Niña occurrences in winter have dramatically decreased since 1977. After a maximum interval between El Niño events from 1974 to 1982, La Niña events have become weaker and have taken place mostly in summer while El Niño has dominated in winter and has become more frequent since 1987.

According to Sekine and Yamada (1996) and Sekine (1998), the ENSO cycle has a feedback from anomalies of winter snow coverage over the Asian continent and summer monsoon winds. In this case, the large-scale processes in the mid-latitude impact on ENSO.

Therefore, the main goal of our study is to find new evidence of ENSO accompanying events in the mid-latitude Northwest Pacific on the basis of meteorological and oceanographic data analyses.

The present work contains:

- a brief background review of the tropic–extratropic relationship associated with ENSO;
- an interpretation of SST anomaly development and movement in the North Pacific using the Complex Empirical Orthogonal Functions (CEOF) method;
- an estimation of the statistical relationship between ENSO and anomalies of meteorological/ oceanographic characteristics in the Northwest Pacific Margin;
- a discussion of typical synoptic situations, their variations, and impact on the subarctic West Pacific Margin.

In the following review earlier studies on the extratropic response to ENSO are discussed which are related to, or promote better understanding of, our findings.

2. Background on the tropic-extratropic relationship associated with ENSO

The extratropic response to ENSO is mostly considered as a global scale phenomenon in the coupled ocean–atmosphere system. It is explained by the ENSO impact on hemispheric patterns of geopotential height and upper ocean temperature anomalies (Bjerknes, 1969; Horel and Wallace, 1981; Trenberth and Paolino, 1981; Alexander, 1992a,b; Lau and Nath, 1990; Palmer, 1993; Molteni et al., 1993).

The part of the variance associated with long-term variability of different scales reaches its maximal values in the subarctic zonal belt. Therefore, the extratropic response to ENSO in the atmosphere seems to be obscured and highly nonlinear (Geisler et al., 1985) due to its interaction with internally generated oscillations. In turn, the internally generated mid-latitude SST variations may overwhelm the signal from anomalies of tropical heating (Trenberth, 1995).

Palmer (1993) and Molteni et al. (1993) argued that, despite very large natural variability of the extratropical circulation, there exist certain preferred regimes with rather persistent flow patterns presumably associated with the land–sea distribution and climatological planetary waves. The effect of tropical SST forcing alters the frequency of occurrence and stability of certain pre-existing regimes (Learning to Predict Climate Variations Associated with El Nino and Southern Oscillation. Accomplishments and Legacies of the TOGA Program, 1996).

The principal questions related to our study are as follows: what kinds of large-scale circulation processes in the North Pacific atmosphere influence the extratropical regimes and, at the same time, are the most closely related to the tropic–extratropic interaction and to ENSO. Those are known to be the meridional Hadley circulation, westerly jet stream and

monsoon circulation. Effects of heating displacement in the tropics on the location and intensity of Hadley circulation and westerly jet stream (Lau and Boyle, 1987; Yang and Webster, 1990; Hou, 1993; Oort and Yienger, 1996), as well as on the monsoon system anomalies (Tanaka, 1982; Schucla and Paolino, 1983; Wu and Hastenrath, 1986; Webster and Yang, 1992; Webster et al., 1997) are actually considered as important physical devices of the extratropic response to ENSO in the atmosphere.

Physical processes of synoptic scale which actualize the ENSO-scale remote linkages in the atmosphere are actually associated with propagation of faster, barotropic (Simmons et al., 1983) and slower, baroclinic (Blackmon et al., 1977; Lau and Boyle 1987; Hou, 1993) waves as well as with changes of extratropical storm tracks (Branstator, 1995) and tropical cyclone activity in the Western Pacific (Chan, 1985; Chen and Weng, 1998).

As for oceanic teleconnections, the poleward ENSO signal propagation in the North Pacific Ocean was described by Johnson and O'Brien (1990a,b). Based on circulation model and observation data analysis they showed that temperature and upper layer thickness anomalies propagate northward along the eastern coast of North America due to coastal Kelvin waves and reach the 50°N latitude in about one year. Westward temperature anomaly propagation to the central Pacific is due to baroclinic Rossby waves excited by coastal Kelvin waves.

Thus, one can suggest that, at least in the North Pacific, both a northward fast ENSO signal in the atmosphere and slow ENSO signal in the ocean exist. Propagation of both these signals is controlled by synoptic-scale processes, atmospheric ones of order of a week, and oceanic ones of order of a few months, which, in turn, interact with larger-scale processes. An oceanic signal propagating northward along the eastern Pacific boundary and westward offshore to the subtropical central Pacific more pronounced while an atmospheric signal is rather obscured in the extratropic area.

It seems that the atmospheric ENSO signal may be dominant in the Northwest Pacific Margin due to its interaction with the Asian monsoon system in southern (tropic-subtropic) and northern (subarctic) areas. This suggestion is supported by previous studies on data analyses in the area of the North Asian monsoon and westerly jet stream.

In this study we examined the relationship at zero or half-year (seasonal) lags between SOI, air temperature in the Northwest Pacific Margin from the southern Japanese Kushu Island and Korean Peninsula (30°N) to the Chukchy Peninsula (70°N), and ice extent in the Sea of Okhotsk. At the same time, we analyzed ENSO (including 1997–98 El Niño–La Nina events) accompanying meteorological situations over the extratropic North Pacific and how their occurrence is related to seasonal/monthly air temperature and ice extent anomalies. To estimate the oceanic response to ENSO in the Northwest Pacific Margin we also analyzed propagation of winter SST anomalies using complex EOF method.

3. Data and Methods

To estimate the propagation of SST anomalies in the North Pacific, the archive of monthly mean SST was used. It consists of 384 time counts for 32 years from 1947–1978 taken in 163 $5° \times 5°$ grid points for the area of 20–55°N, 120°E–120°W. A time period was chosen up to 1978 so that the recent shift in climate regime occurred in 1976 which resulted in changes of occurrence of El Niño–La Niña events is not included in the consideration. It is a subject of further analysis to estimate an impact of this change upon anomaly patterns in the North Pacific.

To study moving features in the anomaly patterns, the complex principal components analysis in time domain was applied to signals composed of original SST data. Theoretical development of the method can be found in Brillinger (1975) and Horel (1984). Conventional (unfiltered) anomalies were computed by subtracting temperature mean values for every month, thus removing the climatic seasonal cycle. Asymmetric filtering (Enting and Robbins, 1989) was applied to obtain signals representing variability in different time scales (Section 4).

Time series of monthly mean air temperature at meteorological stations in the Northwest Pacific Margin for the 20th century, mainly up to 1990, and 10-day mean ice extent for the Okhotsk and Bering Seas from 1960 to 1998 (Plotnikov, 1997) were chosen for estimation of seasonal links with ENSO by correlation analysis (Section 5).

To consider atmosphere conditions over the North Pacific associated with ENSO and their impact on the Northwest Pacific Margin, time series (days/month) of frequency of occurrence were analyzed for six synoptic situations as SLP fields over the mid-latitude North Pacific from 1949 to 1998 based on the classification and calendar developed by Polyakova (1992, 1997). Correlation analysis

was used to reveal their relationship with ENSO based upon both lagged and unlagged correlation estimates (Section 6).

4. Interpretation of SST Anomaly Development and Movement in the North Pacific

The decomposition of ocean/atmosphere fields into normal spatial and temporal components known as an empirical orthogonal function (EOF) analysis is widely applied to reconstruct anomaly patterns in space. Filtering, harmonic and spectral analyses are performed to study variability in time. However, standard EOF analysis is not able to separate moving oscillations from standing ones or directly estimate anomaly propagation. For this reason, an alternative method of complex empirical orthogonal function (CEOF) for detecting moving features is currently employed when eigenvalues and eigenvectors are computed for cross spectrum matrix (frequency domain method; Brillinger, 1975) or complex covariance matrix (time domain method; Horel, 1984). In the latter case, complex signals are first composed of initial scalar fields when an imaginary part is taken as the Gilbert transform of a real part (original data). CEOFs and time series of complex principal components (PCs) obtained are characterized by amplitude and phase (hereafter referred to as spatial/temporal amplitude and phase); power spectra of PC time series are calculated to estimate time-scales of variability.

Movement of monthly mean SST anomalies in the mid-latitude central North Pacific area for the period of 1947–1976 was earlier estimated by Michaelsen (1982) applying CEOF analysis in frequency domain. He showed that SST anomalies propagate in the northeastward direction in a dominant frequency band of about 0.02 cpm (cycles per month; inverse months). The corresponding period of 4.2 years can be associated with the characteristic ENSO period.

Trousenkov (1991) applied CEOF techniques in time domain for SST anomalies in the North Pacific (20°–55°N, 120°E–120°W) based on the archive of monthly mean SST described in Section 3. Figure 1 shows (a) spatial amplitude and (b) phase for the first CEOF (20% of variance). A high amplitude belt spreads in the tropical region and eastern and central Pacific areas, with maximum amplitudes located near the North American coast from 35°N to 45°N. According to the spatial phase, anomalies associated with the first CEOF propagate along the axis between the northeastward and southeastward corners of the basin, tending to bypass the Northwest Pacific area where spatial amplitude is minimal.

The power spectrum of the first PC covers a wide range of time scales from 5 months to 10 years but has an absolute maximum ENSO time scale (3.5–5.3 years). It also has weaker 1.5- and 1-year peaks and intra-annual peaks with periods of 7–8 and 5–6 months (Figure 2a). Lagged correlation coefficients were calculated between the first PC temporal amplitude and SOI/Nino3 Index (Figure 3a). Correlation curves of the PC amplitude with SOI and Nino3 are symmetrical along the *x*-axis which is obviously due to high negative correlation between the SOI and El Niño Index, so it is enough to use either one for further analysis.

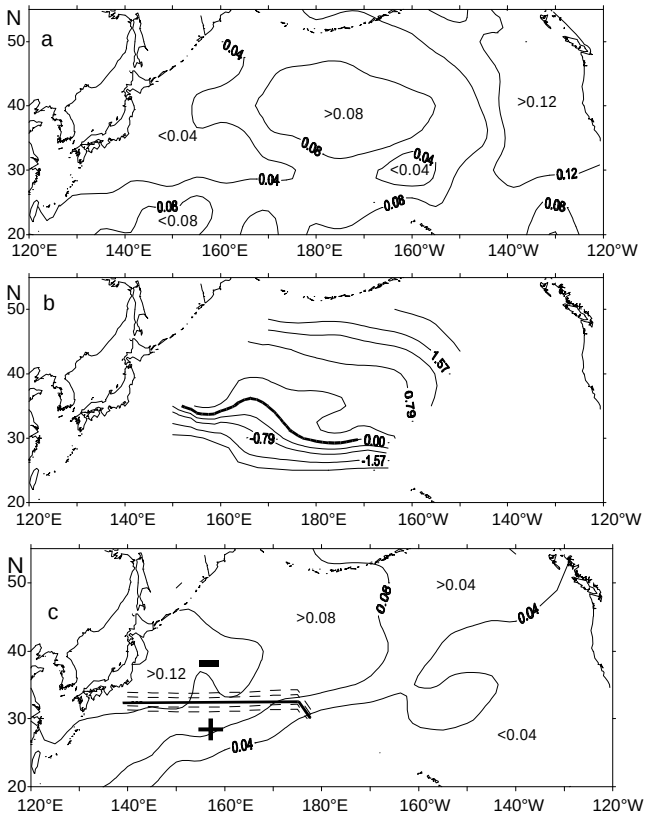

Figure 1. *(a) Spatial amplitude and (b) phase of the first CEOF and (c) spatial amplitude and phase of the second CEOF for the unfiltered monthly SST anomalies in the extra-tropical North Pacific (1947–1978). Phase is given in radians. For the second CEOF, zero phase contour is shown as a thick solid line and phase contours of –p, -p/2, p/2, p are shown as dashed lines, with signs indicating areas of positive (+) and negative (–) phases.*

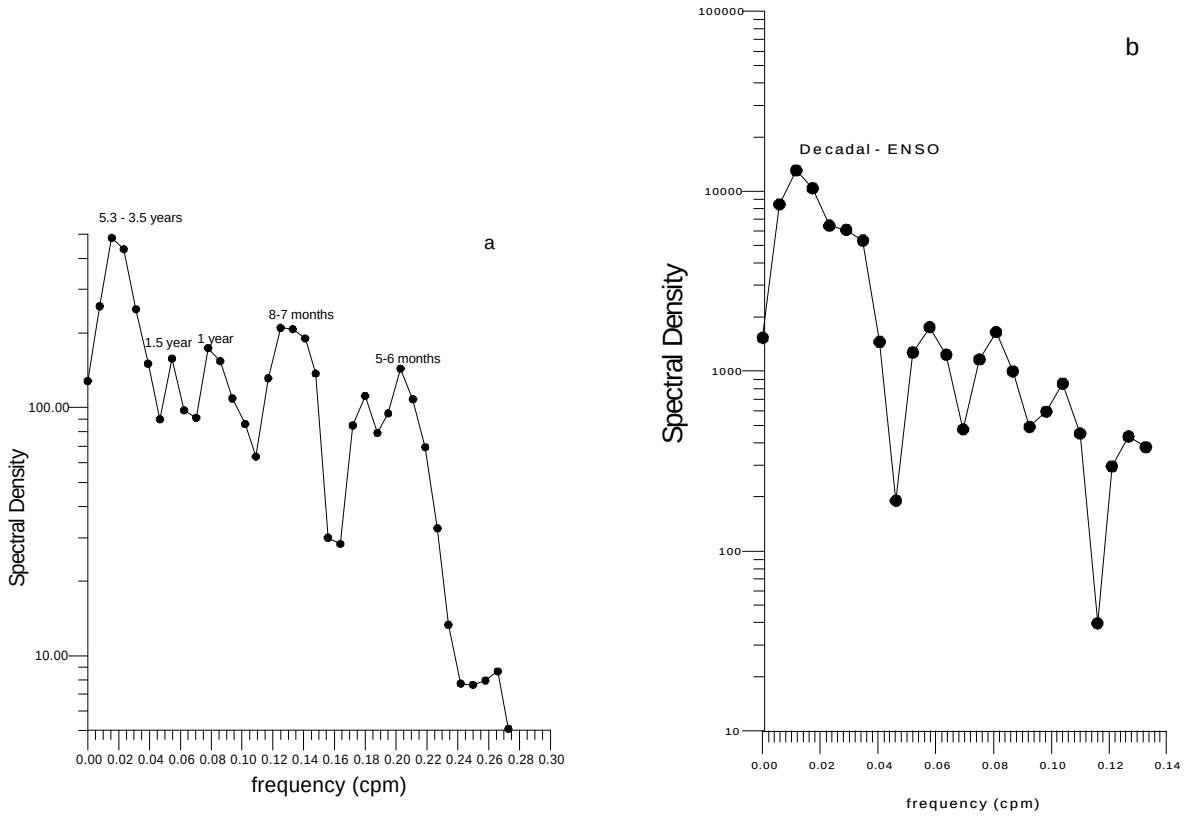

Figure 2. *Power spectra of (a) the first temporal PC for the unfiltered monthly SST anomalies and (b) the second temporal PC for low-pass pre-filtered monthly mean SST in the extra-tropical North Pacific (1947–1978).*

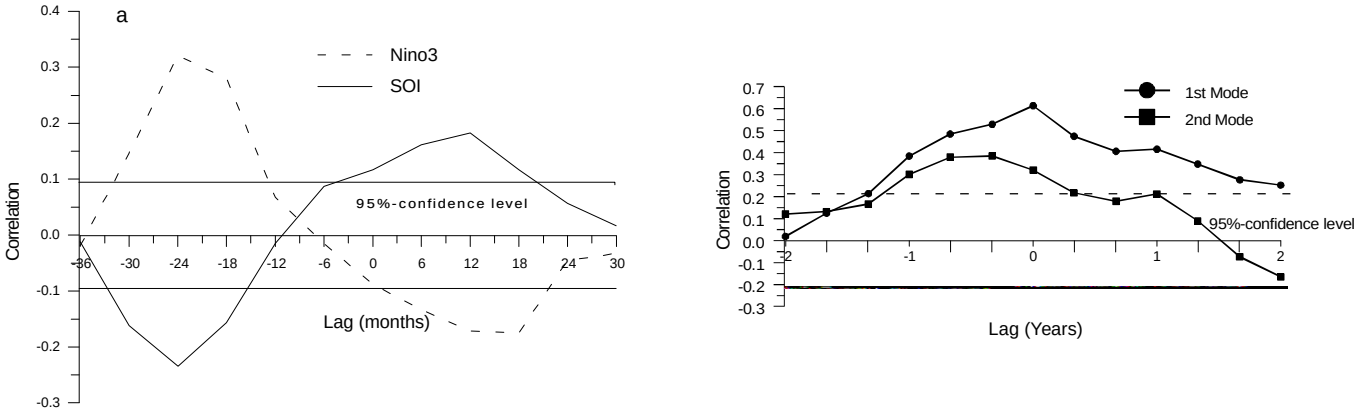

Figure 3. *Lagged correlation of (a) the first temporal PC for the unfiltered monthly SST anomalies with SOI and Niño3 Index and (b) the first and second temporal PCs for the low-pass pre-filtered winter SST anomalies with the low-pass pre-filtered El Niño Index in the extra-tropical North Pacific (1947–1978).*

Substantial asynchronic links with 1.5–1 year (–18, –24 months in the *x*-axis, Figure 3a) SST anomaly delay were obtained as well as weaker but statistically significant links with 1 year (+12 months in the *x*-axis, Figure 3a) SOI/Niño3 Index delay. Asynchronic links obtained are characteristic for the entire North Pacific where the first CEOF spatial amplitude is high with the exception of the Northwest Pacific where the spatial amplitude is low (Figure 1a). Periodicity of the correlation coefficient as a function of lag is about 5 years which corresponds to the ENSO time scale. Positive lagged correlation with SST anomalies behind Niño3 corresponds to positive anomalies over the extra-tropic North Pacific as a whole formed in 1.5–2 years after the El Niño event. This is consistent with general idea of oceanic ENSO teleconnection (Johnson and O'Brien, 1990a,b, and many others). Negative lagged correlation with Nino3 behind SST anomalies points out that ENSO seems to have a positive feedback with extra-tropic North Pacific SST anomalies.

However, the first PC temporal phase (not shown) implies that SST anomalies can propagate in either direction along the northeast–southwest axis as phase mostly decreases with time but increases in some periods. (When the temporal phase gradually increases/decreases, a wave propagates from lower/higher to higher/lower values of spatial phase; abrupt phase jumps are due to its being conventionally bounded in a range from $-\pi$ to π.) This can be explained by the fact that analyzed time series consist of anomalies of varied time scales. So, pre-filtered narrow-band data should be processed to obtain patterns for SST anomalies of a certain time scale.

On the contrary, the second CEOF of unfiltered SST anomalies (12% of variance) shows the standing wave with the amplitude localized in the western Pacific with maximum amplitude in the area of 35°–45°N (Figure 1c). The western subarctic area is in anti-phase with the western subtropical area, the dividing line is stretched along 32–33°N, in the area of the Kuroshio Extension. The contour line of zero phase is also shown in the Figure 1c as a thick solid line and dashed lines represent phases of $-\pi$, $-\pi/2$, $\pi/2$, π. (Abrupt rise and fall of phase on both sides of the zero contour means that the second CEOF is a standing oscillation.)

To separate time scales further analysis was performed based upon filtered time series both of SST and their anomalies.

To estimate contribution of a seasonal signal into propagation of temperature waves in the North Pacific seasonal SST time series were obtained by applying a band-pass filter with a band of 0.05–0.1 cpm (corresponding periods of 9–21 months) to the original SST fields. The CEOF method in time domain was applied to the filtered SST. The general (first) seasonal CEOF (93% of variance) is a standing wave in the subtropical Pacific where the western area is in phase with the eastern one and they both are in the anti-phase with the central area. No moving features were found for the seasonal signal, so, this pattern may be explained by sea–land contrasts and atmosphere–ocean interaction in a annual cycle.

To remove short-time (seasonal and bi-annual) signals from the monthly SST time series a low-pass filter with periods longer than 21 months was applied to the original monthly SST. In this case, with the absence of intra-annual and bi-annual variations in the signal, the general (first) mode (97% of variance) shows no oscillate features and it does not have significant local maxima in its spectrum. The second CEOF (1% of variance) has high amplitudes, mainly in the western subarctic Pacific (the area to the north of 40°N adjacent to Hokkaido and Kuril Islands) as shown in Figure 4a. The spatial phase pattern (Figure 4b) shows that this mode is a superposition of a progressive and standing waves. As for

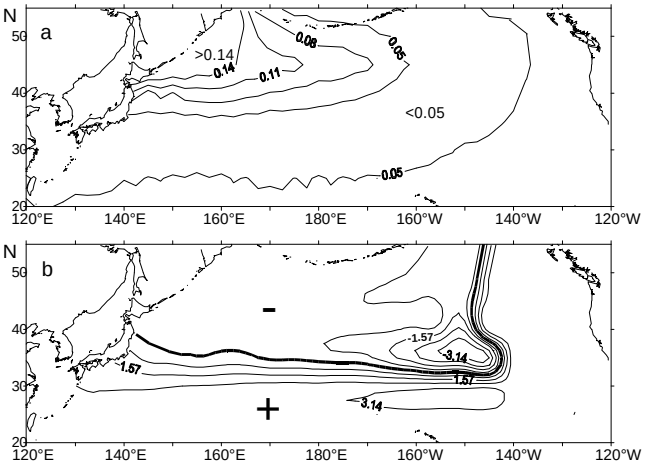

Figure 4. *(a) Spatial amplitude and (b) phase of the second CEOF for the low-pass pre-filtered monthly mean SST in the extra-tropical North Pacific (1947–1978). Phase is given in radians. Contour line of zero phase is shown as a thick solid line.*

the standing oscillation, its pattern is similar to the second mode for conventional SST anomalies but with a sharper outlined area of maximum amplitudes. However, the second PC temporal spectrum has high values in a range of 4.8–10 years with maximum at 7.2 years (Figure 2b).

Thus, analysis for pre-filtered SST time series shows that there are no progressive waves left in general CEOFs for either seasonal or interannual signals. It is concluded that propagating features should be associated with SST anomalies rather than SSTs themselves. Lack of progressive oscillations in the two general modes of low-pass filtered SST component covering 98% of total variance is evidence that moving disturbances are associated with SST anomalies the in seasonal cycle. This gave grounds to believe that winter anomalies would be more informative.

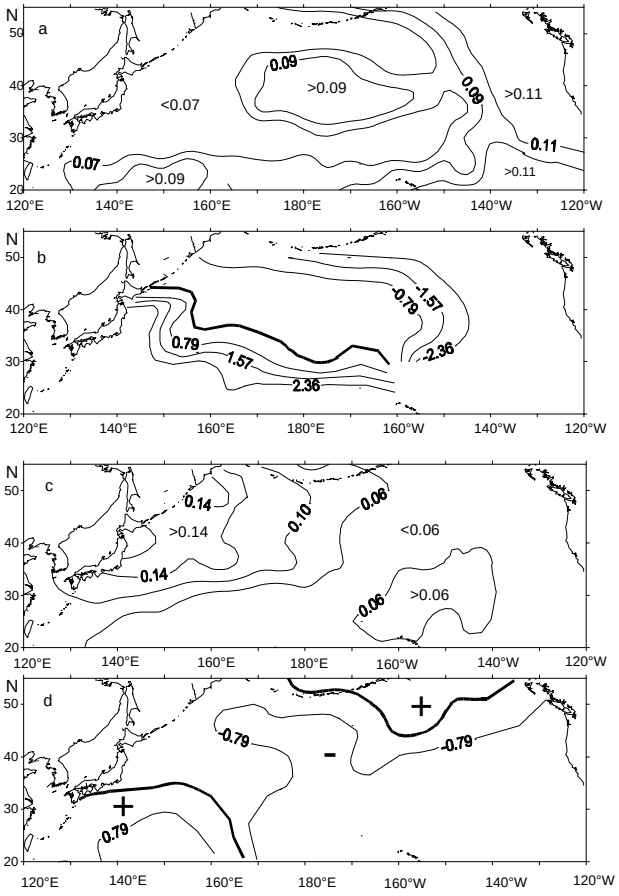

Figure 5. *(a) Spatial amplitude and (b) phase of the first CEOF and (c) spatial amplitude and (d) phase of the second CEOF for the low-pass pre-filtered winter SST anomalies in the extra-tropical North Pacific (1947–1978). Phase is given in radians. Zero phase contour is shown as a thick solid line. Signs indicate areas of positive (+) and negative (–) phases.*

The same low-pass filtering and CEOF procedures were applied to SST monthly anomalies taken for winters only. Time series consist of SST anomalies taken for December, January and February of every year (96 time counts). A maximum of spatial amplitude for the first CEOF (29% of variance) corresponds to the known Kelvin wave propagating along the eastern Pacific coast. Another spatial amplitude maximum corresponds to the Rossby wave propagating in the westward direction from the eastern coast to the central midlatitude Pacific area (Figure 5a) confirmed by the spatial (Figure 5b) and temporal (not shown) phases. Spatial phase gradients suggest that SST anomalies propagate westward from the eastern Pacific margin up to 155–160°W in the belt of 30–40°N (Figure 5b), in line with the Johnson - O'Brien model (Johnson and O'Brien, 1990a, b).

Anomaly wave turns southwestward from the spatial amplitude maximum area (30–40°N, 170°E–160°W). Significant spatial phase gradients and, therefore, southwestward wave propagation are characteristic of the entire western subtropic Pacific. It corresponds to the results of ocean surface level data analysis (ERS 1 satellite three-day repeat altimeter data) on southwestward propagation of waves in the area of 30–40°N, 145–160°E off the Japanese coast (Minster and Gennero 1995).

The first PC temporal amplitude for low-pass prefiltered winter SST anomalies seems to be correlated to the monthly low-pass pre-filtered El-Niño Index time series taken for winters only. Its lagged correlation (Figure 3b) is positive and statistically significant within –1 year (PC amplitude delayed) and +2 year (PC amplitude leading) lag range. It reaches its maximum of 0.61 at a zero lag, i.e. for unlagged correlation. Unlike lagged links of the first PC for unfiltered SST anomalies (Figure 3a), high synchronic correlation of the first PC for low-pass filtered winter SST anomalies with the El Niño Index points out to the possible impact of ENSO-accompanying processes in the winter extratropic atmosphere. The spectrum of the first PC (Figure 6a) has its absolute maximum shifted to decadal time-scales ("red shift") compared to the spectrum for unfiltered SST anomalies (Figure 2a).

Unlike the first CEOF, the second mode for prefiltered winter SST anomalies (16% of variance) shows maximum amplitudes in the western Pacific in the belt of 30°–55°N (Figure 5c). Spatial (Figure 5d) and temporal (not shown) phases reveal the signal propagating from the central Pacific (45°N,

175°E–175°W) in the opposite directions: southwestward in the western subtropic area and northeastward in the eastern subarctic area. This is similar to the finding of Mizuno and White (1983) based on analysis of 300-m temperature data (from 1976–1980, at 30°–40°N, 130°–180°E) that in the Kuroshio Extension area temperature waves propagate westward in the area to the west of the Shatsky Rise (155°E) and eastward to the east of there.

The second PC temporal amplitude also shows a correlation with the pre-filtered winter El Niño Index although lower in value compared to the first mode (Figure 3b). However, in this case, correlation is statistically significant for zero lag and delays up to 1 year only. The spectrum of the second PC (Figure 6b) has its absolute maximum in a wider range including decadal and ENSO scales, compared to the spectrum for unfiltered SST anomalies (Figure 2a). Thus, removing short-scale variations from SST anomalies reveals decadal together with ENSO variations both in the first and second modes.

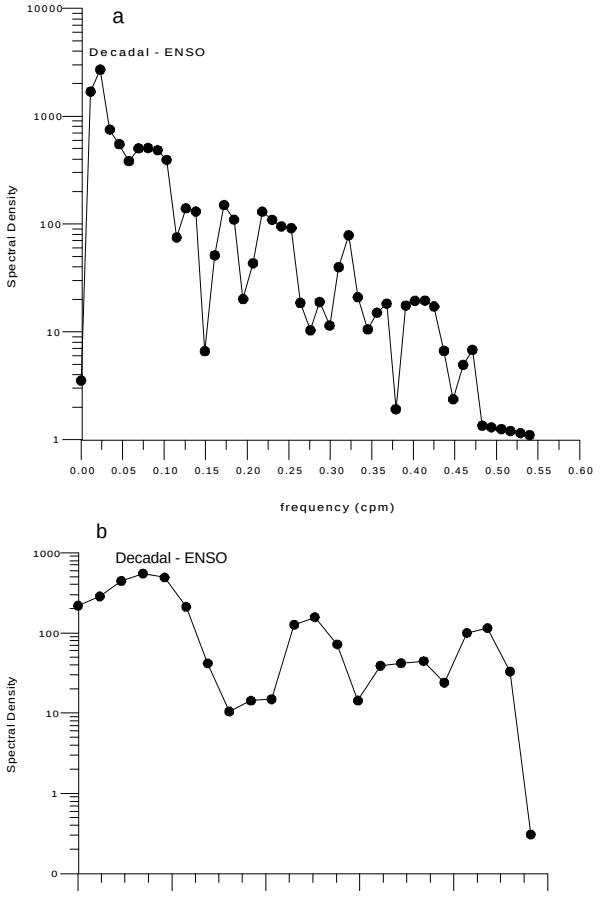

Figure 6. *Power spectra of (a) the first and (b) the second temporal PCs for the low-pass pre-filtered winter SST anomalies in the extra-tropical North Pacific (1947–1978).*

Recently, a substantial interest has arisen to studies on decadal variation which are considered generated in midlatitudes. Analyzing SST anomalies along the coast of the Sea of Japan for the period from 1930/40 to 1984, Watanabe et al. (1986) showed that while 6-year variations dominate in an area adjacent to the Korean Strait, the decadal scale prevails in the northwestern area. Nakamura et al. (1997) applied EOF (not complex) analysis to winter mean SST anomalies for the North Pacific to analyze decadal variations removing ENSO and lower-scale signals. Spatial patterns obtained by Nakamura et al. for the first and second EOFs are similar to our second and first CEOF spatial amplitudes obtained for the pre-filtered winter SST anomalies, correspondingly (Figure 5c,a); namely, the mentioned pairs show common areas of high amplitude. However, compared to Nakamura et al.'s first EOF, in our case, an area of high amplitude for the second CEOF is shifted to the west to the transition area between Oyashio–Kuroshio Current Systems where the most intensive ocean–atmosphere interaction takes place in winter. The presence of both decadal and ENSO variations in SST as well as synchronic correlation of PCs with SOI gives evidence of feedback between decadal and ENSO timescale dynamic processes in the ocean–atmosphere system in this area which is consistent with findings of Sekine and Yamada (1996) and Sekine (1998).

5. Seasonal Links between ENSO and Air Temperature in the Northwest Pacific Margin

Characteristic time scales of infra-annual air temperature variations in the Northwest Pacific Margin were obtained from power spectra for stations located in the area from the Korean to Chukchy Peninsulas. Spectra were estimated based on monthly mean time series for the 20th century, often more then 100 years, taken separately for every month. We chose the three following intervals of interest in the time-scale: biennial (2–3 years), quasi-ENSO (3–7 years), and quasi-decadal (7–13 years) intervals.

As a typical example, periods obtained for stations located around the Japan Sea are shown in the Table 1. It includes all spectral maximums of 95%-significance level and shows that every chosen time interval has, as a rule, the only maximum. Well known biennial variations are present at all stations for almost all months. ENSO and decadal scale variations are also present at almost all stations for

1–2 months at least. Decadal variations become more pronounced at the continental stations, on the one hand, and at the subarctic stations, on the other hand. In particular, one can see from the Table 1 that along the Japanese Islands coast decadal variations are present in winter at the Akita and Supporo stations located to the north of 39°N. As for the Nikolaevsk station located to the north of Tatar Strait at the Okhotsk Sea coast, decadal variations are present for 7 months of a year. This is typical for most stations around the Sea of Okhotsk, the including Kamchatka Peninsula coast.

Table 1. *Characteristic time scales of monthly mean air temperature variations for Russian, Korean and Japanese meteorological stations around the Japan Sea taken from spectra calculated for every monthly time series separately. 95% confidence level is accepted. Underlined are values corresponding to the middle of ENSO (3.0–6.9) or decadal (7.0–12.9) periods.*

Month	Station	Time scale			Station	Time scale		
		2.0–2.9 (biennial)	3.0–6.9 (ENSO)	7.0–12.9 (decadal)		2.0–2.9 (biennial)	3.0–6.9 (ENSO)	7.0–12.9 (decadal)
1	Nikolaevsk	2.1		7.3	Sapporo	2.2		7.8
2	(53°9′N,	2.1		12.8	(45°N,	2.0	4.4	12.8
3	140°4′E)		4.1		141°14′E)		4.1	11.3
4		2.6		11.0		2.6		11.3
5		2.3	5.1			2.6	4.6	
6	1925–1990	2.6			1889–1990	2.0	5.4	
7	(66 years)		6.0		(102 years)	2.2	3.0	
8		2.0		11.0		2.9	6.0	
9		2.0				2.4	6.4	
10		2.4		11.0		2.6		11.3
11		2.4		11.0		2.3	4.6	
12				9.4		2.1	3.6	8.5
1	Vladivostok	2.2			Akita	2.2		8.0
2	(43°7'N,		4.2		(39°26'N,	2.0	4.5	11.6
3	131°5′E)	2.1	3.9		140°5'E)		4.0	11.6
4		2.0		7.3		2.6		
5		2.0	3.3	7.9		2.0	4.7	
6	1881–1990	2.0	3.0		1886–1990	2.3	5.2	
7	(110 years)		3.0		(105 years)	2.9	5.2	
8			5.8				6.5	
9		2.2	3.4			2.2	5.8	
10		2.3	4.2			2.5		
11		2.3;	3.1			2.4	4.3	
12		2.2		9.2		2.4	3.6	9.5
1	Mokpho	2.2		7.8	Fukuoka	2.3	3.7	
2	(34°53'N,		3.9		(33°21'N,	2.2	5.9	
3	126°33'E)	2.3	6.6		130°15'E)		4.0	
4		2.2		8.6			3.0	
5			4.5				4.0	
6	1905–1990	2.2	3.2		1890–1990	2.0		
7	(86 years)		3.1		(101 years)	2.0	3.0; 5.9	
8			6.6			2.9		
9		2.8		7.2		2.8;	6.7	
10		2.6	5.7			2.6		
11		2.4	5.7			2.2	4.3	
12		2.3		9.6		2.3	3.1	

1	Inchon	2.3	4.8		Nagasaki	2.2	3.6	
2	(37°27'N,	2.3	5.7		(32°45'N,	2.2	3.6	9.3
3	126°37'E)		3.9	9.6	129°50'E)		4.0	
4		2.9		8.6		2.2	3.0	
5		2.9		10.8		2.9		
6	1905–1990	2.3			1879–1990	2.1		
7	(86 years)		5.1		(112 years)	2.0	5.6	
8			5.4				3.0	
9		2.0		7.2		2.7		
10		2.6	6.0			2.6		
11		2.3	5.4			2.2	6.2	
12		2.5		8.6		2.3	3.1	10.0

Table 2. *Correlation matrix for time series (1940–1990) of the winter mean air temperature at coastal meteorological stations around the Sea of Okhotsk with each other and Southern Oscillation Index averaged for the same winter (SOI), next summer (SOI, +6) and previous summer (SOI, –6). Only statistically significant correlation is shown (95%-confidence level).*

	Okhotsk	Ajan	Icha	Nikolaevsk	Alexndrvsk	Poronaysk	Abashiry	Nemuro	SOI	SOI, +6 m.	SOI, –6 m.
Magadan	0.93	0.53	0.79	0.42	0.43	0.52	none	none	0.54	none	0.43
Okhotsk		0.66	0.71	0.58	0.52	0.59	none	none	0.58	none	0.38
Ajan			0.48	0.68	0.78	0.69	0.4	0.47	0.41	none	none
Icha				0.46	0.57	0.59	0.46	0.47	0.51	none	0.42
Nikolaevsk					0.73	0.66	0.5	0.52	0.38	none	0.32
Alexndrvsk						0.84	0.71	0.75	0.42	none	0.28
Poronaysk							0.49	0.57	0.56	none	0.43
Abashiry								0.97	none	none	none
Nemuro									none	none	none

Spectra for time series (about 100 years) of winter 3- and 5-month (December–February and November–March) mean air temperature for meteorological stations located around the Japan Sea and SOI are shown in Figure 7. Air temperature spectra exhibit only two maximums, one corresponding to biennial variations and the other maximum shifted to the decadal scale (7–9 years). Figure 7 also shows that spectral density significantly increases from the southeast to the northwest. Spectra estimated for the Okhotsk Sea and Pacific coasts of the Kamchatka Peninsula show similar patterns. This is consistent with the spectrum for the second PC of low-pass filtered winter SST anomalies which has a wide maximum in a range of decadal and ENSO scales (Figure 6b) while the area of maximum spatial amplitudes of this CEOF covers the western subarctic Pacific. As for air temperature time series averaged for summer, spring or fall for stations located around the southern Japan Sea, the dominating maximum corresponds, as a rule, to the typical ENSO time-scale.

Thus, the presence of well pronounced ENSO and decadal scale variations in the subarctic area corresponds to findings based on the analysis of North Pacific winter SST (Nakamura et al., 1997, results of the present study) as well as of Oyashio Intrusion and snow coverage over the eastern Asia (Sekine and Yamada, 1996). Therefore, the relationship between seasonal air temperature anomalies with ENSO should be analyzed.

To reveal seasonal links between SOI and air temperature in the Northwest Pacific correlation analysis was applied. Lagged and unlagged correlation coefficients were calculated between time series of SOI and air temperature averaged for 5 (November–March or May–September) and 3 months (December–February or June–August) at the meteorological stations in the Northwest Pacific Margin. Lagged correlation was estimated between air temperature time series taken for winter and SOI taken for the previous (time lag of -6 months) or next summer (time lag of 6 months). Examples of correlation coefficients calculated for the period of 1940–

1990 are shown in Table 2.

Statistically significant unlagged positive correlation between winter mean air temperature and SOI was found for stations located at the Sakhalin, Siberian and Kamchatka coasts of the Okhotsk Sea. It means that air temperature tends to have a positive anomaly during winter La Niña events and a negative anomaly during winter El Niño events. An example for air temperature at the Ust-Hairuzovo meteorological station located at the Kamchatka coast of the Okhotsk Sea superimposed with North Pacific Index (NPI) and SOI is shown in Figure 8. The correlation coefficient with SOI is statistically significant with a 95%-confidence level and equal to 0.55.

Moreover, total ice coverage in the Okhotsk Sea also shows a linear relationship with SOI (Figure 9). A 10-day mean time series (1957–1989) was calculated by averaging the ice extent during periods of greater ice cover for every year (21–28 of February, 1–10, 11–20 and 21–30 of March, and 1–10 of April). Its unlagged correlation coefficient with SOI is equal to –0.45 with a 95%-confidence level. Its lagged correlation coefficient with SOI for a previous summer (SOI taken 6 months behind) is equal to –0.46 with a 95%-confidence level. Thus, ice coverage increases in years of winter El Niño events or in winters after summer El Niño events and decreases in years of winter La Niña events or in winters after summer La Niña events (Figure 9). (SOI has the highest negative values during El Niño events and highest positive values during La Niña events.)

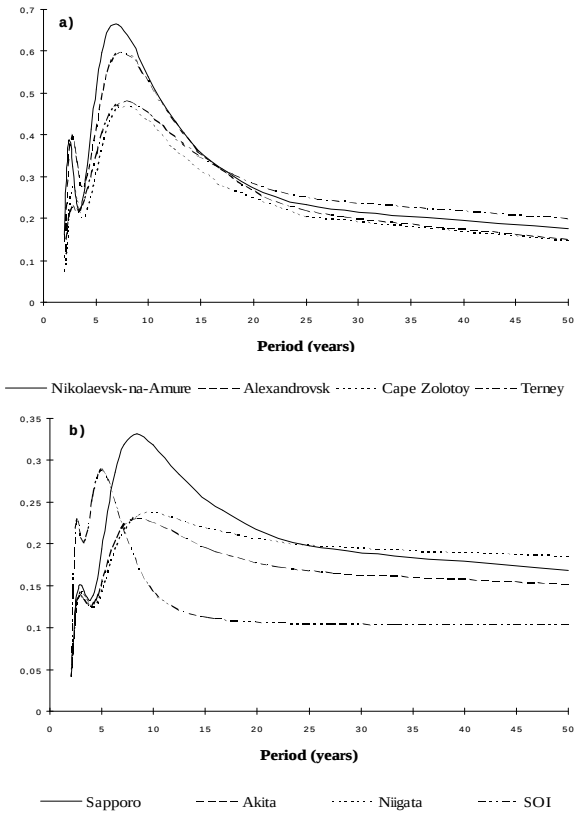

Figure 7. *Power spectra for time series of SOI and winter mean (December–February) air temperature for meteorological stations located around the Japan Sea: at (a) the Siberian coast (Terney, Cape Zolotoy, Nikolaevsk-Na-Amure) and Sakhalin Island (Alexandrovsk) and at (b) the Japanese Islands (Sapporo, Akita, Niigata) and SOI.*

At the same time, air temperature at the meteorological stations situated at the northeast Hokkaido coast (Nemuro and Abashiry) and at the south Kuril Islands, do not have a statistically significant unlagged correlation with the internal Okhotsk/Japan Sea coastal stations or SOI.

There is no lagged correlation between winter air temperature at the Okhotsk Sea coastal stations and SOI of a next summer (+6 months) while the lagged correlation between the mentioned time series and SOI of a previous summer (–6 months) is statistically significant but still smaller compared with the unlagged ones (Table 2). This is in accordance with the presence of synchronic and delayed correlation between the El Niño Index and the second temporal PC for the pre-filtered winter SST anomalies (Figure 3b) while the corresponding spatial CEOF has high amplitudes in the western subarctic Pacific (Figure 5c).

The seasonal mean air temperature time series in the meteorological stations located at the oceanic coast of Kamchatka and adjacent Komandorsky Islands also show statistically significant unlagged correlation with SOI for winter. However, no statistically significant unlagged correlation was found for air temperature and SOI at the Chukchy coast of the Bering Sea, or at the Chukchy coast of the Chukchy Sea.

As for the unlagged correlation between winter (3- or 5-month mean) air temperature at the Japan Sea coastal stations and SOI, the statistically significant coefficients were obtained mainly for the stations situated along the subarctic Northwest Japan Sea coast (Vladivostok, Nakhodka, Terney, Cape Zolotoi, Aleksandrovsk). On the contrary, 5-month summer (May–September) mean air temperature time series show a high unlagged correlation with SOI at the southern stations located along the southeastern coast of the Japan Sea (Akita,

Adgihara, Fukuoka). The significant correlation between 3-month summer (June–August) air temperature and SOI is revealed only for the most southern stations, for example Fukuoka.

So, a significant local maximum of the ENSO time scale in the spectrum of monthly mean air temperature was found for most meteorological stations

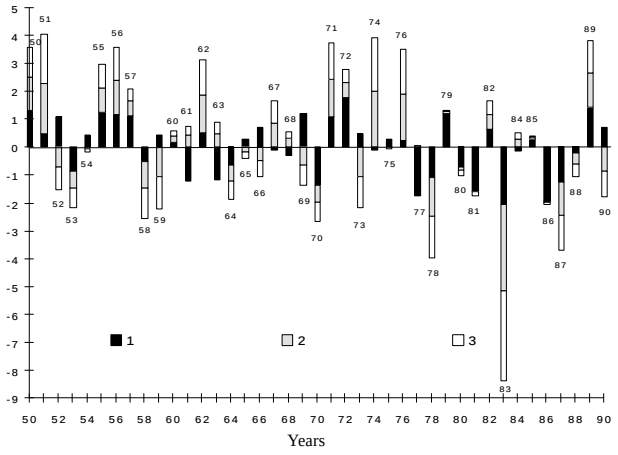

Figure 8. *Time series (1950–1990) of normalized winter anomaly of (1) NPI, (2) SOI, and (3) air temperature at the Ust-Hairuzovo meteorological station located at the Okhotsk coast of Kamchatka Peninsula. (SOI positive anomalies correspond to La Niña event, negative anomalies correspond to El Niño event).*

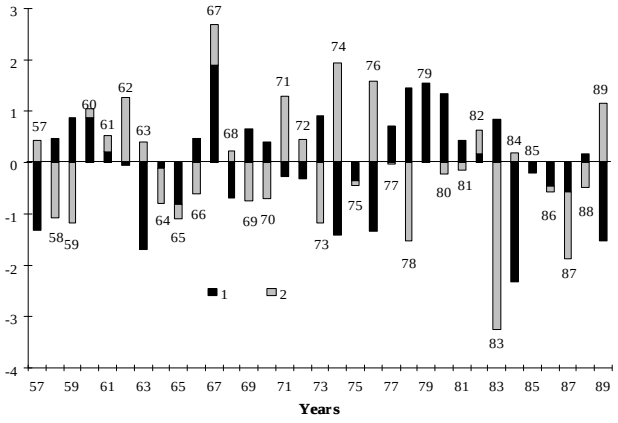

Figure 9. *Time series (1957–1989) of the Sea of Okhotsk ice extent (1) normalized anomaly and (2) normalized winter anomaly of SOI. (SOI positive anomalies correspond to the La Niña event, negative anomalies correspond to the El Niño event).*

in the Northwest Pacific Margin, but air temperature and SOI are related in a different way in the southern (South Japan Sea coast and Korean Peninsula), mid (Okhotsk Sea coast and Kamchatka Peninsula) and northern (Bering Sea coast and Chukchy Peninsula) areas. This difference is associated with asymmetry of the seasonal temperature anomalies in an annual cycle. Air temperature over the South Japan Sea is more under influence of ENSO-accompanying dynamic processes in the extratropical summer atmosphere, whereas air temperature over the North Japan Sea, Okhotsk Sea and Kamchatka Peninsula is mostly subjected to the impact of the ENSO accompanying processes in the winter atmosphere.

NPI measuring intensity of the Aleutian Low also has a statistically significant unlagged correlation with SOI for winter (Figure 8) but not for summer. Correlation coefficients for 5- and 3-month winter mean time series are equal to 0.58 and 0.41, respectively. Besides, lagged correlation coefficients between winter NPI and SOI taken for a previous summer (–6 months lag) are statistically significant as well and equal to 0.49 and 0.45, for 3- and 5-month averaging, respectively. At the same time, the NPI spectrum has a well known decadal spectral maximum, which is also present in the time series of air temperature (Table 1) over the Western Subarctic Pacific Margin. Ice extent in the Sea of Okhotsk shows a decadal maximum in the spectrum as well (Plotnikov, 1997).

According to air temperature and SST analyses one can suggest that ENSO and decadal scale variations in the North Pacific are connected via both annual–biennial oscillations of the Asian Monsoon and ocean–atmosphere interaction in the western mid-latitude (subarctic/subtropic) and central subtropic Pacific.

6. Typical Synoptic Situations, their Variations, and Impact on the Subarctic Northwest Pacific Margin

Polyakova (1992, 1997) developed the heuristic classification based on daily sea surface pressure (SLP) fields and suggested six principal types of atmosphere synoptic circulation over the North Pacific (Figures 10–15). The choice of original observations rather than averaged, for example monthly data, gave classes which keep information on synoptic processes.

Positions of cyclone tracks as well as of the Aleutian Low Pressure and Subtropic High Pressure Centers were chosen as classifying attributes for atmospheric circulation patterns. Characteristic synoptic situations (classes) presented as six SLP fields correspond to known atmospheric circulation patterns over the North Pacific area obtained earlier by (Wallace and Gutzler, 1981) and over the Northern Hemisphere (Barnston and Livezey, 1987) using EOF analysis of averaged SLP fields. In particular, Polyakova's expert situations reflect the Pacific–North American (PNA), East–West (EW), Zonal Dipole (ZD) patterns. The latter is similar to the Pacific Transition (PT) pattern in the hemispheric classification (Barnston and Livezey, 1987).

It was shown earlier that due to ENSO events over the Northern Hemisphere "...changes in the extratropical circulation immediately begin to change the jet stream and the associated storm tracks, so that the heat and vorticity fluxes caused by the transient eddies in the extratropics are also altered." (Branstator, 1995; citation from *Learning to Predict Climate Variations Associated with El Nino and the Southern Oscillation*, 1996). This gives grounds to believe that Polyakova's calendar of six atmosphere circulation pattern occurrences may be closely connected with ENSO accompanying events in the mid-latitude Northwest Pacific.

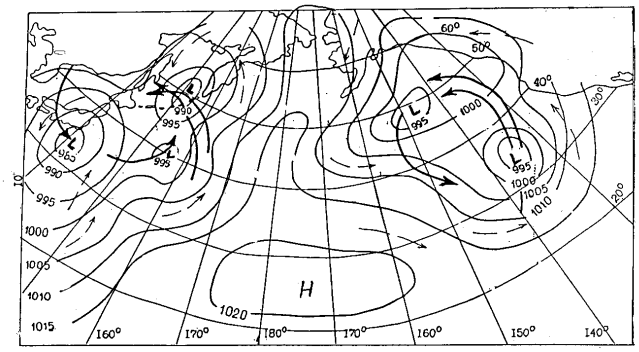

Figure 10. *The Okhotsk–Aleutian (OA) synoptic situation associated with northwestward cyclone tracks in the Okhotsk Sea adjacent to the Pacific and north-eastward tracks near North America as well as with the central position of Subtropic High Pressure, strongly meridional type in the Eastern and Western Pacific. Air mass transport is shown by thin arrows, cyclone tracks are shown by thick arrows.*

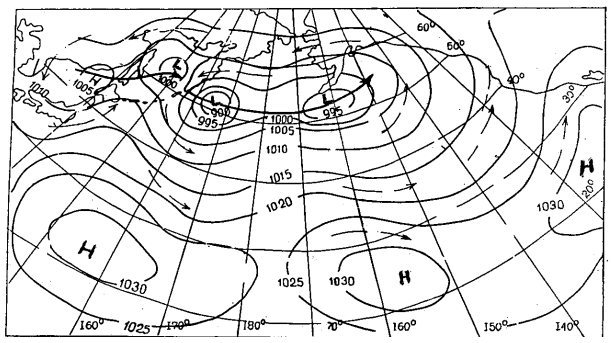

Figure 11. *The Aleutian-Zonal (AZ) synoptic situation associated with zonal cyclone tracks in Subarctic Pacific (50°–55°N) from the Sea of Okhotsk to the North America as well as with both zonally stretched Aleutian Low and Subtropic High Pressure. Air mass transport is shown by thin arrows, cyclone tracks are shown by thick arrows.*

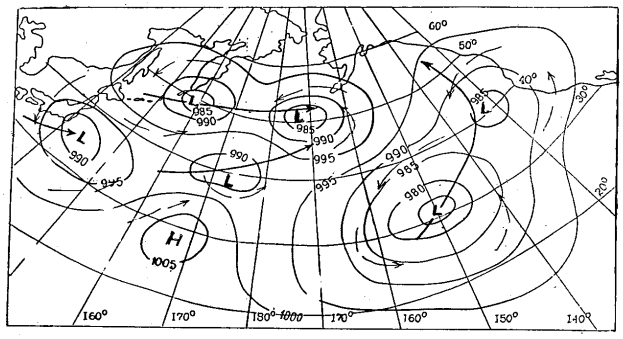

Figure 12. *The Cyclones Over the North Pacific (CN) synoptic situation associated with cyclonic activity over mid-latitude (subtropic and subarctic) North Pacific, with western position of the Subtropic High Pressure and with eastward cyclone tracks in the western and central Pacific and northward tracks in the eastern Pacific. Air mass transport is shown by thin arrows, cyclone tracks are shown by thick arrows.*

Three situations show a more or less pronounced meridional (Figures 10, 12, 14) and three situations show quasi-zonal (Figures 11, 13, 15) circulation patterns over the North Pacific. The former ones are associated with sea–land temperature contrasts, while the latter ones may be considered as related to south–north temperature contrasts. Higher frequency of occurrence of zonal or meridional types may accompany weakening or strengthening of both

the Asian winter and summer monsoons in the Northwest Pacific Margin, respectively. It is especially true for the subarctic Northwest Pacific area where the highest variance of both air temperature and SST anomalies of a seasonal cycle was found. A characteristic example for low-frequency variations in the subarctic Northwest Pacific is also the South Oyashio Intrusion (Hanawa, 1995; Sekine, 1996).

Thus, the classification used in the present study can be a basis for the estimation of interannual variations in both the Asian Monsoon and circulation patterns in the North Pacific atmosphere via anomalies of synoptic situation frequency of occurrence and cyclone track changes in transitions from one situation to another. Time series were composed of monthly frequency of occurrence (days per month) for these situations taken from 1949 to 1997 and averaged for 3- (December–February, June–August) and 5-month (November–March, May–September) winter or summer periods. To estimate the linear relationship with ENSO, time series of SOI were subjected to the same kind of averaging. It should be noted that the years 1990 and 1992 are missing from the Polyakova's calendar. This was taken into account when the SOI time series were composed. The occurrence of the six synoptic situations is shown in Figure 16. It is easy to see that the first four types occur more often than the last two ones.

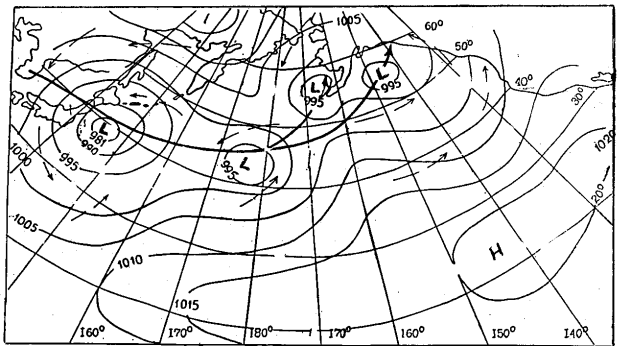

Figure 13. *The Northwest (NW) synoptic situation associated with cyclonic activity over the western Subtropic and eastern Subarctic Pacific with cyclone tracks in northeastern direction and with eastern position of Subtropic High Pressure. Air mass transport is shown by thin arrows, cyclone tracks are shown by thick arrows.*

The first two types, especially the Okhotsk-Aleutian (OA) situation, meridional for the whole North Pacific, correspond to the penetration of south cyclones with characteristic weather patterns into the northern Japan and southern Okhotsk Seas and Kuril area of the Pacific. On the other hand, the internal Okhotsk Sea is subjected to cold air mass transport from Siberia in winter. This sharpens the land–sea contrast and strengthens the winter monsoon. The OA situation (Figure 10) represents the classical meridional dipoles with a high pressure ridge over the central Pacific from the subtropic to subarctic area and low pressure over the eastern and

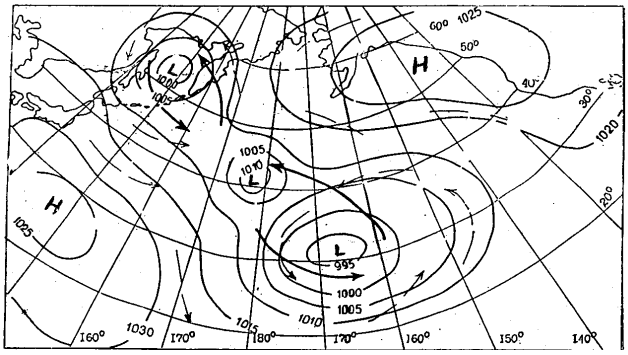

Figure 14. *The Okhotsk–Hawaii (OH) synoptic situation associated with unusual cyclone tracks over the Central Pacific and Sea of Okhotsk as well as the high pressure over North America and extreme western position of the Subtropical High Pressure. Air mass transport is shown by thin arrows, cyclone tracks are shown by thick arrows.*

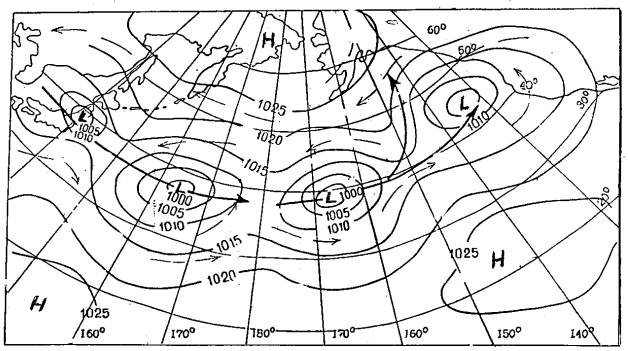

Figure 15. *The Southern–Zonal (SZ) synoptic situation associated with strong zonal eastward cyclone tracks in the Western Central Pacific (35°–49°N) and northward tracks in the Eastern Pacific. Air mass transport is shown by thin arrows, cyclone tracks are shown by thick arrows.*

western Pacific. Due to its high frequency of occurrence it is often present in the monthly mean fields. Northward tracks of south cyclones dominate over the western and eastern Pacific Ocean. For the western Pacific, cyclones come from the Philippine Sea through the Kuroshio–Oyashio area to the Kuril Pacific area, northern Japan and southern Okhotsk Seas.

The Aleutian-Zonal (AZ) situation (Figure 11) corresponds to a zonal dipole with low pressure in the subarctic and high pressure in the subtropic Pacific representing a pattern of an active winter monsoon. Northeastward cyclones move mostly along the land–sea margin from the East China Sea through the Japan Sea to the southern Okhotsk Sea and then turn eastward to cross the subarctic Pacific. Time series for the AZ situation winter mean frequency of occurrence shows both unlagged and lagged (6 months ahead) negative correlation with SOI. Correlation coefficients satisfy to a 95%-confidence level and are equal to –0.047 and –0.44, respectively, which means that the AZ situation is more frequent during winter El Niño events.

The Cyclones Over the North Pacific (CN) synoptic situation (Figure 12) reveals a meridional circulation pattern in the eastern Pacific with a western position of the weakened Subtropic High Pressure, northward cyclone tracks over the Eastern Pacific, and eastward tracks over the Western Pacific.

The Northwest (NW) synoptic situation (Figure 13) exhibits an almost zonal circulation dipole pattern but still has asymmetric features. It is characterized by the southeastern position of Subtropic High with eastward cyclone tracks over the Kuroshio–Oyashio Extension area in the western Pacific and northeastward tracks over the eastern subarctic Pacific. Both the CN and NW situations have a similar effect on the Okhotsk Sea due to cyclone tracks located over the southern Sea. The NW situation frequency of occurrence shows a positive unlagged correlation with SOI of 0.37, slightly above the 95%-confidence level. It means that the NW situation is less frequent during winter El Niño events.

Two last synoptic situations (Figures 14 and 15) are very rare events compared to the previous ones (Figure 16). The Okhotsk–Hawaii (OH) situation represents a kind of exotic feature of the atmosphere circulation over the North Pacific. It exhibits a diagonal dipole similar to an extreme phase of PNA with low pressure over the subarctic and central Pacific and high pressure over North America. The latter prevents northward propagation of the cyclone in the eastern Pacific area. Subtropical High Pressure is located in an extreme southwestern position blocking the northward cyclone tracks in this area. There are rather cold (subarctic) cyclones above the Okhotsk Sea in winter.

The Southern-Zonal (SZ) situation (Figure 15) corresponds to a zonal dipole with an extreme southern position of the subarctic low pressure system, high pressure over the Bering Sea and Alaska, eastward cyclone tracks in the subtropic Pacific area and northeastward cyclone tracks over subarctic eastern Pacific. Both these situations cause cold winter air temperature anomalies in North America, but their impact on the Northwest Pacific is not significant.

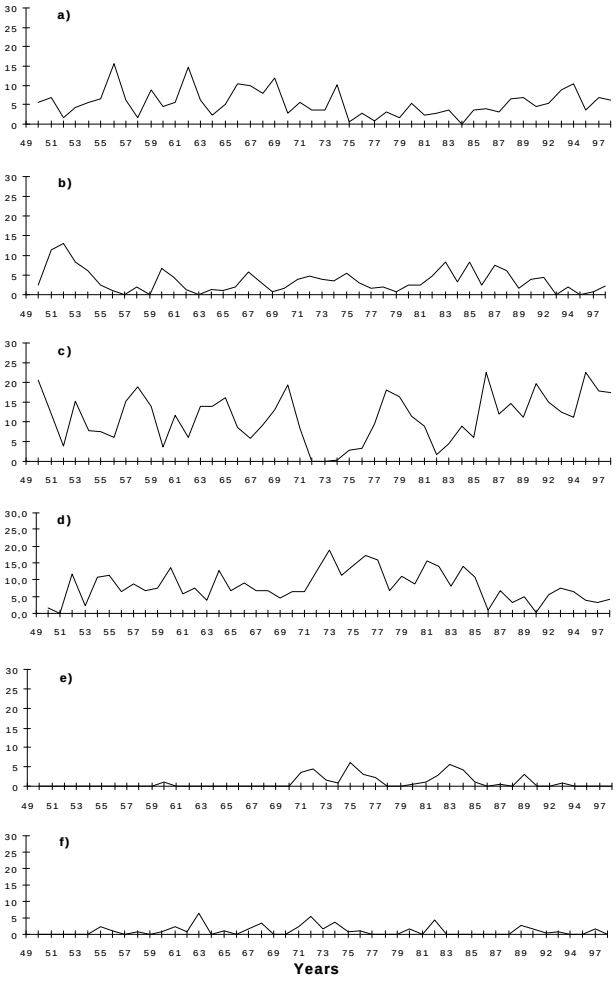

Figure 16. *Five-month (November–March) winter mean time series (1949–1998) of frequency of occurrence for (a) Okhotsk–Aleutian, (b) Aleutian–Zonal, (c) Cyclones Over the North Pacific, (d) Northwest, (e) Okhotsk–Hawaii, and (f) Southern-Zonal synoptic situations over the North Pacific.*

Figure 17 shows the time series (1949–1998) of sum frequency of occurrence (days/month) for CN and NW situations in (a) winter (including December of a previous year) and in (b) summer (May–September mean time series were used). Strong and medium El Niño events in winter are also marked. Minimums in the chart for (a) winter and maximums in the chart for (b) summer coincide with mostly El-Niño events, namely, the frequency of occurrence is low during the winter El Niño event in 1966 and reaches its local minimum during the winter El Niño events in 1973, 1983, 1987, and 1997, while it reaches local maxima in the summers of 1952, 1958, 1966, 1973, 1983, 1987, and 1992 following the winter El Niño events of the same years.

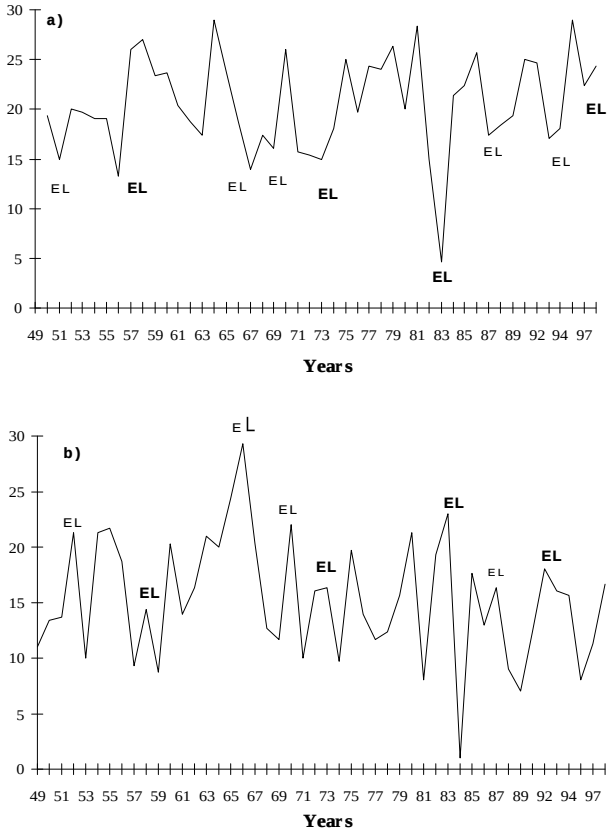

Figure 17. *Time series (1949–1998) of sum frequency of occurrence for CN and NW synoptic situations over the North Pacific in (a) winter (for November–February mean values) and (b) summer (for May–September mean values). El Niño events are marked by EL symbols.*

Thus, years of El Niño events dominating in winter are characterized by substantial anomalies in an annual cycle of the extratropic synoptic circulation patterns over the North Pacific. It seems that certain physical processes which control the accompanying ENSO effects in winter atmosphere over the mid-latitude Northwest Pacific are prominent in the cyclone track changes.

7. Conclusions

When analyzing conventional SST anomalies for the whole extratropic North Pacific (unfiltered monthly mean SST anomalies including anomalies of an annual cycle), the power spectrum has a maximum at the ENSO scale and a lagged correlation with SOI dominates, with SST being 1.5–2 years behind or 1 year ahead of the Niño3 Index. When analyzing interannual winter SST anomalies for the whole extratropic North Pacific (low-pass filtered wintertime monthly mean SST anomalies), an unlagged correlation with ENSO dominates and both ENSO and decadal scale variations are revealed.

In both cases the first CEOFs have maximums in the eastern and central Pacific while the second CEOFs are located in the Northwest Pacific. However, for the interannual winter SST anomalies the spatial core of the second mode is shifted to the north and confined in the transition area between the Oyashio and Kuroshio Currents where the most intensive ocean–atmosphere interaction takes place in winter. Presence of both decadal and ENSO variations in the SST anomalies as well as its unlagged/lagged significant correlation implies possible feedback between low-frequency variations of the two mentioned time scales in the mid-latitude Pacific and particularly in the Northwest Pacific also outlined by Sekine (1998).

The significant local maximums of the ENSO scale in spectra of monthly mean air temperature are pronounced for most of the seasons and meteorological stations in the Northwest Pacific Margin. Nevertheless, air temperature and SOI are related, in a different way, in the southern (South Japan Sea coast and Korean Peninsula), mid (Okhotsk Sea coast and Kamchatka Peninsula) and northern (Bering Sea coast and Chukchy Peninsula) areas. The principal difference is associated with the asymmetry of seasonal temperature anomalies in an annual cycle. Air temperature over the southern Japan Sea is under greater influence to ENSO-

accompanying dynamic processes in the extratropical summer atmosphere, while air temperature over the northern Japan Sea, Okhotsk Sea and Kamchatka Peninsula is mostly subjected to the impact of the ENSO accompanying processes in the winter atmosphere.

According to air temperature and SST analyses, one can suggest that ENSO and decadal scale variations in the North Pacific are connected via both annual–biennial oscillations of the Asian monsoon system and ocean–atmosphere interaction in the western mid-latitude (subarctic/subtropic) and central subtropic Pacific.

ENSO-accompanying processes in the Northwest Pacific increase frequency of occurrence of certain synoptic circulation patterns over the North Pacific associated mainly with cyclone track changes in the western margin. The ENSO signal with the lag of about half a year is associated with the Northwest Pacific ocean memory in a seasonal cycle. The ENSO signal with the lag of about one year is probably conditioned by both oceanic SST anomalies propagating from the tropic–equatorial Pacific to the extratropic areas and by the atmosphere circulation response to these anomalies.

References

Alexander, M.A. 1992a. Midlatitude atmosphere–ocean interaction during El Niño. Part I: The North Pacific Ocean. *J. Climate, 5,* 944–958.

Alexander, M.A. 1992b. Midlatitude atmosphere-ocean interaction during El Niño. Part II: The Northern Hemisphere Atmosphere. *J. Climate, 5,* 959–972.

Barnston, A.G. and Livezey, R.E. 1987. Classification, seasonality and persistence of low-frequency atmospheric circulation patterns. *Mon. Wea. Rev., 115,* 1083–1125.

Bjerknes, J. 1969. Atmospheric teleconnections from the equatorial Pacific. *Mon. Wea. Rev., 97,* 163–172.

Blackmon, M.L., Wallace, J.M., Lau, N.-C. and Mullen, S.L. 1977. An observational study of the Northern Hemisphere wintertime circulation. *J. Atmos. Sci., 34,* 1040–1053.

Branstator, G.W. 1995. Organization of stormtrack anomalies by recurring low frequency circulation anomalies. *J. Atmos. Sci., 52,* 207–226.

Brillinger, D.R. 1975. *Time Series Data Analysis and Theory.* Holt, Rinehart and Winston, 500 pp.

Chan, J.L. 1985. Tropical cyclone activity in west Pacific in relation to the El Niño/Southern Oscillation phenomenon. *Mon. Wea. Rev., 113,* 599–606.

Chen, T.C. and Weng, S.P. 1998. Interannual variation in the tropical cyclone formation over the western north Pacific. *Mon. Wea. Rev., 126,* 1080–1090.

Enting, I.G. and Robbins, F.J. 1989. Asymmetric filters for analyzing time series of atmospheric constituent data. *Tellus, 41A,* 109–114.

Geisler, J.E., Backmon, M.L., Bates, G.T. and Munoz, S. 1985. Sensitivity of January climate response to the magnitude and position of equatorial Pacific sea surface temperature anomalies. *J. Atmos. Sci., 42,* 1037–1049.

Hanawa, K. 1995. Southward penetration of the Oyashio water system and the wintertime condition of midlatitude westerlies over the North Pacific. *Bull. Hokkaido Natl. Fish. Res. Inst., 59,* 103–115.

Hirst, A.C. 1986. Unstable and damped equatorial modes in simple coupled ocean–atmosphere models. *J. Atmos. Sci. 43,* 606–630.

Horel, J.D. and Wallace, J.M. 1981. Planetary-scale atmospheric phenomena associated with the Southern Oscillation. *Mon. Wea. Rev., 109,* 813–829.

Horel, J.D. 1984. Complex principal component analysis: theory and examples. *J. Clim. Appl. Meteorol., 23,* 1660–1673.

Hou, A.Y. 1993. The influence of tropical heating displacements on the extratropical climate. *J. Atmos. Sci., 50,* 3553–3570.

Johnson, M.A. and O'Brien, J.J. 1990a. The role of coastal Kelvin waves on the northeast Pacific Ocean. *J. Marine Systems, 1,* 29–38.

Johnson, M.A. and O'Brien, J.J. 1990b. The Northeast Pacific Ocean response to the 1982–1983 El Niño. *J. Geophys. Res., 95(C5),* 7155–7166.

Lau, K.M. and Boyle, J.S. 1987. Tropical and extratropical forcing of the large-scale circulation: a diagnostic study. *Mon. Wea. Rev., 11,* 400–428.

Lau, N.-C. and Nath, M.J. 1990. A general circulation model study of the atmospheric response to extratropical sea surface temperature anomalies observed in 1950–79. *J. Climate, 3,* 965–989.

Learning to Predict Climate Variations Associated with El Niño and Southern Oscillation. Accomplishments and Legacies of the TOGA Program. 1996. National Academy Press. Washington, p. 235.

Michaelsen, J. 1982. A statistical study of large-scale, long-period variability in North Pacific sea surface temperature anomalies. *J. Phys. Oceanogr., 12,* 694–703.

Minster, J.-F. and Gennero, M.-C. 1995. High-frequency variability of western boundary currents using ERS 1 three-day repeat altimeter data. *J. Geophys. Res.,* 100(C11), 22,603–22,612.

Mizuno, K. and White, W.B. 1983. Annual and interannual variability in the Kuroshio current system. *J. Phys. Oceanogr., 13,* 1847–1867.

Molteni, F., Ferranti, L., Palmer, T.N. and Viterbo, P. 1993. A dynamical interpretation of the global response to equatorial Pacific sea surface temperature anomalies. *J. Climate, 6,* 777–795.

Nakamura, H., Lin, G. and Yamagata, T. 1997. Decadal climate variability in the North Pacific during the recent decades. *Bull. Amer. Meteorol. Soc., 78(10),* 2215–2225.

Oort, A.H. and Yienger, J.J. 1996. Observed interannual variability in the Hadley circulation and its connection to ENSO. *J. Climate, 9,* 2751–2767.

Palmer, T.N. 1993. A nonlinear dynamical perspective on climate change. *Weather, 48,* 314–326.

Philander, S.G.H., Yamagata, T. and Pacanowski, R.C. 1984. Unstable air–sea interactions in the tropics. *J. Atmos. Sci.,* 41, 604–613.

Plotnikov, V.V. 1997. Space-time relations between ice conditions in the Far Eastern Seas. *Meteorol. Gidrol., 3,* 77–85 (Rus.).

Polyakova, A.M. 1992. Method of Super Long Term Forecast of Ice Covering of the Okhotsk Sea. *The Seventh International Symposium on Okhotsk Sea and Sea Ice. Cold Research Association, Mombetsu, Japan,* 375–376.

Polyakova, A.M. 1997. The types of atmospheric circulation over the North Pacific and climate variations in the North Pacific. *Pacific Oceanological Institute. Proceedings of Annual Session, 1994*. Dalnauka, Vladivostok, Russia, 98–105 (Rus.).

Schucla, J. and Paolino, D.A. 1983. The Southern oscillation and long-range forecasting of the summer monsoon rainfall over India. *Mon. Wea. Rev., 111,* 1830–1837.

Sekine, Y. 1996. Anomalous Oyashio intrusion and its teleconnection with Subarctic North Pacific circulation, sea ice of the Okhotsk Sea and air temperature of the northern Asian continent. *Proceedings of PICES Workshop on the Okhotsk Sea and Adjacent Areas., Vladivostok, June 19–24, 1995. Canada, 1996,* 177–187.

Sekine, Y. and Yamada, F. 1996. Atmosphere and ocean global teleconnection around the Okhotsk Sea. *The 11th International Symposium on Okhotsk Sea and Sea Ice, 25–28 February 1996, Mombetsu, Hokkaido, Japan. Abstracts*, 148–150.

Sekine, Y. 1998. On the teleconnection processes around the North Pacific with reference to the decadal variations in atmosphere and ocean. *Seventh Annual PICES Meeting, Abstracts, October 14–25, 1998. Fairbanks*, p. 39.

Simmons, A.J., Wallace, J.M. and Branstator, G.W. 1983. Barotropic wave propagation and instability, and atmospheric teleconnection patterns. *J. Atmos. Sci., 40,* 1363–1392.

Tanaka, M. 1982. Interannual fluctuations of the tropical winter monsoon circulation and its relationship to the Walker circulation. *Tropical Ocean – Atmos. Newslett., 12,* 4–5.

Trenberth, K.E. and Paolino, D.A. 1981. Characteristic patterns of variability of sea level pressure in the Northern Hemisphere. *Mon. Wea. Rev., 109,* 1169–1189.

Trenberth, K.E. 1995. El Niño / Southern Oscillation. *in* Climate Change: Developing Southern Hemisphere Perspectives, T.W. Giambelluca and A. Henderson-Sellers (eds.), Wiley, New York, chap. 6.

Trousenkov, S.T. 1991. Identifying waves in climate signal processing. *Proc. Intern. AMSE Conf. "Signals & Systems". Warsaw, Poland, July 15–17, 1991*, Vol. 5, 145–153

Wallace, J.M. and Gutzler, D.S. 1981. Teleconnections in the geopotential height field during the Northern Hemisphere winter. *Mon. Weather Rev., 109,* 784–812.

Walker, G.T. 1924. Correlation in seasonal variations of weather IX: A further study of world weather. *Mem. Indian Meteor. Dept., 24 (4)*, 275–332.

Watanabe, T., Hanava, K. and Toba, Y. 1986. Analysis of year-to-year variation of water temperature along the coast of Japan Sea. *Prog. Oceanogr.,17,* 337–357.

Webster, P.J. and Yang, S. 1992. Monsoon and ENSO: selectively interactive systems. *Quart. J. Roy. Meteorol. Soc., 118,* 877–926.

Webster, P.J., Dixit, S. and Palmer, T.N. 1997. Intraseasonal variability of the Monsoon system and its relationship to monsoon predictability on interannual timescales: the concept of nudged chaos. *Joint Assemblies of IAMAS and IAPSO*, JMP1-31.

Wu, M.C. and Hastenrath, S. 1986. On the interannual variability of the Indian monsoon and the Southern oscillation. *Arch. Meteor. Geophys. Biocl., B39,* 239–261.

Wyrtki, K. 1975. El Niño – The dynamic response of the equatorial Pacific Ocean to atmospheric forcing. *J. Phys. Oceanogr*., 5, 572–584.

Yang, S. and Webster, P.J. 1990. The effect of summer tropical heating on the location and intensity of the extratropical westerly jet streams. *J. Geophys. Res., 95(D11),* 18,705–18,721.

Zhang, Y. and Wallace, J.M. 1996. Is climate variability over the North Pacific a linear response to ENSO? *J. Climate, 9,* 1468–1478.

Observations of El Niño off Oregon: July 1997 to Present (October 1998)

Robert L. Smith, A. Huyer, P.M. Kosro and J.A. Barth
College of Oceanic & Atmospheric Sciences
Oregon State University
Corvallis, OR 97331-5503, U.S.A.
e-mail: rsmith@oce.orst.edu

Every few months since July 1997 we have made CTD/ADCP sections off Newport, Oregon (44.6°N) from the coast to 150 km; a base of historical (1962–69) hydrographic data exists for this section. See our website (Monitoring the Coastal Ocean off Oregon: El Niño and beyond) under http://www.oce.orst.edu/po/coastal.html

The surface layer off Oregon was already warmer than normal in July 1997 (Figure 1a). The largest anomalies (>6°C) occurred offshore (>90 km) in July 1997, and inshore (<50 km) in September 1997 (Figure 1a). In September 1997, the surface layer was everywhere warm (>17°C) with low salinity; subsurface slope waters were >1ºC above normal with an isotherm slope indicating northward advection (Figure 1a). In November 1997 (Figure 1a), the surface layer was 1°C warmer than normal; subsurface waters over the slope were even warmer than in September and steric height rose steeply toward shore over 60 km, consistent with strong northward flow on the shelf (Figure 2). In February 1998 (Figure 1a), all water on the shelf was >12°C (>2°C above normal). Temperatures over the shelf remained above normal from July 1997 to June 1998 but were near normal by August 1998 (Figure 1b). Temperature and salinity fields suggest that upwelling was suppressed from September 1997 to June 1998. (The PFEL Upwelling Index for 45°N was negative or anomalously weak from June 1997 to June 1998.) Subsurface waters over the upper slope (100–400 m) remained warmer than normal from July 1997 through September 1998 (Figure 1). The winter and spring sections showed evidence of enhanced poleward advection, with a local anomaly maximum near the shelf break. The geostrophic currents were consistent with ADCP data (Figure 3) showing a strong current jet flowing poleward beyond the shelf break off Newport during the El Niño winter (November 1997 and February 1998). This poleward jet was surface-intensified with speed ~ 0.5 m/s, width ~ 20 km, and extending to depths > 200 m. By August 1998 the equatorward surface jet associated with normal coastal upwelling was present over the shelf, shelf temperatures were near normal, and the upwelling index was above the mean for August and September 1998.

Sections were also made at several latitudes between Newport, Oregon and San Francisco, California in November 1997, April 1998, and August 1998. These extended cruises showed much alongshore homogeneity. In November 1997, sections at 39°, 42°, 43.2°, and 44.7°N all showed the steric height of the sea surface rising steeply toward shore (~20 cm in ~ 60 km), while the 7° and 8°C isotherms slanted down toward the continental slope, indicating enhanced poleward flow over the shelf and upper slope (Figure 2). In April 1998, steric height profiles were flat (at 39° and 44.7°N) or slanting down toward the coast (at 42° and 43.2°N), indicating that the anomalous poleward flow had weakened or ceased. In August 1998, these sections show evidence of near-normal coastal upwelling inshore although subsurface waters offshore remained warmer than normal; they also show the 6.5° and 9°C isotherms diverging toward shore, suggesting geostrophic poleward flow with a subsurface core offshore of the continental slope. At this time, the ADCP observations along each section showed a band of poleward flow 20–40 km wide, with a subsurface maximum centered at 150–200 m, typical of the scales of the poleward undercurrent but with the core of the flow detached from the continental slope and offshore of the shelf break by 15 to 40 km (Figure 3).

Satellite-tracked drifters (drogued at 15 m) were released off Newport on all of the 1998 cruises (Figure 4). Eight drifters released off Newport in January 1998 (Figure 4a) moved coherently to the north, with strongest (up to 0.65 m/s) poleward flow near the continental shelf break. Four eventually

beached between 47° and 56°N, one was still off Vancouver Island in October, and two reached 49.5°N (and one 48°N) before reversing direction about 1 March. These observations are consistent with above normal sea level, warm water and enhanced poleward advection typical of El Niño conditions in winter. Of the seven drifters released off Newport in April 1998 (Figure 4b), the five released over the shelf and slope were advected by variable wind-driven currents, including some initial northward motion. Through August and September most drifters were moving equatorward and offshore, delineating the meandering jets of the California Current (Figure 4f); by October some drifters from the January, April, June and August releases off Newport (44.6°N) were between 35° and 39°N (Figure 4a–d). The drifters released in late September (Figure 4e) initially moved offshore and southward but, with the onset of fall storms, have not yet shown consistent trajectories.

See our web-site (Monitoring the Coastal Ocean off Oregon: El Niño and beyond) under: http://www.oce.orst.edu/po/coastal.html.

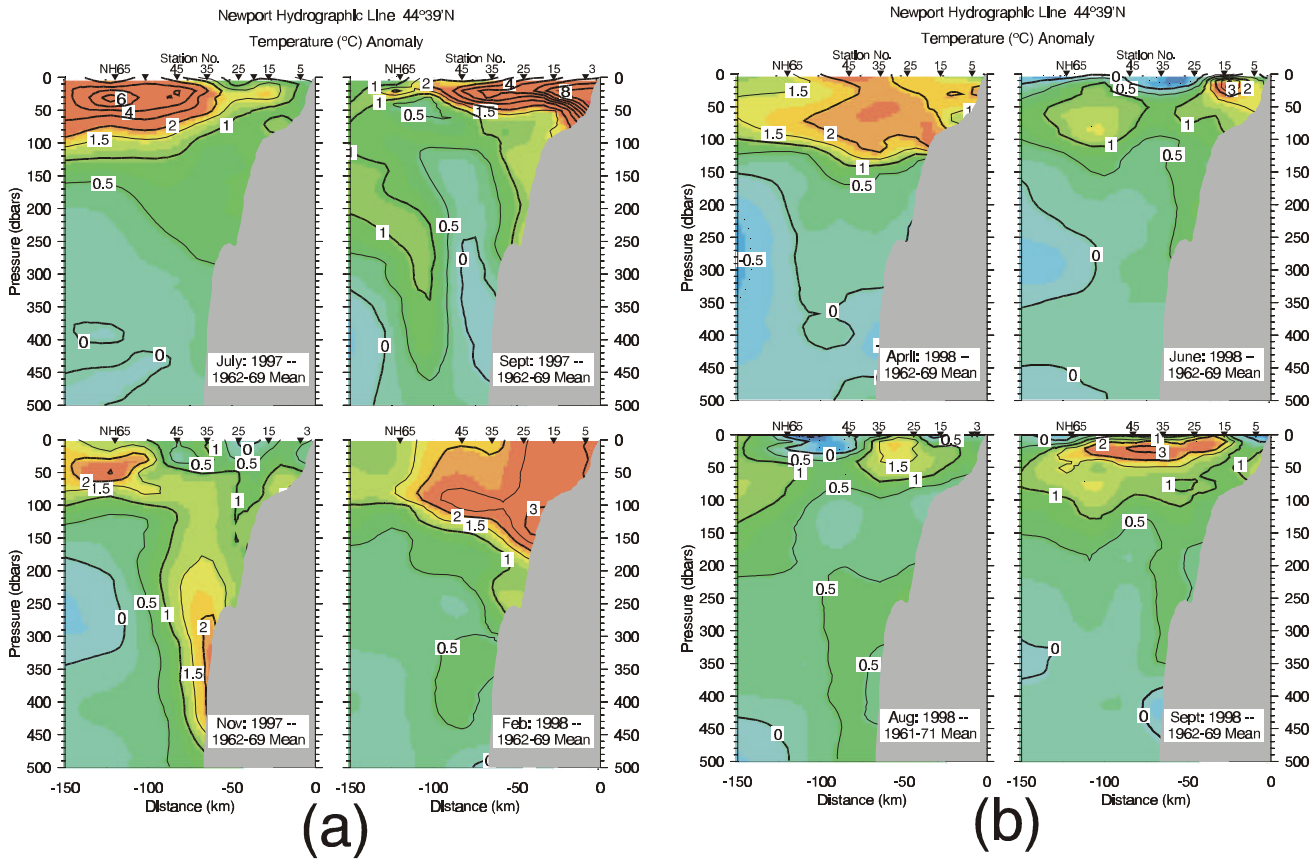

Figure 1. *Distributions of temperature anomalies from the historical average (1961–1971 for August, 1962–1969 for all other months) along the Newport Hydro Line at 44° 40'N (a) July, Sept., Nov. 1997, and Feb. 1998, (b) April, June, August and September 1998.*

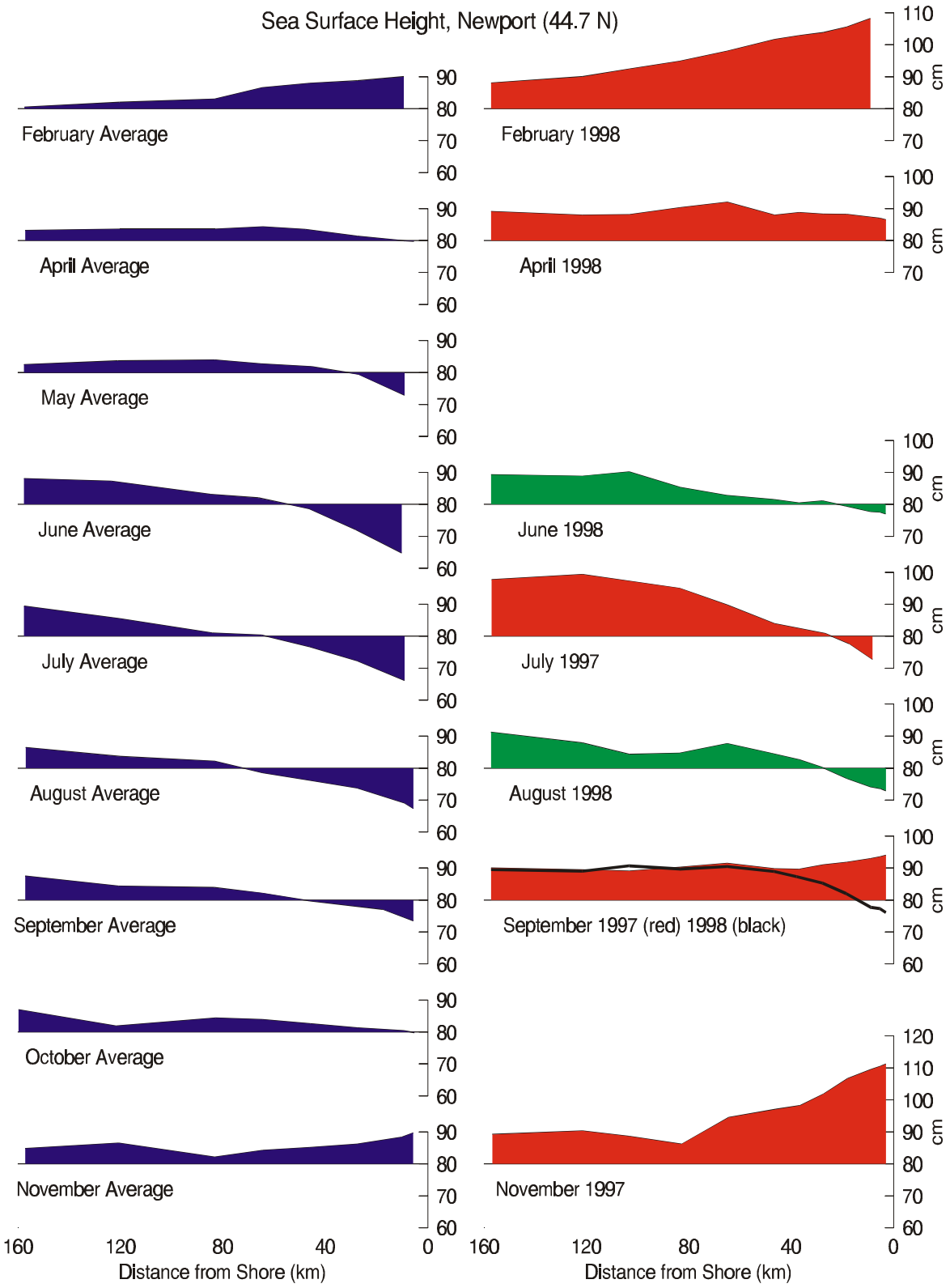

Figure 2. *Offshore profiles of the steric height of the sea surface (relative to 500 dbar), calculated from historical-average (left) and contemporary (right) density data along the Newport Hydro Line. The fill-color of the contemporary profiles indicates whether the section was during (red) or after (green) the 1997–8 El Niño.*

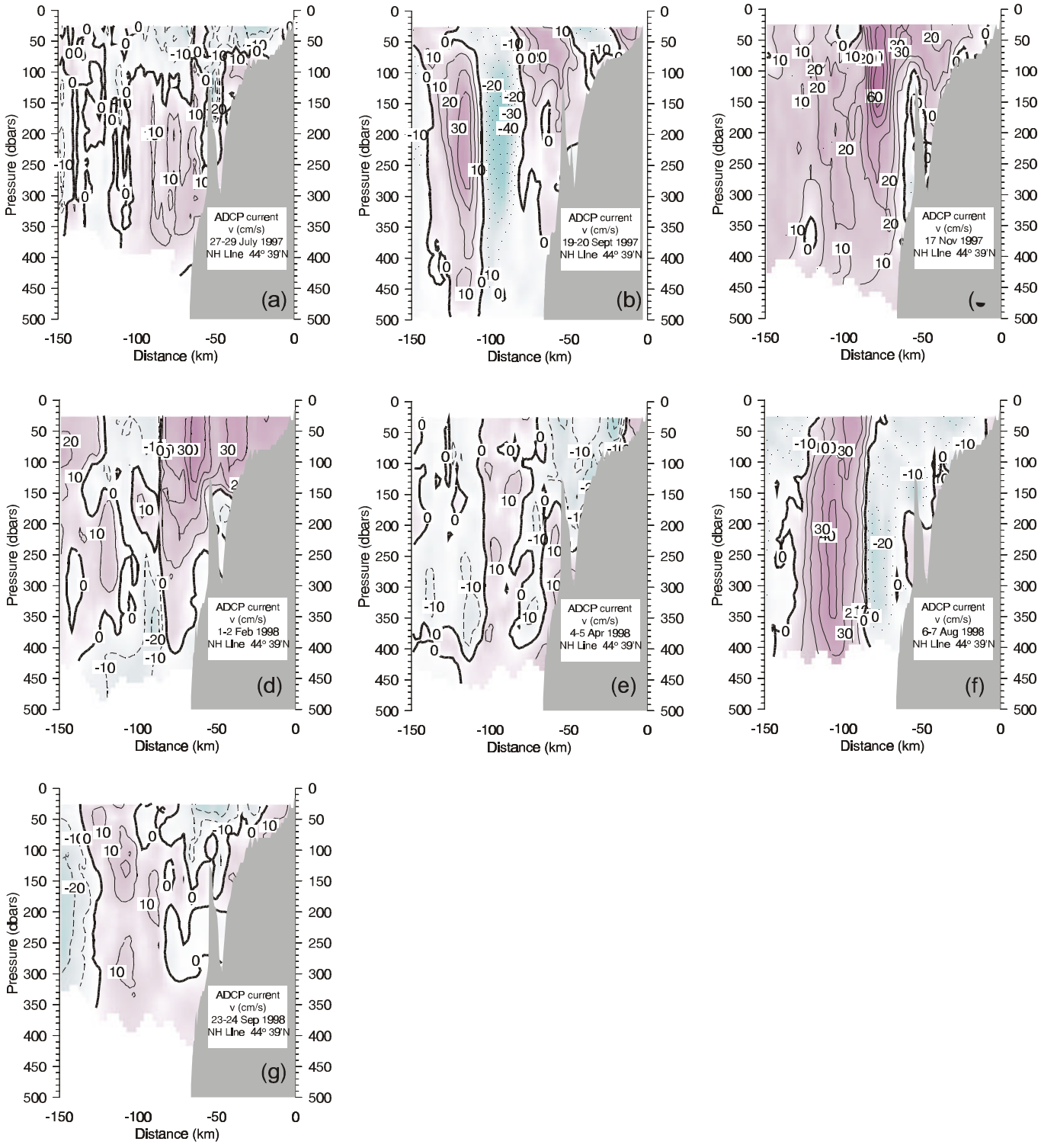

Figure 3. *Distributions of alongshore current (positive northward) measured with the ADCP on the Newport Hydro Line (a) 28–30 July 1997, (b) 19–20 Sept. 1997, (c) 15–16 Nov. 1997, (d) 1–2 Feb. 1998, (e) 5 April 1998, (f) 6–7 August 1998, and (h) 24–25 Sept. 1998.*

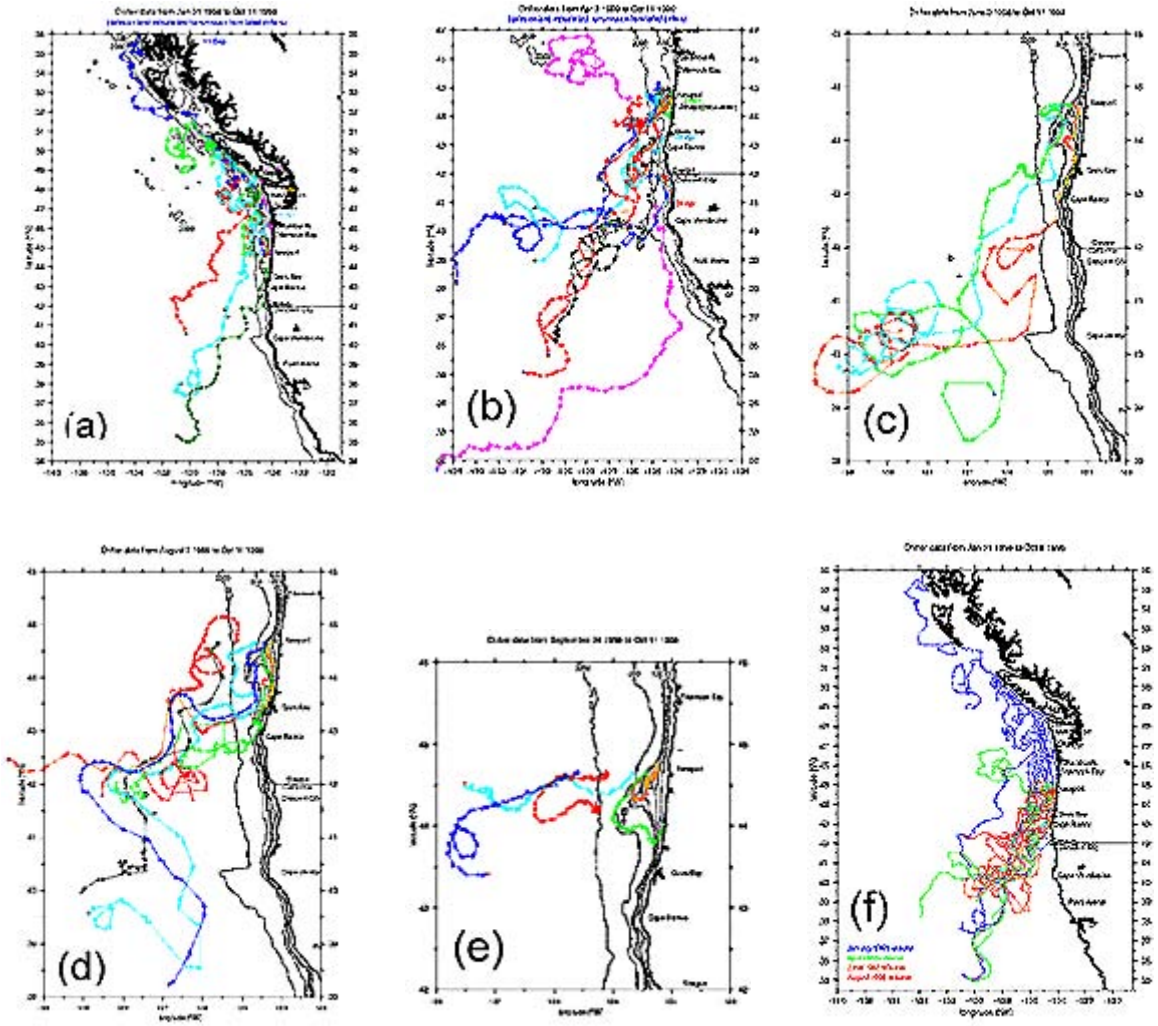

Figure 4. *Trajectories of satellite-tracked drifters deployed during the project: a) 31 Jan. to 11 Oct. 1998, (b) 3 April to 11 Oct. 1998, (c) 3 June to 11 Oct 1998, (d) 7 Aug. to 11 Oct. 1998, (e) 24 Sept. to 11 Oct. 1998, (f) summary of drifters deployed along Newport Hydro Line, 31 Jan. to 11 Oct. 1998.*

Biological Effects of the 1997–1998 EL Niño Event off Oregon: Nutrient and Chlorophyll Distributions

Patricia A. Wheeler and Jon Hill
College of Oceanic and Atmospheric Sciences
Oregon State University
Corvallis OR 97331 U.S.A.
e-mail: pwheeler@oce.orst.edu

Abstract

As part of the west coast GLOBEC long-term observation program we began measuring nutrient and chlorophyll distributions off the Oregon coast in July 1997. Three types of sampling have been conducted: a broad scale sampling in July 1997 (with R. Emmett, NOAA/NMFS) included eleven transects extending from the shore to 120 mi. offshore, high frequency sampling along the Newport hydroline (with B. Peterson, NOAA/NMFS), and additional sampling along 1–5 other transects every few months (with R. Smith et al. Oregon State University). General features of the broad scale survey include evidence of more upwelling, increased nutrients and higher chlorophyll in the southern half of the region compared with the northern half. High frequency sampling along the Newport hydroline showed less upwelling, lower nutrients and lower chlorophyll compared to non-El Niño years. Comparison of the nutrient and chlorophyll distributions with physical data will be presented to suggest the magnitude of the impact of changes in upwelling dynamics on primary production.

Goals of the biological studies of the Northeast Pacific (NEP) GLOBEC and El Niño sampling are to address three questions:

1. How do shifts in climate affect the distribution of nutrients and primary production?
2. How did the 1997–1998 El Niño condition affect nutrients and primary production off Oregon?
3. How do variations in physical and biological processes off Oregon affect poleward moving coastal and California Current waters?

Methods

We used three spatial/temporal schemes for sampling. During July 1997 we sampled 11 transects extending from 42–47°N and 124–127°W (Fig. 1). Our NEP-GLOBEC sampling included 2–5 transects off Oregon and northern California (Figure 1) during September and November 1997, and January, April, and August 1998. In addition, high-frequency sampling (once or twice a month) was carried out along the inner portion of the Newport line (Figure 1).

Results

The spatial distribution of temperature, nitrate, chlorophyll, and organic carbon in surface water (43–47°N and 124–127°W) is shown in Figure 2. Characteristics allow us to distinguish four regions as summarized in Table 1.

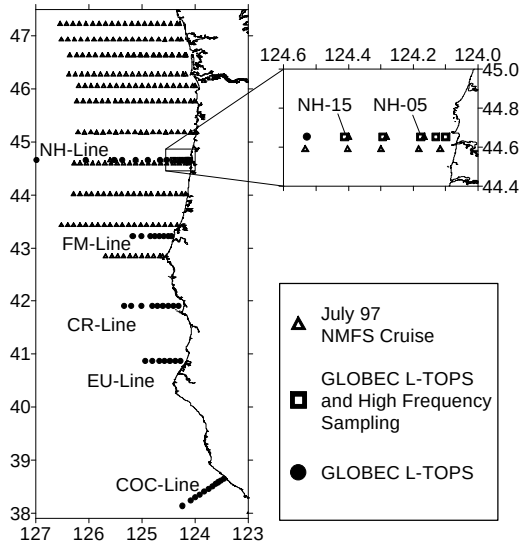

Figure 1. *In situ sampling map, 1997–98 NE Pacific, GLOBEC-L-TOPS.*

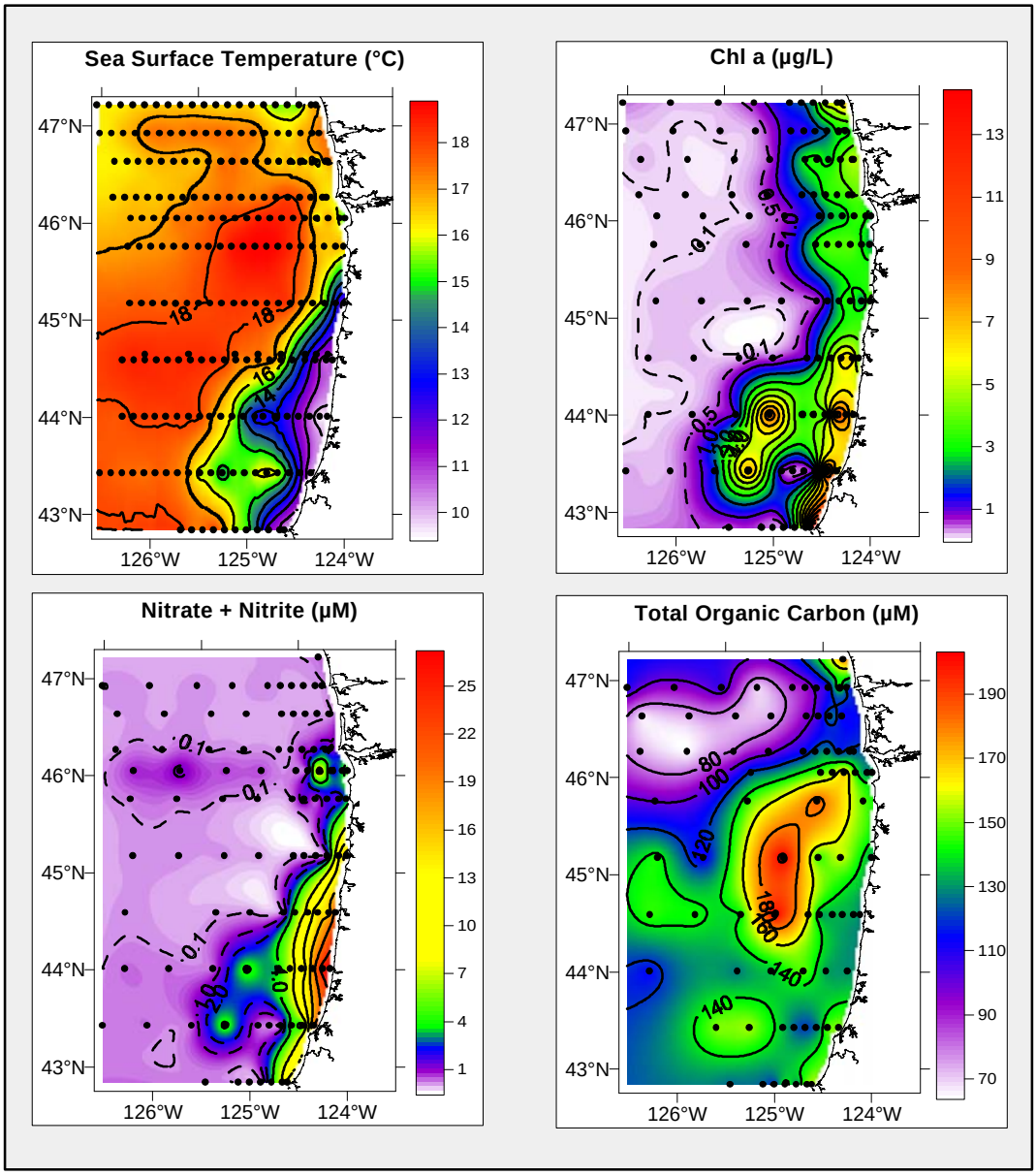

Figure 2. *Sea surface data from July 9–21, 1997. The chlorophyll, carbon, and nutrient samples were collected from 3 meters below the surface. Temperature data were taken by hand and reflect actual surface values.*

High-frequency sampling along the Newport transect showed that El Niño conditions resulted in a 2°C increase in surface temperature (Figure 3), a 50% reduction in integrated nitrate (Figure 4), and a 70% reduction in integrated chlorophyll (Figure 5).

Results from the September 1997 GLOBEC Newport transect confirm the low nutrient levels in the upper 20–30 m along the Newport line all the way from 160 m offshore to the coastline (Figure 6). These low-nutrient conditions were accompanied with low chlorophyll levels and a subsurface chlorophyll maximum at about 30 m (where nitrate levels were about 1 µM) (Figure 6). By August 1998 normal upwelling conditions had returned, accompanied by much higher chlorophyll levels throughout the water column and a chlorophyll maximum in the surface water near the coastline (Figure 6).

Table 1. *Regional comparison.*

Region	Temp (°C)	NO_3^- (μM)	Chl (μg/L)	TOC (μM)
Offshore	18	< 0.1	< 0.1	< 80
Columbia River Plume	18	< 1.0	0.1–0.5	140–200
N. Coast	16	2–6	2–4	120–140
S. Coast	10–14	6–26	2–14	120–140

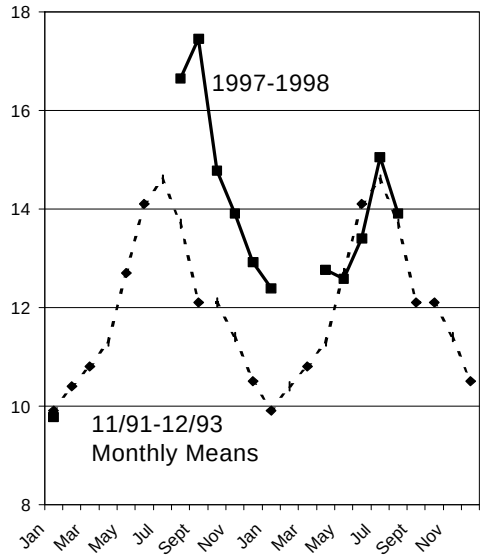

Figure 3. *Surface temperature at NH-20.*

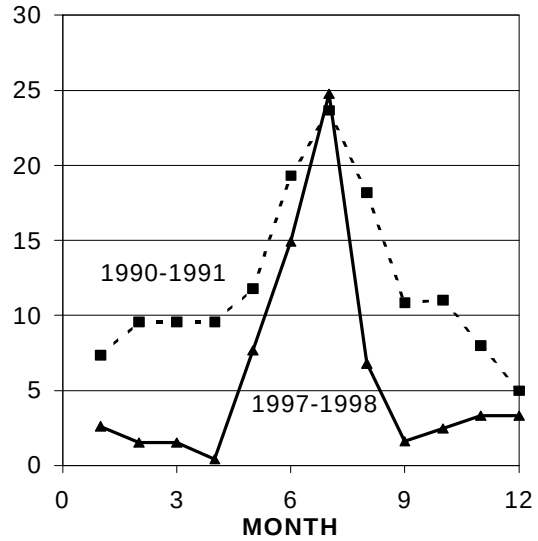

Figure 4. *Integrated nitrate (g/m^2).*

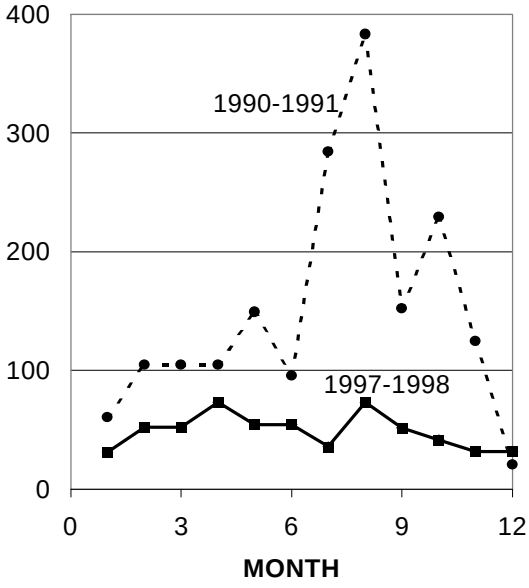

Figure 5. *Integrated chl (mg/m^2).*

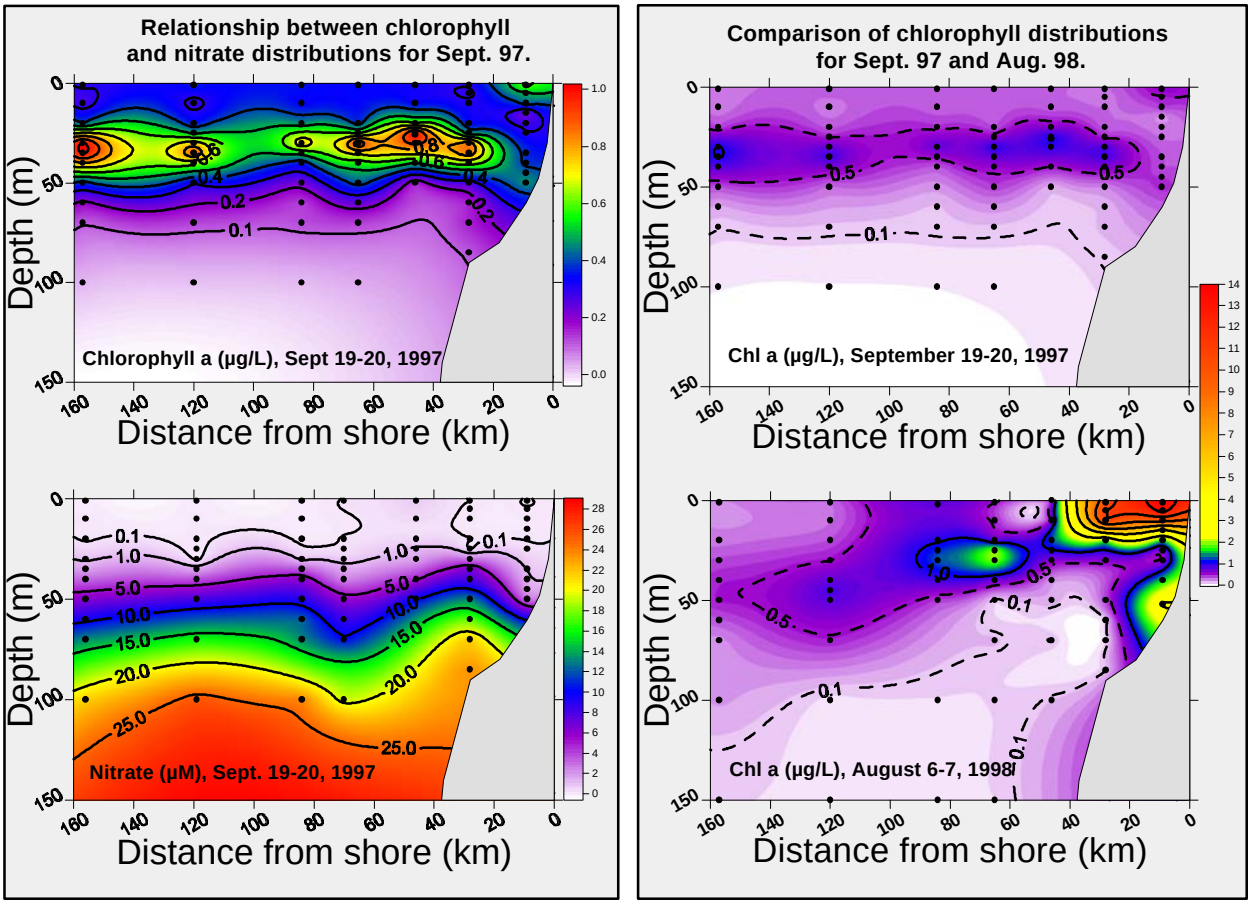

Figure 6. *NH-Line (off Newport, OR), chlorophyll and nitrate.*

Conclusions and Future Work

The 1997–1998 El Niño resulted in significantly warmer and nutrient depleted water off the coast of Oregon. The low levels of nutrients are probably the primary cause for the reduced levels of chlorophyll and primary production. By August 1998 conditions had returned to normal in terms of the total standing stock of chlorophyll and the patterns of distribution with depth.

During the next two years of sampling we hope to provide further analysis of the causes and consequences of variations in lower trophic level activity along the coast of Oregon and its influence on the characteristics of southward flowing water in the California Current.

References

Hill, J. and Wheeler, P.A. 1999. Variations in concentrations and C:N ratios of dissolved and particulate organic carbon and nitrogen in Oregon coastal and offshore waters. ASLO Ocean Science Meeting, Santa Fe, New Mexico, February 1–5.

Hill, J. Temporal and spatial distribution of DOC and DON in the surface waters off the Oregon coast. Master's Thesis, Oregon State University, in preparation (1998).

Corwith, H. Comparison of nutrient and chlorophyll levels off the coast of Oregon betweenEl Niño and non-El Niño years. Master's Thesis, Oregon State University, in preparation (1999).

Hydrography and Zooplankton off the Central Oregon Coast during the 1997–1998 El Niño Event

William T. Peterson
NOAA/NMFS/Northwest Fisheries Science Center (NWFSC)
Hatfield Marine Science Center
2030 S. Marine Science Drive
Newport, OR 97365 U.S.A.
e-mail: bpeterso@sable.nwfsc-hc.noaa.gov

I had the good fortune to initiate monitoring of hydrography and zooplankton offshore of Newport, Oregon prior to the 1997–98 El Niño event. Stations 1, 3, 5, 10 and 15 miles off Newport (44º 40'N) were sampled biweekly beginning in May 1996. The zooplankton at these same stations were sampled repeatedly from 1969–1973 and in 1978 thus providing a baseline to which modern measurements could be compared. In this brief note, I compare present observations to data from the 1970s.

In 1997, upwelling began as usual in late March indicating the onset of the spring transition. A boom in zooplankton production followed in April. In May, northerly winds weakened, upwelling relaxed, Columbia River Plume Water moved onto the shelf, and zooplankton numbers began to decline. The intrusion of warm Columbia River Plume Water was indicated by a salinity minimum in June (Figure 1). A minor upwelling event occurred in mid-June and a third (and final) upwelling event lasting

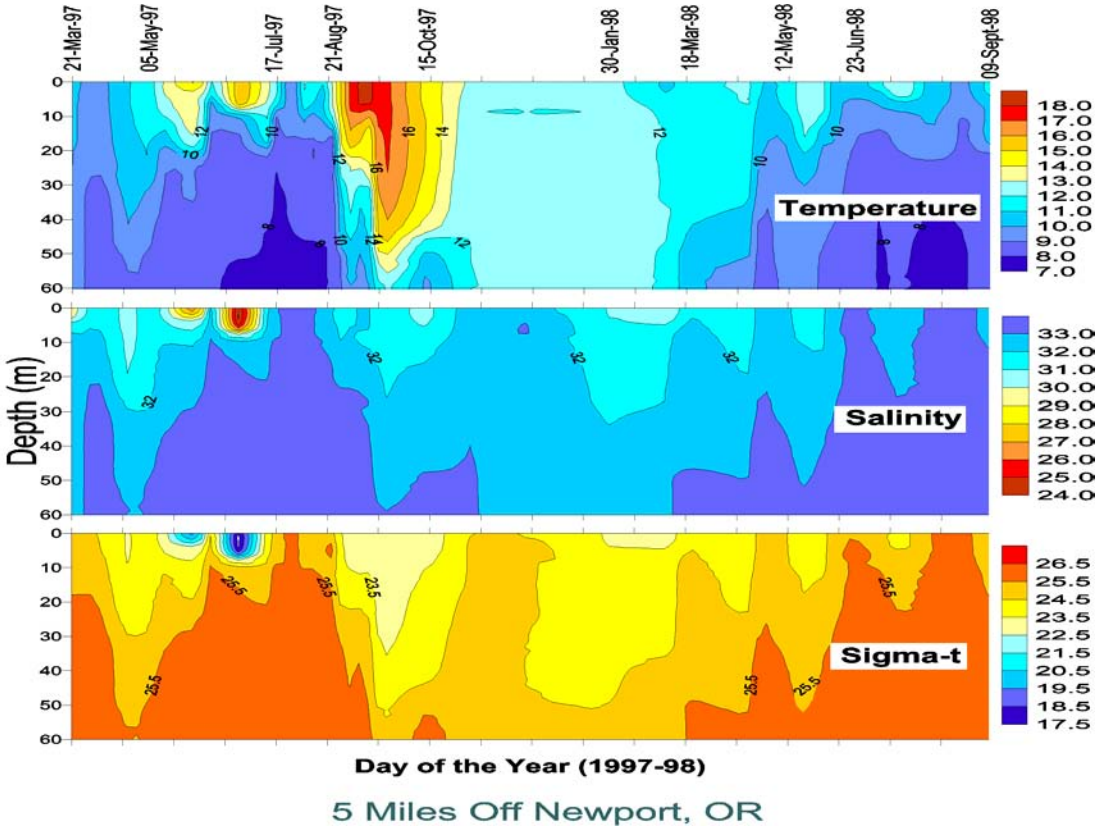

Figure 1. *Time series of temperature, salinity and sigma-t 5 miles off Newport, Oregon.*

five weeks occurred from 12 July through 19 August. The latter showed little biological response; subsequently, upwelling ceased altogether. Sea surface temperatures on the shelf warmed from 12º to 17ºC during the period of extended relaxation from May until mid-July. Surface waters cooled to 10ºC during the July/August upwelling event. From 20–26 August, a strong southwesterly storm moved north along the Oregon coast, resulting in a large downwelling event, with warm waters penetrating to near the sea floor at our baseline station at NH 5 (Figure 1). Surface waters warmed to a record temperature of 18.5ºC, warmer by 1 degree than any observation made during the 1983 El Niño event (Figure 2a, b, c), and warmer than 5ºC compared to climatological temperatures measured at this same station in the early 1970s. After the September peak, the sea surface cooled rapidly and wintertime temperatures were no warmer than 1–2ºC.

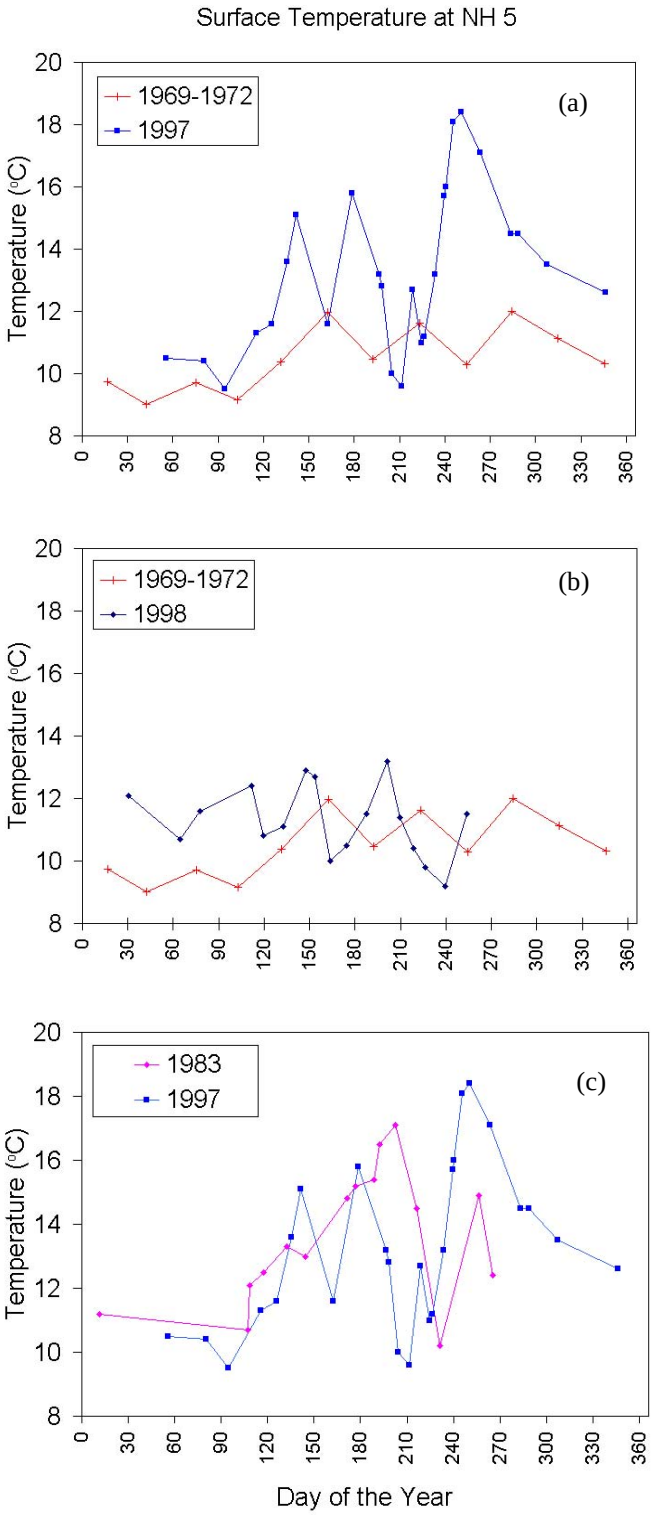

Figure 2. *Comparison of sea surface temperatures at station NH 5 for (a) 1969–1972 and 1997, (b) 1969–1972 and 1998, and (c) 1983 and 1997.*

Secchi depths were deep during both the early and late summer 1997 warm events, averaging 10 m during June/July and exceeding 15 m during the late-summer warming event. Usual secchi depths are on the order of 3–5 m during the summer upwelling season (Figure 3a, b). During the winter of 1997–98 secchi depths remained deep, then shoaled to 3–4 m in the summer of 1998.

The copepods captured in shelf waters during April/May and during the July/August upwelling events were boreal species. During relaxation of upwelling in May/June and August/September, species captured were those normally found in waters offshore of Oregon (Table 1). During the winter months of 1997/98, the zooplankton were typical of those expected with the Davidson Current — i.e., species with southern and offshore affinities. In spring 1998, these same southern and offshore species continued to dominant the zooplankton through at least mid-June, chiefly because southwesterly storms were frequent and upwelling had not become firmly established.

In contrast to the 1982–83 El Niño, very few unusual zooplankton, fish or bird species were seen in Oregon's coastal waters. Thus, the greatest effect of the 1997/98 El Niño on the zooplankton community was firstly, a reduction in biomass and production of local zooplankton species due to a shortened upwelling season in 1997, a delayed start of upwelling in 1998, and secondly, changes in community structure due to advection onshore of species which are normally found off Northern California and/or in waters well offshore of Oregon. The "usual" boreal coastal zooplankton species did not begin to increase in numbers until late July 1998; by September, the most common and abundant species, *Pseudocalanus mimus*, *Acartia clausii*, *A. longiremis*, and *Centropages abdominalis*, had population sizes only 10 to 20% of normal.

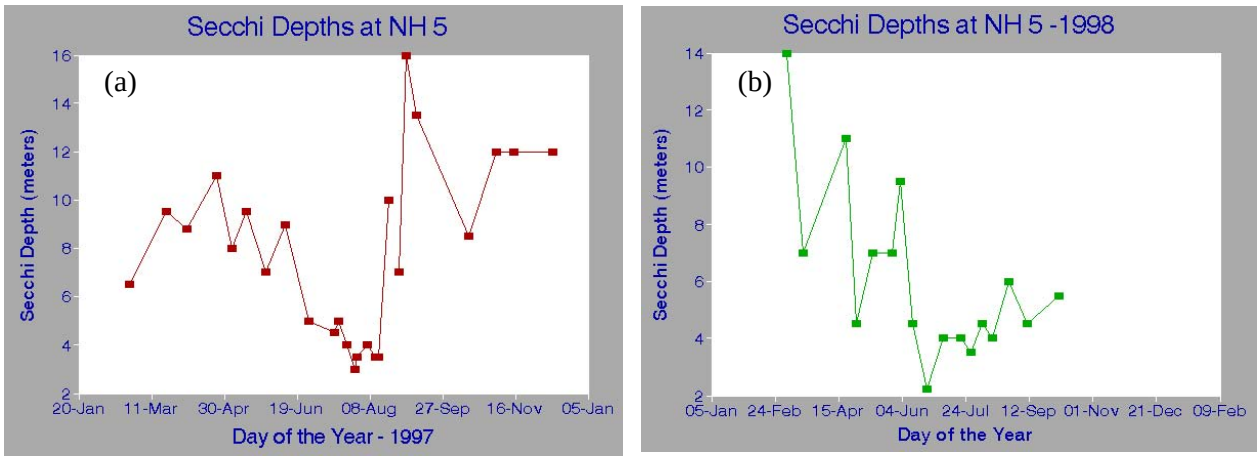

Figure 3. *Comparison of secchi depths at station NH 5 for (a) 1997 and (b) 1998.*

Table 1. *Density (number per cubic meter) of zooplankton species collected at a station five miles off Newport OR (water depth 60 m) during the summer of 1997 from June through September. The "warm event" began on 20 August and reached a maximum in mid-September, bringing with it warm water copepod species to the Oregon shelf.*

	Date (June through September)									
	6/27	7/15	7/23	7/30	8/6	8/14	8/21	8/28	9/2	9/9
Cool Water Species										
Calanus marshallae	17	49	125	31	46	553	559	61	5	0
Pseudocalanus mimus	461	1470	1719	678	207	796	987	173	184	22
Paracalanus parvus	159	219	1218	130	84	103	102	555	495	710
Centropages abdominalis	168	1138	72	157	103	73	17	17	0	0
Acartia longiremis	0	0	54	104	65	225	204	113	25	4
Oithona similis	537	601	1737	574	245	474	493	113	709	372
Warm Water Species										
Calanus pacificus	0	4	0	0	0	0	0	17	36	32
Calanus tenuicornis	0	0	0	10	4	0	0	9	5	2
Eucalanus californicus	0	0	0	0	4	0	0	52	15	0
Ctenocalanus vanus	0	0	0	0	0	0	17	9	15	10
Acartia danae	0	0	0	0	0	0	0	0	15	6
Corycaeus anglicus	0	0	0	0	0	0	0	26	76	64
Dolioletta gegenbaurii	0	0	0	0	0	0	0	130	71	22

A possible long-term trend may be evident: as compared to the summers of the 1970s when sampling was carried out at the same stations as those which I am currently sampling (Peterson and Miller, 1975), during the summers of 1996–1998, numbers of the copepod *Paracalanus parvus* are at least 100-fold higher; numbers of *Calanus marshallae* are lower by a factor of 2–3 (Figures 4 and 5). A similar result has been found for the two *Acartia* species listed above as well as for *Centropages* (not shown). *Pseudocalanus mimus* numbers (Figure 6) showed little change when 1996 and 1997 were compared to the early 1970s; however, as noted above, the population off Oregon collapsed in August 1997 and has not yet become re-established.

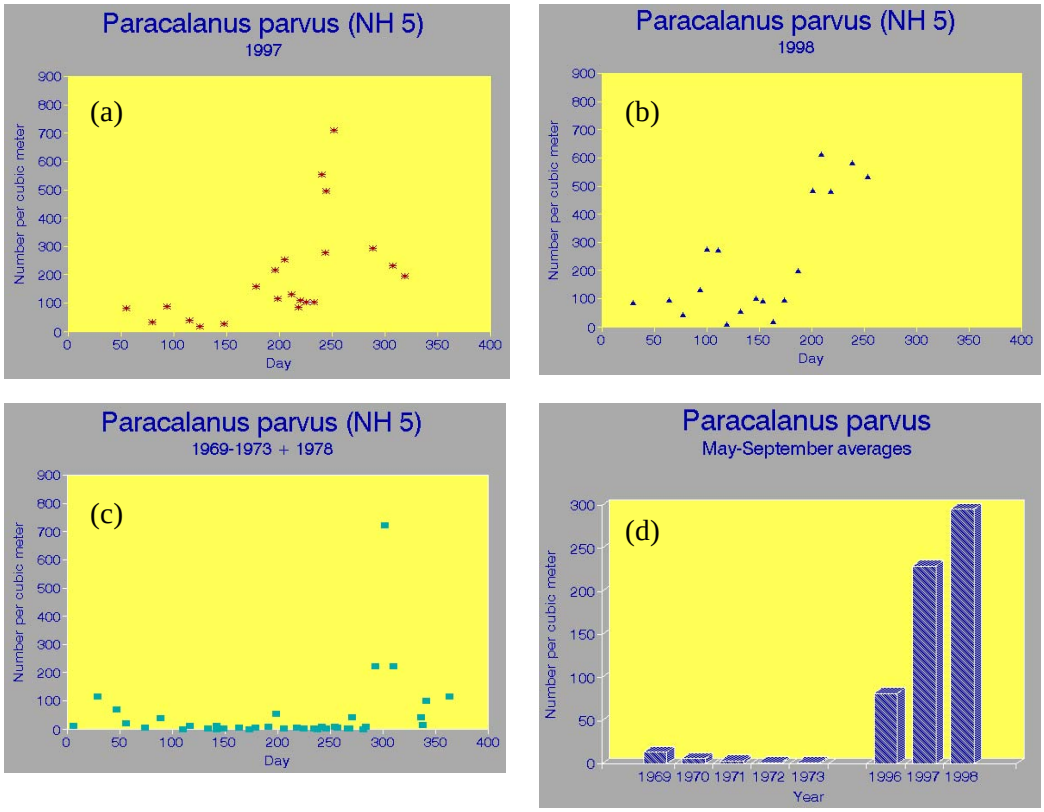

Figure 4. *Comparison of <u>Parcalanus parvus</u> populations for (a) 1997, (b) 1998, (c) 1969–1973 and 1978, and (d) histogram comparing data from 1969–1973 with 1996, 1997, and 1998.*

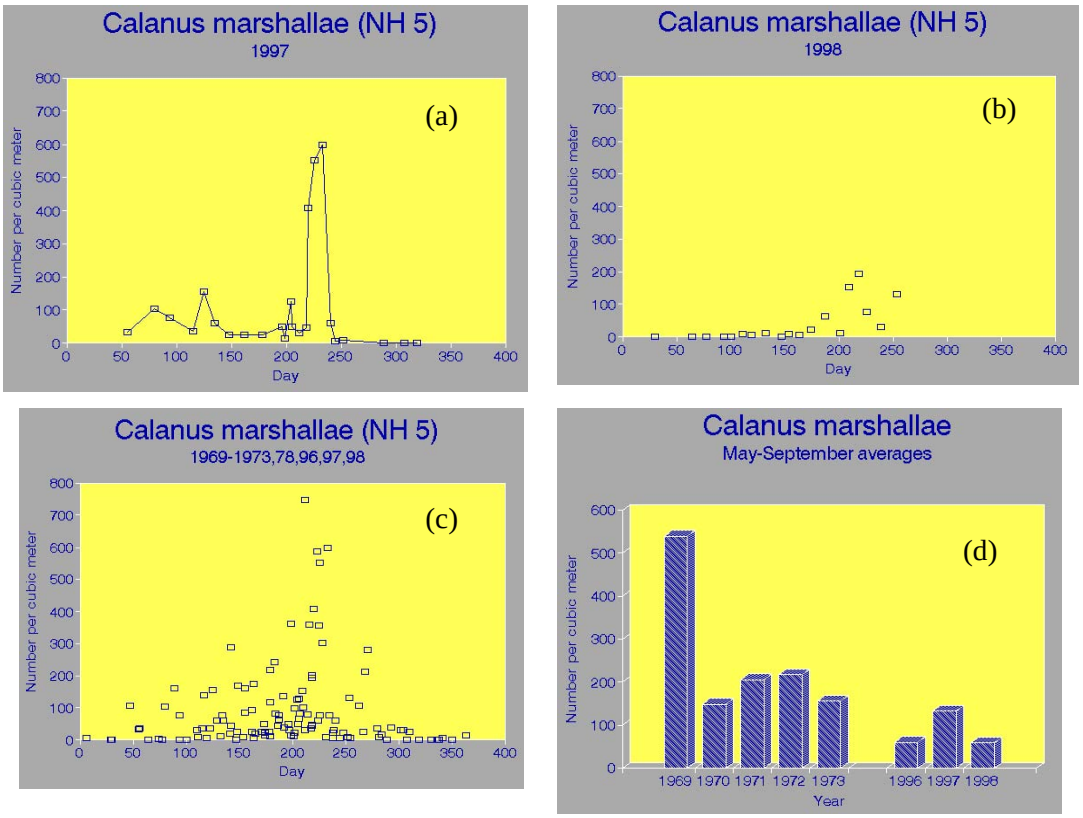

Figure 5. *Comparison of <u>Calanus marshallae</u> populations for (a) 1997, (b) 1998, (c) 1969–1973, 1978, and 1996–1973, and (d) histogram comparing data from 1969–1973 with 1996, 1997, and 1998.*

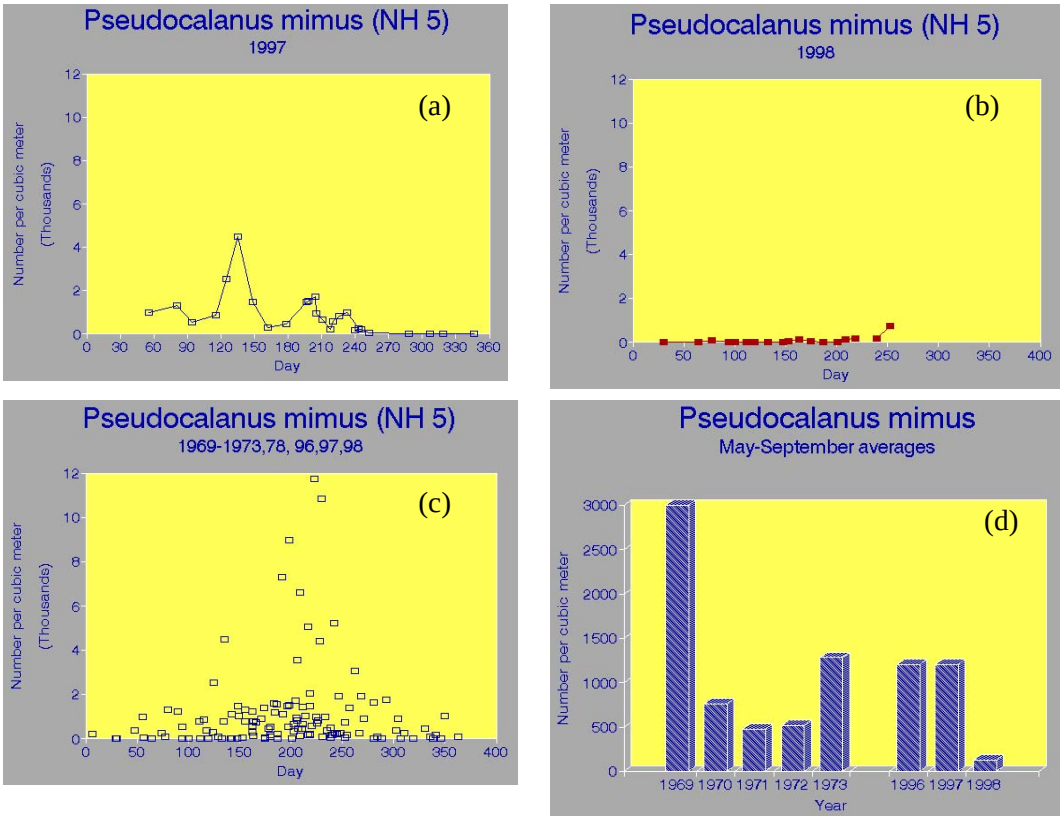

Figure 6. *Comparison of Pseudocalanus mimus populations for (a) 1997, (b) 1998, (c) 1969–1973, 1978, and 1996–1998, and (d) histogram comparing data from 1969–1973 with 1996, 1997, and 1998.*

The degree to which the warm water event of late-summer 1997 is linked to the equatorial El Niño event remains an open question — there is evidence, presented in the PICES/El Niño session by Jim Overland, that the warming was due to anomalous atmospheric patterns off the west coast of the U.S. that may have been teleconnected to the equatorial weather patterns associated with the movement of the "warm pool" from the western Pacific to near the dateline.

The effects of the "warm event" of the summer of 1997 on chlorophyll and copepod egg production rates are discussed in Gomez-Gutiérrez and W. T. Peterson (in press).

A listing of the key events observed during the "warm event" is shown below:

Key Events observed during the 1997–1998 "warm event"

1997	
Last week of March	Spring transition initiated
April	El Niño begins at equator
15 May	Warming trend begins in N. Pacific
early June	Brief upwelling event off Oregon (ca. 5 days duration)
mid-June	Warming trend resumes
14 July	Upwelling begins off Oregon
19 August	Upwelling ends off Oregon
21 August	Offshore and southern copepod species appear on shelf; remain dominant through winter and spring/summer 1998
18 September	Maximum temperature observed, 18.4ºC
22 September	Autumn cooling begins
October–March	Winter cooling to 12ºC (approx. 1–2ºC warmer than normal)

1998	
mid-March	Spring transition begins
late April	End of el Niño; first big coastal upwelling event
12 May	Some boreal coastal copepod species begin to re-appear on shelf
12 June	First large phytoplankton bloom
28 July	Boreal coastal copepod species first begin to increase in numbers
16 September	First southwesterly storm

References

Gomez-Gutiérrez, J. and Peterson, W. 1999. Egg production rates of eight copepod species during the summer of 1997 off Newport, Oregon, USA. *J. Plankton Res.* In press

Peterson, W.T. and Miller, C.B. 1975. Year-to-year variations in the planktology of the Oregon upwelling zone. *Fish. Bull. U.S. 73*, 642–653.

El Niño Sea Level Signal along the West Coast of Canada

William Crawford,[1] Josef Cherniawsky,[1] Michael Foreman[1] and Peter Chandler[2]

[1] *Fisheries and Oceans Canada*
Institute of Ocean Sciences
Sidney, BC, Canada
e-mail: crawfordb@dfo-mpo.gc.ca

[2] *Madeira Research*
North Saanich, BC, Canada

During strong El Niño winters, sea levels along the West Coast of Canada typically rise about 10 to 20 cm above seasonal heights and remain above normal for several months. During the 1997/98 El Niño, sea levels rose 10 cm in May 1997, 20 cm in the autumn, and 30 cm in January and February 1998, all along the Pacific Coast of Canada. Monthly average sea levels at Tofino, British Columbia (49° 09′N, 125° 55′W), during the 1997/98 El Niño (Figure 1) were as high as observed during the 1982/83 El Niño, and were far above seasonal values. Only the January 1914 monthly mean reached a height along Canadian shores comparable to the four months of January and February 1983 and 1998. Pressure-adjusted sea levels are not shown here, but were about 10 to 20 cm or so above seasonal values in winter.

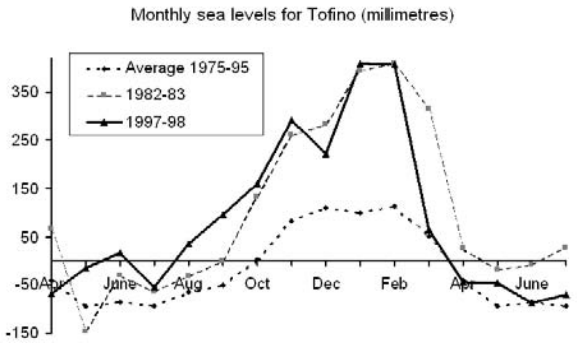

Figure 1. *Monthly average sea level at Tofino, British Columbia (49° 09'N, 125° 55'W) for sixteen-month periods in 1982–83, 1997–98, and for the average seasonal cycle between 1975 and 1995.*

The offshore extent of the rise in adjusted sea level is evident in TOPEX/Poseidon satellite altimetry data. This satellite measures sea surface elevation relative to the ellipsoid, and adjusted (atmospheric pressure compensated) sea levels are computed using air pressure data from global weather analysis models. We obtained 2-day delay data (TOPEX only) from the National Oceanographic Data Center for Satellite Altimetry. After applying our own tidal corrections, we found that adjusted sea levels on the continental shelf were about 10 cm above normal at mid-continental shelf during January and February 1998, and maintained high levels well beyond the outer edge of the continental shelf. The rise was especially high off the west coast of the Queen Charlotte Islands.

Off the west coast of North America, an upward slope of the sea surface toward shore implies northward transport, and usually northward transport of heat. TOPEX/Poseidon (T/P) measurements provide anomalies in sea surface elevations due to barotropic and baroclinic currents in the water column. Water property measurements along Line-P (Figure 2) provide measurements of dynamic heights due to baroclinic currents. Comparisons of these two types of measurement provide insight into the relative contributions of baroclinic and barotropic motion. The Line-P stations 3, 9 and 13 are 45, 22 and 11 km respectively from T/P crossover points (Figure 2). A crossover point denotes the geographical spot where the northwestward track of the T/P satellite crosses the southeastward track of this satellite. At these locations we have twice as many data points. In addition, the sampling time interval allows more accurate computation of tidal

heights, which must be removed from the record prior to their use in non-tidal current studies.

Figure 3 presents T/P sea levels at three cross-over points compared to dynamic heights at the nearest Line-P station. The T/P data were provided to us by NASA Ocean Altimeter Pathfinder Project. Between September 1992 and the end of this record in 1997 there were 194 cycles of T/P data, each providing 2 observations at each of these three cross-over points. We removed the tidal signals using our own tidal analysis on these data, and also removed a local 5.3-year mean at each crossover point. Finally, we adjusted each of the three lines along the vertical axis to remove a difference in the means in these three comparisons with dynamic heights. Therefore it is the variability about these means that provides useful information.

The large triangles in this figure denote the individual dynamic heights of the sea surface relative to 1000-m depth as measured during vessel transects along Line-P at stations 3, 9 and 13. Water properties at station 4 below 730 m were transferred to station 3 where the bottom depth is only 730 m. The other two stations are in water deeper than 1000 m.

Line-P station 3 lies on the near-shore side of the continental shelf. It is 45 km away from the nearest satellite crossover point station, which is beyond the outer edge of the continental shelf. We believe this separation accounts for the generally higher winter sea levels observed in T/P data compared to the dynamic heights, since winter sea level elevations are typically higher near shore than along the outer shelf. Although T/P data extend only to the last few days of 1997, they clearly show the sea level rise during the 1997/98 El Niño, in autumn and early winter.

The line-P stations plotted in the bottom two graphs in Figure 3 lie closer to cross-over points and therefore the dynamic height variability follows the T/P sea levels more closely. At station 13 where the separation is only 11 km, the rms difference between T/P sea levels and dynamic heights is only 3.0 cm.

Of interest here is the phase reversal in seasonal cycles between stations 3 and 9 in Figure 3. Ekman divergence associated with the build-up of the Aleutian low pressure system in winter generally lowers sea levels in mid Gulf of Alaska, as observed at T/P crossover points at 49.014°N, 128.978°W, and 49.014°N, 131.811°W. However, the near-shore winds in this low pressure system blow in a direction that pushes currents to the north and raises sea level on the continental shelf in winter, as observed at the T/P crossover point at 49.014°N, 126.142°W.

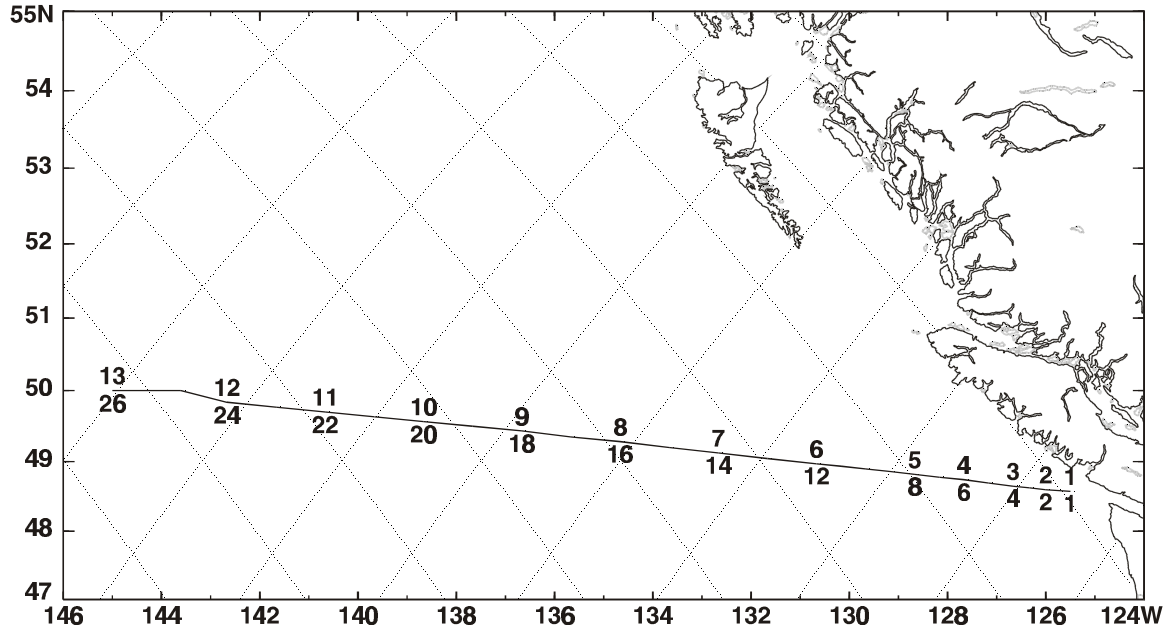

Figure 2. *Tracks of TOPEX/Poseidon satellite (dotted lines) and Line-P water sampling stations. Both old and new Line-P station numbers are presented. The new station numbers (1 to 26) are used in this paper.*

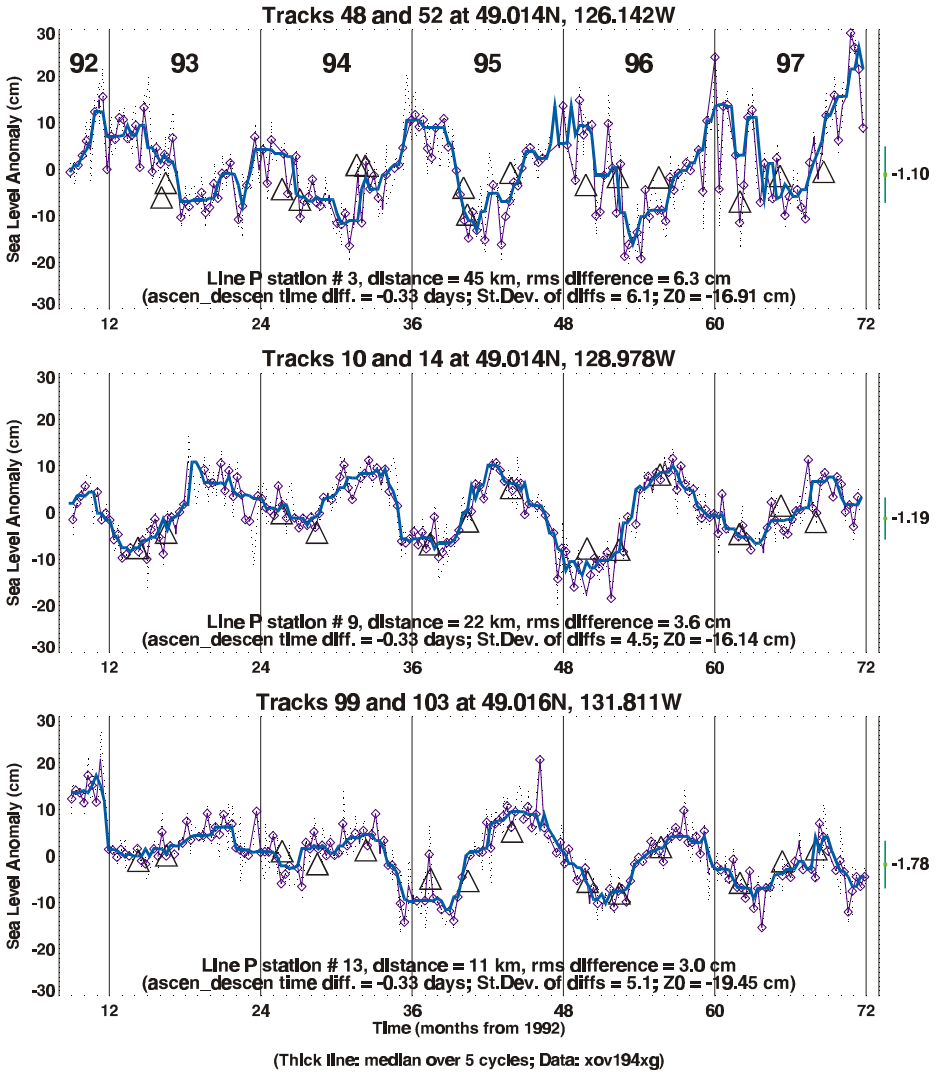

Figure 3. *Time series of T/P sea level (dotted line) at track crossovers near Line P stations 3, 9, and 13 (see Figure 1) during September 1992–December 1997. Dotted lines joint every available point; small triangles are averages over ascending-descending pairs; thick solid lines are 5-point running medians. Triangles show Line-P dynamic topography (steric height) values relative to 1000 m.*

We have examined records of dynamic topography from 35 winter cruises along Line-P between 1969 and 1998. In February 1998, at Line-P station 4 in 1300 m of water, the surface dynamic height relative to 1000 m was 10 cm higher than observed during any of the other 34 cruises. Second and third highest levels were found in the winters of 1992 and 1987 respectively. These three highest values were observed during recent El Niño winters, and we expect that northward transport of heat during the past decade may have been significantly above normal due to these El Niño-related events.

We have applied our own tidal corrections to T/P data because the normal T/P data products use tidal constituents provided by global tidal models. Typically, these models are inaccurate over continental shelves. In deeper waters the global tidal models provide reasonable de-tiding of records for examination of large-amplitude features. One such feature observed is an eddy that began off the west coast of the Queen Charlotte Islands in February 1998. An image of this eddy, as observed by TOPEX and ERS-2 imagery, is provided in Figure 4.

This eddy is the largest of several that began in the past El Niño winter. A recent modelling study suggests these eddies are more frequent during El Niño winters when northward transport along the Canadian and Alaskan coast is stronger (Melsom, Meyers, Hurlburt, Metzger and O'Brien personal communication, 1998). An Electronic version of

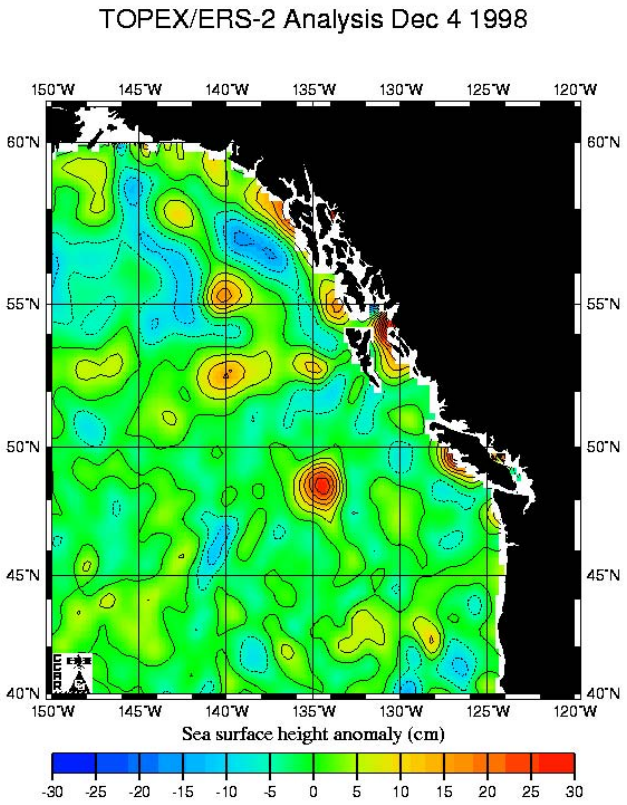

Figure 4. *Spatial variability of sea levels as measured by TOPEX and ERS-2 satellites for the time period near December 4, 1998. Processing has enhanced the mesoscale variability. This image is available at the web site* http://www-ccar.colorado.edu/~realtime/global-real-time_ssh/ *provided by the Colorado Center for Astrodynamics Research at the University of Colorado, Boulder.*

this manuscript can be found at web site http://www.coaps.fsu.edu/~stricher/EI_revision/.) The T/P and ERS-2 record shows such eddies to be spawned off this coast almost every winter.

After generation in February 1998 off the Queen Charlotte Islands, the eddy moved westward until mid April. Whereas most such eddies in other years track westward, this one moved southward between April 1998 and press time in December 1998. Based on studies of other eddies, it is expected to survive for at least a year and possibly as long as three years.

A Line-P cruise through this eddy in September 1998 showed it to be more than 1000 m deep, with water characteristics typical of the West Coast of the Queen Charlotte Islands in winter. It might be a major source of nutrients for waters above and in the upper thermocline.

Acknowledgments Two-day delay TOPEX data provided by NODC Laboratory for Satellite Altimetry at Silver Spring, Maryland, with special assistance from Bob Cheney and John Kuhn. TOPEX/Poseidon data 1992–97 provided by NASA Ocean Altimeter Pathfinder Project, with special assistance from Richard Ray and Brian Beckley.

The El Niño Signal along the West Coast of Canada – Temperature, Salinity and Velocity

Howard Freeland and Rick Thomson
Institute of Ocean Sciences
Sidney,B.C. V8L 4B2, Canada
e-mail: freelandhj@dfo-mpo.gc.ca

The Institute of Ocean Sciences, or its predecessors, have occupied a series of 26 stations extending from the mouth of the Juan de Fuca Strait to Ocean Station Papa, at 50°N and 145°W, since 1956. This line of stations is commonly called Line-P (see Figure 1). In the early years the line was occupied many times per year, but in recent years the line is routinely occupied in February, May and August of each year. The value of this long time series became particularly evident during the El Niño event of 1997/98 as we had good control over the definition of "normal" conditions along Line-P.

Having a definition of "normal" evidently allows the definition of a mean field and thence, an anomaly. In Figure 2 we show a plot of the temperature anomaly field associated with the 1982/83 El Niño event. It was astonishing that the temperature anomalies penetrated so deep. Ideally one would like to have computed the velocity anomalies associated with this event. We can compute velocity fields for both the mean state and for the observed conditions in March 1983, and subtract one from the other. The result makes no sense and is not shown here. The obvious conclusion from this exercise is that in that calculation we are missing a large barotropic signal associated with the 1982/83 event.

In the remainder of this note we will attempt to outline the evolution of the scalar fields through the 1997/98 El Niño event. We will then use TOPEX/Poseidon data to allow a more realistic estimate of the velocity anomaly field, and from that an estimate will be made of the anomalous heat flux associated with this El Niño event. In describing the evolution of the scalar fields we were greatly assisted by the existence of the Department of Fisheries and Oceans (DFO) El Niño Watch Program. This allowed us to use new resources to increase the sampling along Line-P. Thus, we have 10 anomaly sections between August 1997 and July 1998, inclusive. Some of these were obtained as part of the routine scientific surveys along Line-P. Some were

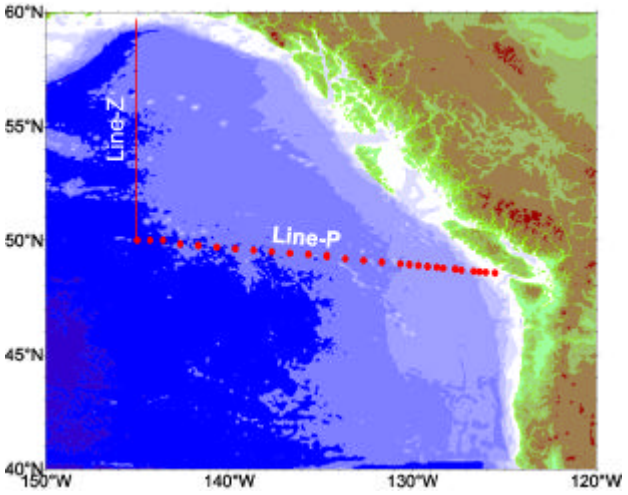

Figure 1. *Location of the stations comprising Line-P off the west coast of Canada.*

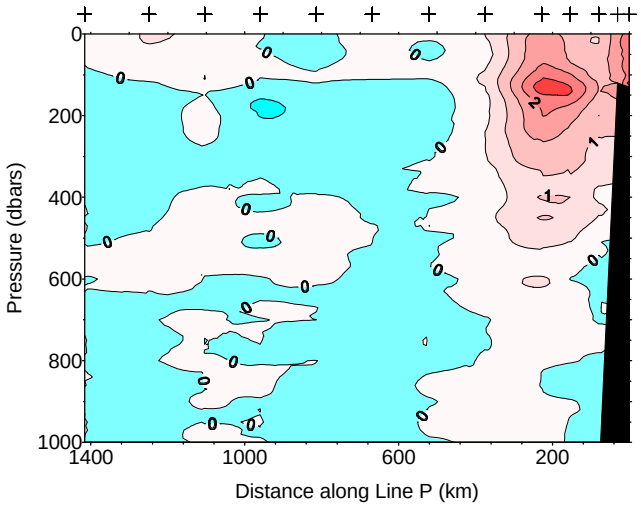

Figure 2. *Temperature anomalies versus depth and distance offshore along Line-P in March 1983.*

partial surveys, courtesy of the Canadian Coast Guard, and some were shallow surveys along the entire length of Line-P, courtesy of Department of National Defence AXBT surveys. By this means, the 1997/98 El Niño was observed more thoroughly than any previous climate event.

Figure 3 shows a selection of images illustrating the development of the 1997/98 El Niño of British Columbia. The first period, February 1997, shows conditions in the N.E. Pacific Ocean before the El Niño began. As expected, sea surface temperature anomalies are weak throughout the area of concern, and temperature anomalies are small along Line-P, at all depths. A significant salinity anomaly is visible as a longitudinal feature near a pressure of 120 dbar. This is reflected by the general shallowing of the mixed layer in the N.E. Pacific that has been reported elsewhere. By the autumn of 1997 a major warming event has occurred throughout the Pacific and we see extensive coastal warming throughout the N.E. Pacific The warming is visible at the surface but shows no penetration below the top few tens of metres. Again, as in February 1997, the only significant salinity anomaly is due to the shallow mixed layer, compared with the 1956 to present climatology. By the fall of 1997 the sea surface height was a little above normal, but shortly afterwards sea surface height anomalies began to grow rapidly (see paper by Crawford in this report). Coincident with this large change in sea level we began to see temperature anomalies at depth through the winter of 1997/98. This is illustrated in Figure 3 with the sections for February 1998, which is chosen to be the time when sea level reached its greatest height above normal. At this period, sea surface temperature anomalies remain large throughout the coastal regions of North America, but now the largest subsurface temperature anomalies appear, both suggestive of northward advection along the coast.

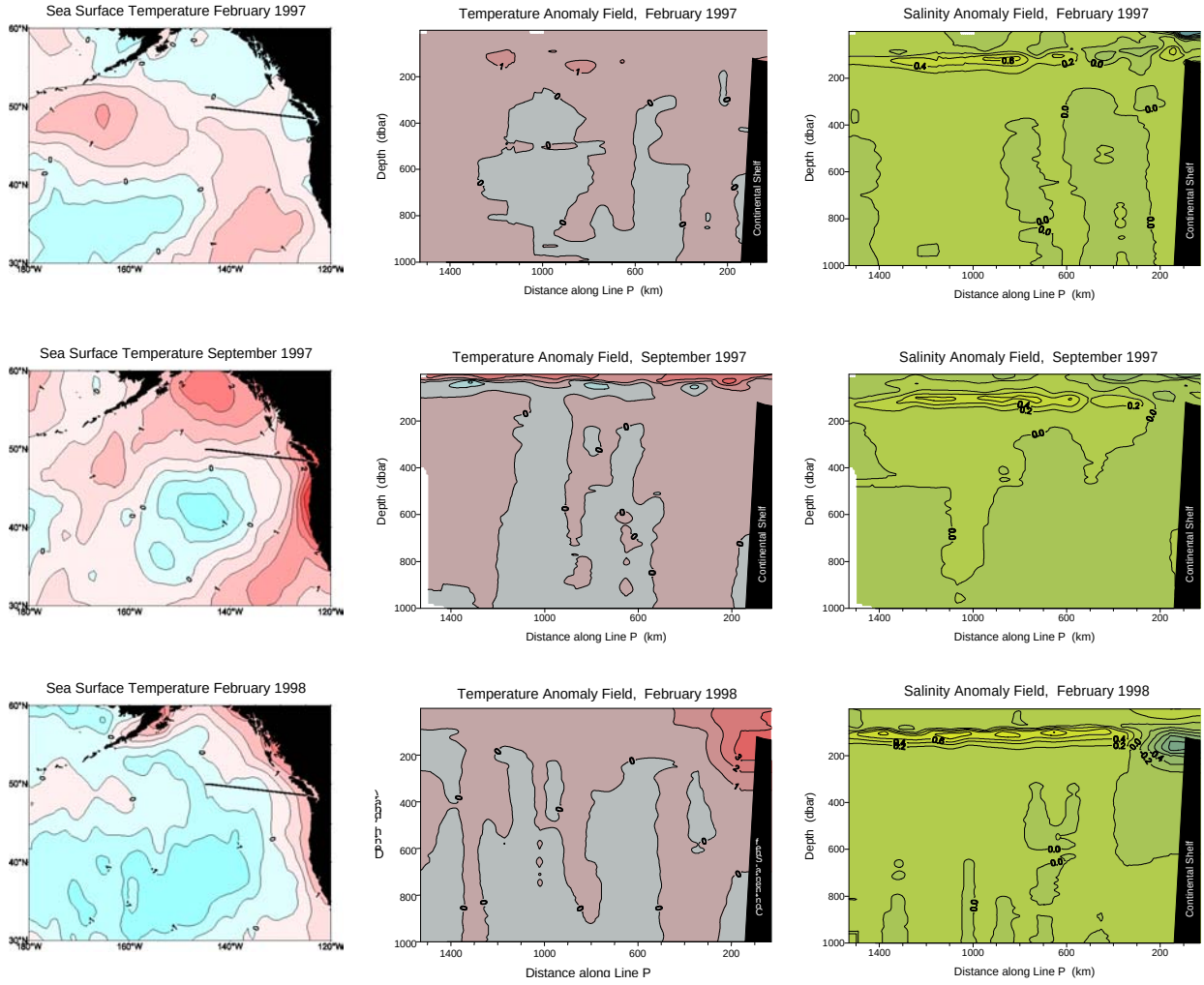

Figure 3. *Sea surface temperature (SST), and cross-sections of temperature and salinity anomaly for February 1997, September 1997 and February 1998. The solid line on the SST maps shows the position of Line-P.*

We suggest that the early, superficial warming in the N.E. Pacific is due to an atmospheric teleconnection and that this superficial warming induced a small sea level change owing to thermal expansion. The sea level change seen after November 1997 is far larger than could be explained by thermal expansion, and we propose that this event is due to the arrival of a Kelvin wave from the south. This fits with the observations of a deep anomaly appearing during the winter of 1997/98.

We can estimate the velocity anomaly field in the following way:

Absolute velocity = (g/f) × (surface pressure gradient) + (geostrophic velocity computed relative to the surface).

We can calculate the geostrophic velocity field (relative to the surface) both from the February 1998 observations, and the long-term mean fields for February, set up the above equation for both February 1998 and the long-term mean and look at the difference, thus:

Velocity anomaly = (g/f) × (surface pressure gradient anomaly) + (geostrophic velocity anomaly relative to the surface).

The surface pressure anomaly is strictly not known, but here we choose to represent that by the difference in sea level as seen by TOPEX/Poseidon, between February 1998 and February 1997, i.e. El Niño sea level minus pre-El Niño sea level. Then, having computed the velocity anomaly (v'), we can multiply by the temperature anomaly field (T') to estimate the heat flux anomaly, $T'v'$.

The velocity anomaly field illustrated above is supported by various ancillary observations. Current meters on the continental slope installed in support of the DFO El Niño Watch Program suggest very clearly that flows at the shelf edge were anomalous and that the typical northward flow in February 1998 was about 10 cm/s above normal. Profiling Alace floats deployed near Station Papa suggest that any velocity anomaly is in the direction along Line-P, with near zero anomaly perpendicular to Line-P.

The heat flux in Figure 4 are in cgs units. Integrating under the contour of $T'v' = 1.0$ cal s^{-1} cm^{-2} we estimate the total heat flux transported by the El Niño ocean signal in February 1998 as 6.8×10^{12} cal s^{-1}. To give some idea of the magnitude of this flux, it would be sufficient to warm the coastal area north of Line-P 200 km from the coast and to a depth of 200 metres by 1°C in 70 days. It would be interesting to run a model analysis of the ocean response in 1997/98 and estimate the total heat required in the ocean, north of Line-P. By this means we should be able to estimate the importance of the oceanic teleconnection in the high latitude ocean response.

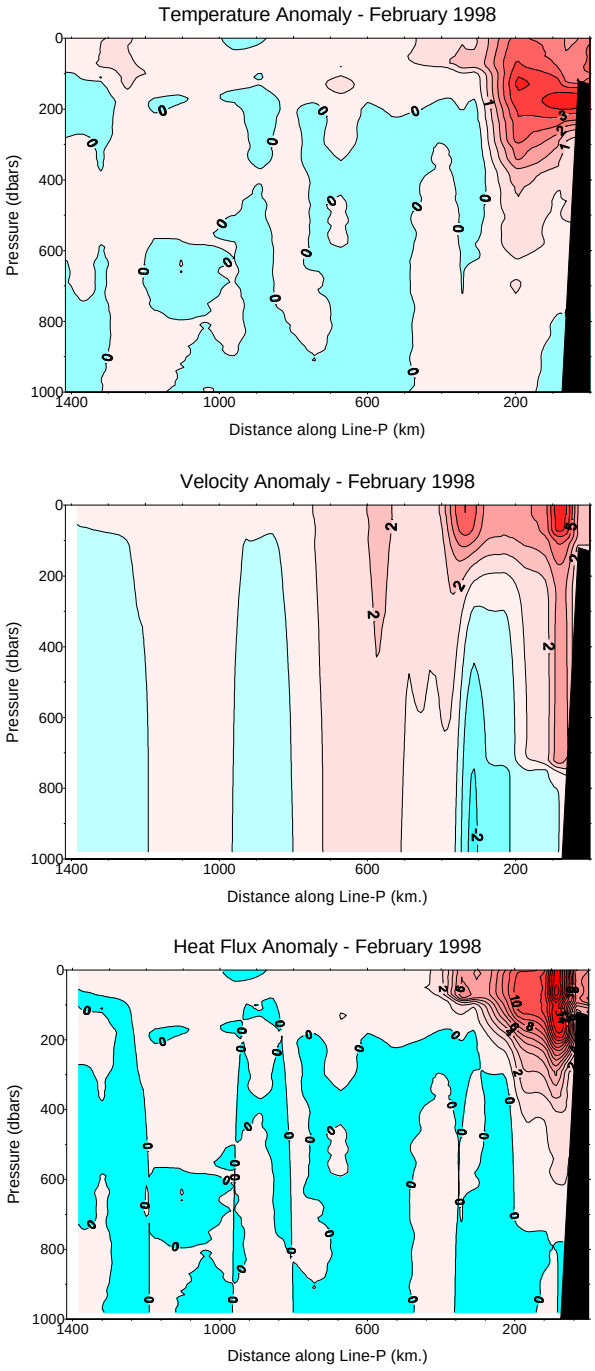

Figure 4. *Anomalies of temperature, velocity and heat flux in February 1998.*

In summary, we successfully observed the evolution of the temperature and salinity anomalies off the coast of British Columbia as various phases of the El Niño affected the coastal regions. The late response may be an oceanic Kelvin wave that transports heat to the north. We have estimated the heat flux associated with this event and would like to make a comparison with model analyses.

Impact of the 1990s El Niños on Nutrient Supply and Productivity of Gulf of Alaska Waters

Frank Whitney,[1] David Mackas,[1] David Welch[2] and Marie Robert[3]

[1] *Fisheries and Oceans Canada, Pacific Region*
Institute of Ocean Sciences
Box 6000, Sidney, B.C. V8L 4B2, Canada
e-mail: whitneyf@dfo-mpo.gc.ca

[2] *Pacific Biological Station*
Hammond Bay Rd.
Nanaimo, B.C. V9 R 5K6, Canada

Institute of Ocean Sciences
[3] *Box 6000, Sidney, B.C. V8L 4B2, Canada*

Over the past few decades, surface waters of the Gulf of Alaska have been gently warming. In the 1990s, we are also setting records for warmest waters since observations began in the 1930s. Coastal temperatures at British Columbia lighthouses (e.g. Amphitrite Point and Kains Island, Figure 1) were very warm during the summer of 1997 (Figure 2), besting previous temperature maxima by more than 1°C. The monthly averaged T at Amphitrite Point, for example, was 16.0°C in September 1997, topping the 1979 record of 14.9°C. Coastal trends generally mimic that seen in equatorial waters. In both regions, warming is measured over time, and periodic El Niños produce major warm anomalies. A notable exception is that the 1972 El Niño does not appear in Lighthouse temperature records.

In open ocean, the highest measured winter temperatures were observed in 1994. Coincident with this was a thinning of the mixed layer (a trend Freeland et al. (1997) have observed over the past 40 years at Ocean Station Papa (OSP)) and a reduction in the nutrient supply to the mixed layer (Whitney et al., 1998). As a result of reduced winter nutrient supply, nitrate depletion has become more widespread in the 1990s. Between 1989 and 1994, nitrate depletion spread from 250 km to almost 600 km offshore along Line P. This loss of nutrient has resulted in abnormally low chlorophyll levels in recent summers (Figure 3) compared with the recent average, and a substantial reduction in primary productivity in late summer (Whitney et al., 1998).

This work allowed estimates of loss of new production in an area covering 290,000 km^2 off the coast of Vancouver Island. Between 1989 and 1994, a decline of about 2 million tonnes of phytoplankton carbon was calculated. However, surveys had not been made along the coast of Alaska during this period. When it was evident that a major El Niño was building in 1997, more detailed sampling was begun both along Line P and to the north coasts of B.C. and Alaska. Over the past couple of years, we have been able to chart the area that experiences nitrate depletion in summer (Figure 1), and now see that virtually all the shelf waters in the Gulf are affected.

More frequent surveys along Line P provided much better seasonality to nutrient supply and utilization. On the shelf, 1997–98 winter nutrient levels were less than half those of an average year in the 1970s, and nitrate depletion occurred in April rather than May (Figure 4). It also appears that coastal upwelling has been much weaker through the summer of 1998, since nutrient levels remained low. This trend was also seen in open ocean stations, to at least 225 km offshore.

Assuming that nutrient deficiency is spreading in the Gulf of Alaska, much the same way it has been along Line P, then shelf productivity has been substantially impacted. B.C. juvenile salmon are known to spend several months in coastal waters as they migrate northward through spring and summer (D. Welch, unpublished data). The weakened nutrient supply suggests that they are migrating through water that may have only 50 to 60% of the primary production that was seen in the 1970s. The decline in open ocean survival (Welch et al., submitted) of some of these stocks in the 1990s may be linked to changes in coastal nutrition.

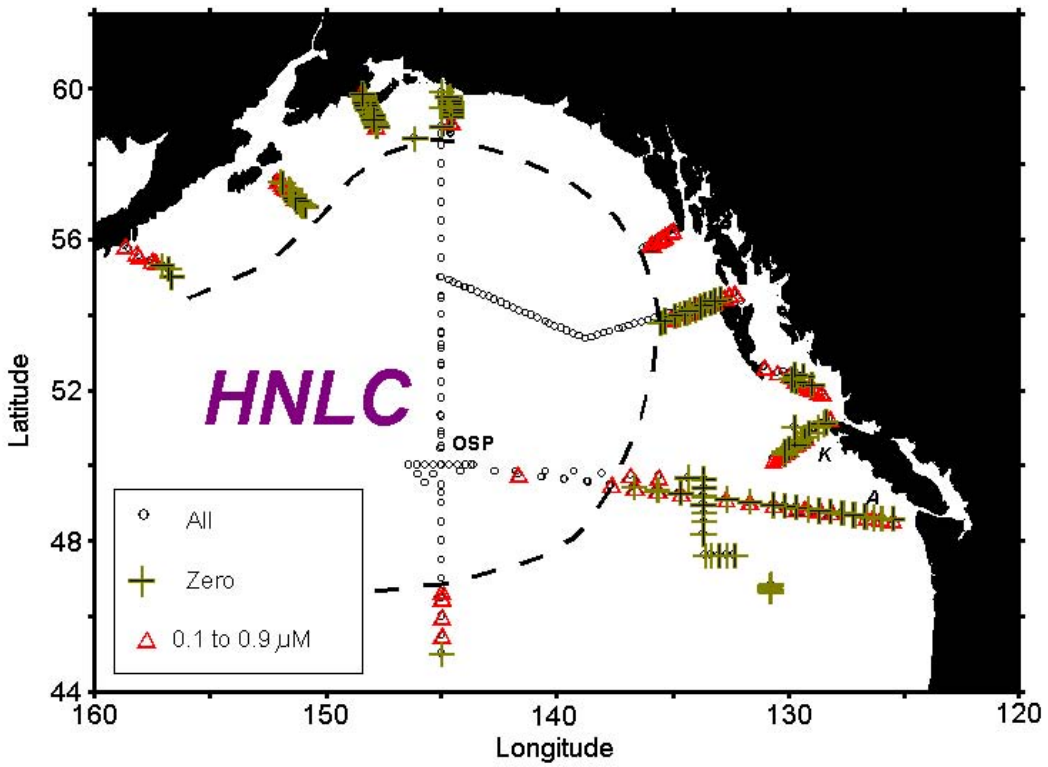

Figure 1. *Gulf of Alaska, showing surface sampling locations for summers of 1997 and 1998. The dashed line shows the approximate bounds of high nutrient–low chlorophyll (HNLC) water. Ocean Station Papa (OSP), Amphitrite Point (A) and Kains Island (K) sampling locations are marked.*

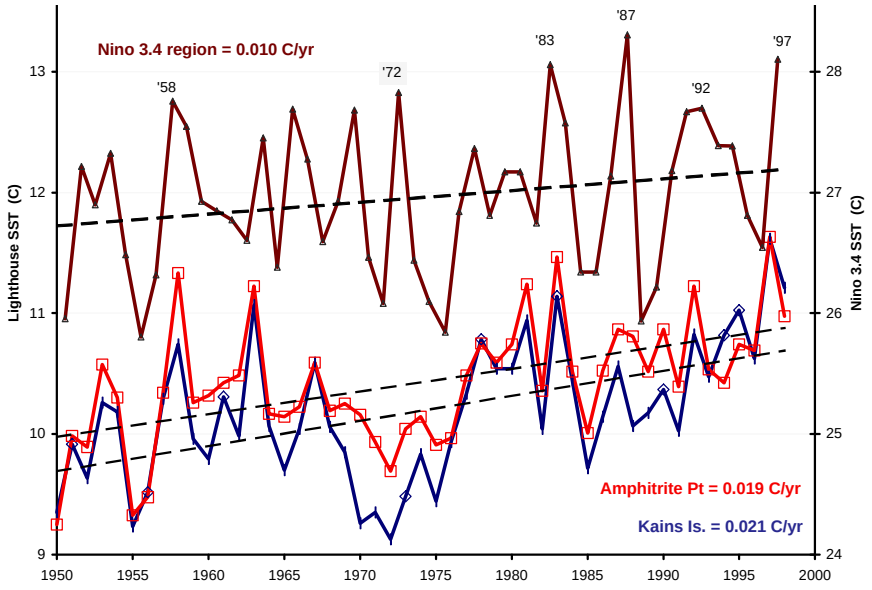

Figure 2. *SST averaged yearly for the equatorial Niño 3.4 region and two lighthouse stations. Linear regressions show a warming trend in each area.*

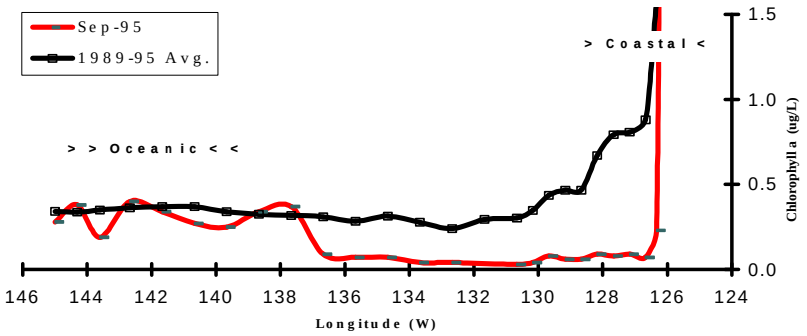

Figure 3. *Chlorophyll a levels in surface waters along Line P. Low concentrations in September 1995 correspond to nitrate-depleted waters; high coastal values to upwelling.*

A result of mixed layer thinning is the increase in average light levels that phytoplankton receive, which would advance the onset of spring growth (as suggested in Freeland et al. (1997)) and should stimulate earlier development of grazers. Mackas et al. (1998) have observed a 2 month earlier development of one of the major subarctic Pacific copepods, *Neocalanus plumchrus*, at OSP. Such shifts in communities must create mismatches in timing of predator and prey interactions.

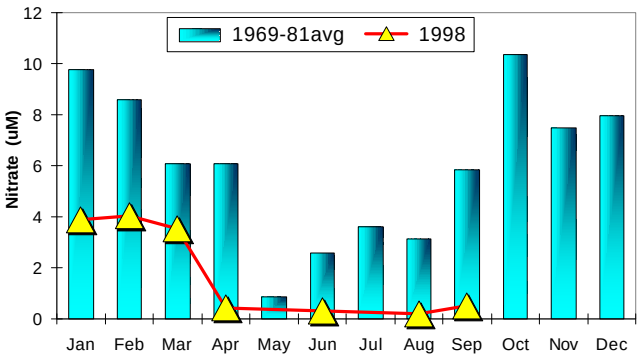

Figure 4. *Average nitrate concentration in the coastal 75 km of Line P during the 1970s and 1998.*

Thus the changes we have been observing in coastal and open ocean in the Gulf of Alaska are consistent with a warming of surface waters. The increased buoyancy of the mixed layer results in less winter supply of nutrient, which decreases the amount of phytoplankton biomass that is produced, which in turn impacts the productivity of the entire region.

References

Freeland, H.J., Denman, K.L., Wong, C.S., Whitney, F. and Jacques, R. 1997. Evidence of change in the winter mixed layer in the northeast Pacific Ocean. *Deep-Sea Res., 44*, 2117–2129.

Mackas, D.L., Goldblatt, R. and Lewis, A.G. 1998. Interdecadal variation in developmental timing of *Neocalanus plumchrus* populations at Ocean Station P in the subarctic North Pacific. *Can. J. Fish. Aquat. Sci.* ***55***, 1–16

Welch, D.W., Ward, B.R., Smith, B.D. and Eveson, J.P. 1999. Influence of the 1990 ocean climate shift on British Columbia steelhead (*O. mykiss*) populations. *Fish. Oceanogr.* (submitted)

Whitney, F.A., Wong, C.S. and Boyd, P.W. 1998. Interannual variability in nitrate supply to surface waters of the Northeast Pacific Ocean. *Mar. Ecol. Prog. Ser. 170*, 15–23

Dissolved Gas Measurements at Stn. P4 during the 97–98 El Niño

Craig McNeil, David Farmer and Mark Trevorrow
Institute of Ocean Sciences
Sidney, B.C., Canada
e-mail: mcneilc@dfo-mpo.gc.ca

Preliminary results and interpretation of measurements obtained at the N.E. Pacific El Niño monitoring station P4 during September 1997 to May 1998 are presented. Station P4 is situated in the vicinity of 48° 39' N and 126° 40' W approximately 75 km west of Vancouver Island, British Columbia, Canada in a water depth of approximately 1,300 m. An instrument package, consisting of a SBE16 DO CTD and an upward-looking sonar, was deployed on a subsurface mooring at a mean depth of ~20 m. Time series measurements, recorded with a 1-h sampling period, include total dissolved air pressure or gas tension, dissolved oxygen and nitrogen concentrations, fluorescence, water temperature and salinity, and acoustical back-scatter intensity.

Data Overview

Figure 1 displays a summary of the data. The instrument package remained at around 20 m depth for the majority of the deployment, although it was drawn down to depths in excess of 50 m for a short period during a storm on year day 415. Water temperatures in November 1997 (year day 280) were around 15°C. Water temperature at 20 m depth continued to cool until mid-January 1998 (year day 380). Dissolved oxygen, measured by a Beckman probe on the SBE16, appeared super-saturated by approximately 20–30% for the first 25–30 days of the deployment and then remained reasonably stable, close to saturation. Winkler calibration samples are indicated. The initial decline in dissolved oxygen concentration is suspect and probably associated with a calibration change during what appears to be a 'settling in' period of the sensor. This is apparent by comparing the dissolved oxygen sensor measurements with the gas tension signal as follows.

Gas tension is the dissolved air pressure. The signal is approximately 20% pO_2 (dissolved) and 80% pN_2 (dissolved). As dissolved N_2 is relatively biologically inert, the sensor responds, like an oxygen sensor, to variations in dissolved oxygen concentration. The accuracy of the gas tension measurement, however, is remarkable. Its absolute error is ± 0.01% yr^{-1} (the error bar is thinner than the plotted line). Unfortunately it stopped working on day 450 due to a pressure housing leak, but not before the spring bloom.

A bloom event is identified during mid-March, lasting approximately 10 days. The bloom is reflected in the dissolved oxygen measurements, the gas tension measurements and the fluorometer measurements, providing three completely independent means of determining the timing, duration and size of the bloom. We used a WETLABS WETStar fluorometer. The calibrations appear good (*cf.*, bottle sample). The fall bloom and spring bloom periods are identified. The spring bloom occurs shortly after a storm. The bloom appears to be triggered by a very calm period when there is no significant surface wave activity or bubble plume penetration (to be discussed). Peak Chl levels of ~ 4 $\mu g\ l^{-1}$ were recorded.

The meteorological and wave measurements we use are from the Environment Canada buoy # 46206 located at 48° 50' N and 125° 60' W. Shown also for comparison is a time series of the power at the inertial period (f_I) of the CTD pressure period, which serves as a crude indicator of storm activity. Bubble cloud penetration depth is measured using an upward-looking sonar at 200 kHz, located at the top of the mooring with an unobscured view of the surface.

These data may be compared with historical measurements and differences interpreted in terms of the impact of the El-Niño on N.E. Pacific productivity.

Historical Measurements

Figure 2 displays CTD casts taken during January, February and March 1998 at Stn. P4. The effect of the El Niño is clearly seen in the unusually warm and saltier surface waters, reaching peak levels sometime during February. Note that the surface waters at 150 m are changing temperature by 3°C during January to March.

Our data are presented in Figure 3 and compared with the historical annual average at Stn. P4 and indicate the waters at 20 m depth are approximately 3°C warmer than usual and saltier by approximately 0.5. Shown as error bars on the historical data are the standard deviations.

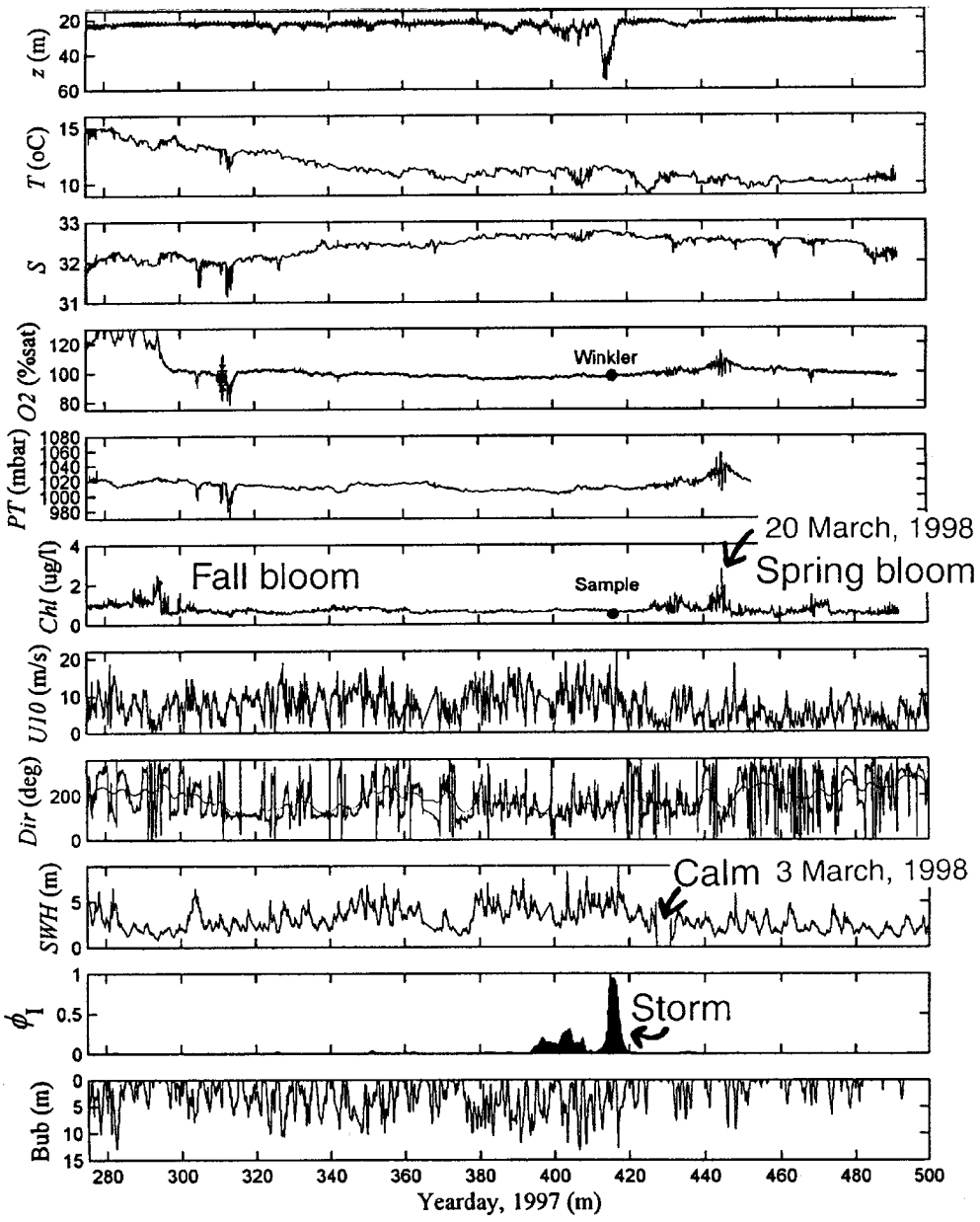

Figure 1. *Data recorded during September 1997 to April 1998 at Stn. P4, showing: instrument depth; water temperature and salinity; dissolved oxygen saturation level; total gas tension; chlorophyll concentration; wind speed, direction and significant wave height from a MET buoy 50 km away; energy in the inertial frequency band from the CTD pressure record at 30 m depth; bubble cloud penetration depth from an upward-looking sonar.*

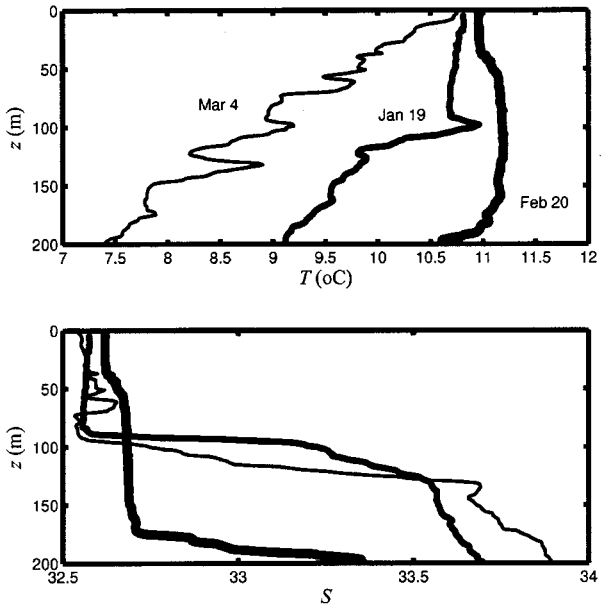

Figure 2. *CTD measurements at Stn. P4 during 1998 (from IOS, Sidney, B.C.).*

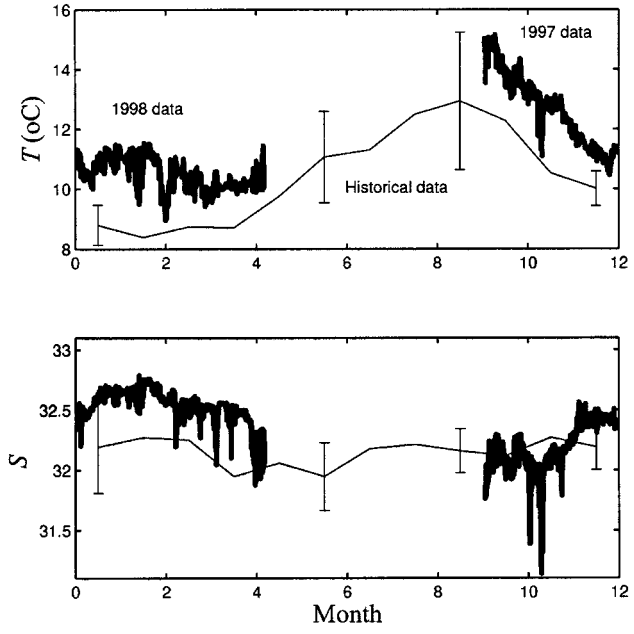

Figure 3. *Temperature and salinity time series at Stn. P4. Bold line shows data collected during September 1997 to April 1998, thin line shows historical annual average and standard deviations from records during 1959–1990 (Tabata and Weichselbaumer, 1992).*

Primary Production Estimates

What is the primary production rate derived from these data? There are two preliminary comparisons to make:

1. daily change in Chl concentrations,
2. daily change in dissolved O_2 concentrations.

Assuming a C:Chl ratio by weight of 60 and the observed change in Chl (inferred from fluorescence changes) of say 1 ug l^{-1} day^{-1}, we calculate a primary production rate of 1.2 gC m^{-2} day^{-1} assuming a 20-m layer depth. Such an estimate is crude as it does not account for daily redistribution of the biomass, changes in the fluorescence with time of day or grazing by zooplankton.

Similar calculations can be made using the observed dissolved oxygen changes. Again, we neglect redistribution of oxygenated water and biomass and assume that mixing extends to h = 20 m depth. From the observed daily saturation level change in dissolved oxygen of Δs = 20%, and the mean dissolved oxygen solubility, b = 280 mmol m^{-3}, we may estimate the productivity as $hb\Delta s/\Delta t$ (McNeil and Farmer, 1995). This leads to a net production rate of 1.12 molO_2 m^{-2} day^{-1}. Using a photosynthetic quotient, PQ = O_2:CO_2, of 1.2 (typically in the range of 1.1–1.2; Kirk, 1983) would imply a carbon production rate of 0.93 mol CO_2 m^{-2} day^{-1}, or 11 gC m^{-2} day^{-1}. This is a factor of ten times more than that derived from the change in fluorescence.

The above analysis indicates the levels of uncertainty associated with these kinds of estimates. We do, however, expect the estimate derived from fluorescence to be less than that derived from oxygen as fluorescence is typically quenched during the day as a result of light exposure (Denman and Gargett, 1988). The magnitude of this effect is not known for these data. It would, therefore, be inappropriate to combine the above results to infer a C:Chl ratio. We note once again that dissolved oxygen has been measured by two independent methods and both methods provide the same result giving credibility to this production estimate during the bloom of 11 gC m^{-2} day^{-1}.

Questions to be Addressed

Several questions have been identified by this preliminary look at the data:

- How will primary production estimates from these data compare with sediment trap data at the site?
- Is the timing of the spring bloom, or the magnitude of the spring bloom, different from non El Niño years?
- Is the export efficiency of carbon from the upper ocean different between El Niño and non El Niño years?

We invite other investigators to help address these questions through correspondence and data comparison.

Acknowledgements We thank Frank Whitney, Howard Freeland, Ken Denman and Angelica Peña for discussions and use of their data, and Kevin Bartlett for assistance with data collection and processing.

References

Denman, K.L. and Gargett, A.E. 1988. Multiple thermocline barriers to vertical exchange in the subarctic Pacific during SUPER, May 1984. *J. Mar. Res.*, *46,* 77–103.

Kirk, J.T.O. 1983. *Light and Photosynthesis in Aquatic Ecosystems*. Cambridge University Press, Cambridge, England, 401 pp.

McNeil, C.L. and Farmer, D.M. 1995. Observations of the influence of diurnal convection on upper ocean dissolved gas measurements. *J. Mar. Res*., *53,* 151–169.

Tabata, S. and. Weichselbaumer, W.E 1992.An update of the statistics of oceanographic dada based on hydrographic/CTD casts made at Stations 1 through 6 along Line P during January 1959 through September 1990. *Canadian Data Report of Hydrography and Ocean Sciences, No. 108,* 317 pp.

Data Compilation and Preliminary Time Series Analysis of Abundance of a Dominant Intertidal Kelp Species in Relation to the 1997/1998 El Niño Event

Kristen L.D. Milligan,[1] Colin D. Levings [2] and Robert E. DeWreede[1]

[1] *Botany Department*
University of British Columbia
Vancouver, British Columbia, V6T 1Z4
Canada
e-mail: milligan@monmouth.com

[2] *Department of Fisheries and Oceans, Canada*
Coastal and Marine Habitat Science Section
West Vancouver Laboratory, 4160 Marine Drive
West Vancouver, British Columbia, V7V 1N6
Canada

Introduction

The primary goal of this study was to document effects of the 1997/1998 El Niño event on intertidal macroalgal abundance in Barkley Sound, British Columbia, Canada. Population fluctuations in the dominant intertidal kelp species *Hedophyllum sessile* were documented from June 1991 to May 1998. The extensive baseline data prior to 1997 provides a database to evaluate current intertidal kelp population trends from summer 1997 to the present. The authors recognize that the spatial scale of this survey is limited. However, this data set is unique for Barkley Sound since it is the only known long-term population study compiled for this geographic area. Eight sites were sampled in Trevor Channel (Figure 1). The most detailed surveys were taken at four sites on Prasiola Point.

These data provide a solid baseline against which present trends in macroalgal biomass and densities can be compared. The 1997/1998 El Niño increased coastal, Northeast Pacific water temperatures during approximately May 1997 to March 1998. The peak temperatures ranged from 17°C to more than 18°C (unpublished data from the Institute of Ocean Sciences, Canada). These temperatures and associated low nutrient levels (Zimmerman and Kremer, 1984) have the potential to negatively affect the sporophyte production and maintenance of kelp populations. These *Hedophyllum sessile* data from before, during, and after the 1997/1998 El Niño can thus be used to evaluate impacts of this warm-water event on kelp populations in the intertidal zone.

Hedophyllum sessile (Laminariales, Phaeophyceae) is found in the mid-intertidal zone on shores in the northeast Pacific Ocean, ranging from Attu Island, Alaska to northern California (Widdowson, 1965). The juvenile plant has a short flattened stipe (up to 5 cm) which rapidly disappears as the blade becomes sessile on the holdfast. Adult plants are characterized by a large blade (up to 0.6 m^2 total surface area) and no stipe, attached by numerous haptera (root-like attachment structures) arising from the thickened basal margins of the plant. Juveniles recruit in spring and summer months. *H. sessile* is a dominant intertidal kelp species which forms dense canopies within which various invertebrate and fish species are found. For example, *H. sessile* provides substratum and habitat for spawning Pacific Herring.

Methods

Data collected

Data collected were: kelp percent cover, adult and juvenile density, reproductive status, a biomass index, and cover of various understory species. Data on *Hedophyllum sessile*'s adult and juvenile density at Prasiola Point were included in this report because they directly quantify mortality. These data were arranged in a time series to evaluate trends in these parameters.

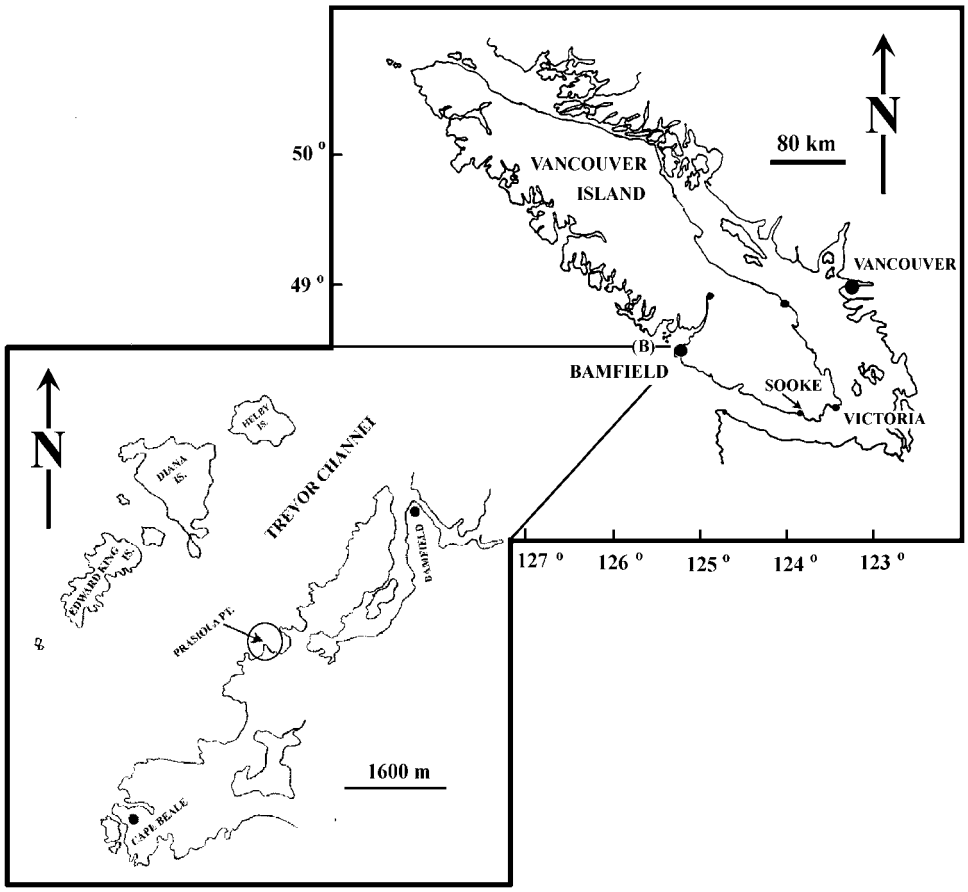

Figure 1. *Hedophyllum sessile sampling locations in Barkley Sound, British Columbia. In total, eight sites in Trevor Channel were sampled. Four sites at Prasiola Point (encircled on the left-hand map of Trevor Channel) were intensively studied. This report only includes data from Prasiola Point.*

Historical data compiled

Historical data on juvenile and adult densities were compiled from Druehl and Elliott (1996) and from DeWreede's macroalgal monitoring program (unpublished data, see acknowledgments). These data were examined for continuous time series and for compatibility of data sets between sites and times. Four sites from Druehl and Elliott (1996) and all DeWreede's sites (a total of four at Prasiola Point) were chosen for re-sampling in spring 1998. Druehl and Elliott's sites were not analyzed for trends because data were not consistent enough to provide a reliable baseline.

Data collected and analyzed for post-El Niño status

Historical sites were visited in May 1998. At Prasiola Point, adult density and juvenile densities (# per m^2) were quantified by randomly placing twenty 0.25 m × 0.25 m quadrats on permanent transect lines in the middle of the *Hedophyllum sessile* zone. All of the sites at Prasiola Point were pooled to produce a single, continuous data series from 1991 to 1998. Because different sites at Prasiola Point were sampled in different years, any given date in the 1991–1998 time series had a total of 20 quadrats, except in May 1998 when the total number of quadrats sampled was 40.

Results

Juvenile and adult densities were negatively affected from June 1997 to February 1998 (Figures 2 and 3). Peak recruitment normally occurs in late spring/early summer months. June 1997 was unique from all other sample dates because (in a site which always had successful recruitment) it was the first documented summer month with zero recruitment

(Figure 2). Data from the most recent field sampling (May 1998) indicated that juvenile densities were similar to those found in spring and summer months in 1991 to 1996 (e.g. April and June 1996; Figure 2).

In May 1998, adult densities in previously dense kelp beds were low and there was no apparent increasing trend in adult densities. These beds will only recover if the newly recruited juveniles (in May 1998; Figure 2) survive.

Conclusion

Recruitment of *Hedophyllum sessile* sporophytes was measured on Prasiola Point in 1991, 1992, 1995, 1996, 1997, and 1998. June 1997 was the first summer date during this time period when there was no recruitment. Low juvenile densities were reported in subsequent sample dates, with juvenile densities recovering in May 1998. The low 1997 recruitment event presumably correlates with effects of El Niño-induced oceanographic conditions such as high water temperature and associated low nutrient concentrations (Zimmerman and Kremer, 1984; Deysher and Dean, 1986). Low sporophyte recruitment in 1997 was followed by low adult density. Extremely low adult densities in May 1998 on Prasiola Point may thus be a result of the previous year's recruitment failure.

These data suggest that *Hedophyllum sessile* was negatively impacted from May 1997 to the present and is recovering. This also indicates that if water temperatures (and/or a correlated variable such as nutrient concentrations) had remained at a level which physiologically stresses algal production, these kelp populations would continue to decline. However, this prediction can only be appropriately tested by monitoring other kelp beds in Barkley Sound for trends related to water temperature (and nutrient concentrations). This study also demonstrates that an extensive monitoring program for inshore macroalgal habitats is a valuable tool for evaluating effects of environmental change.

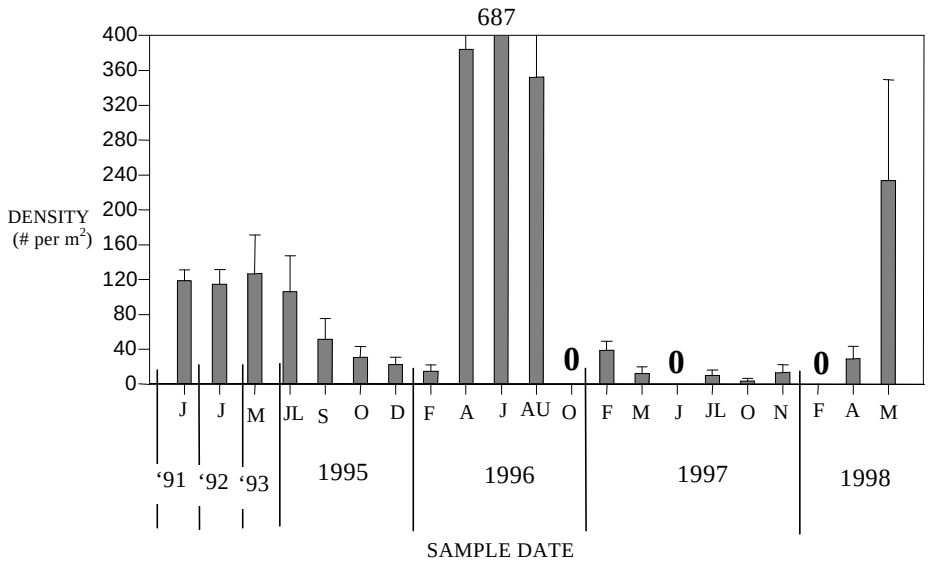

Figure 2. *Juvenile sporophyte density. Densities (+ SE; n = 20 for all dates except May 1998 when n = 40) are pooled means for all sites sampled at each time. Months are abbreviated: A = April, AU = August, D = December, F = February, J = June, JL = July, M = May, N = November, O = October, S = September. "687" above J-96 is the mean density. "**0**" indicates zero individuals.*

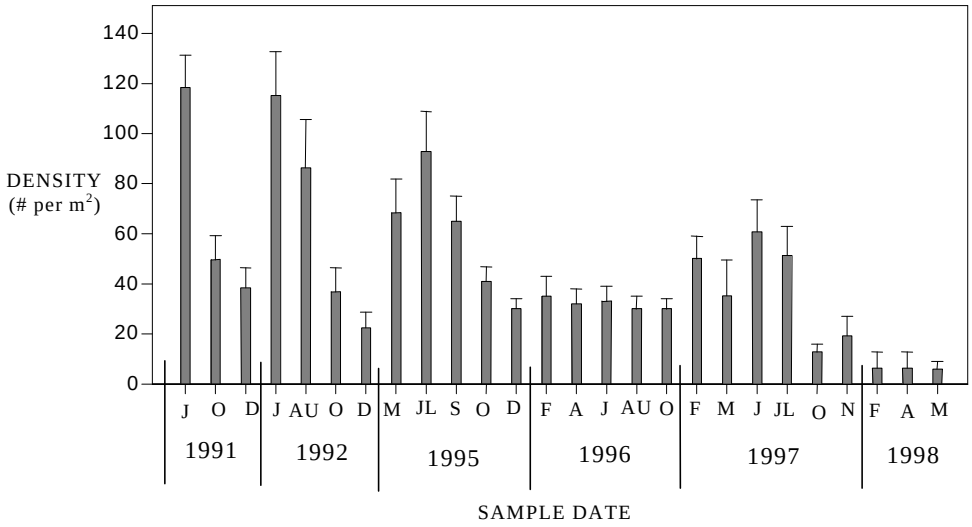

Figure 3. *Adult sporophyte density. Densities (+ SE; n = 20 for all dates except May 1998 when n = 40) are pooled means for all sites sampled at each time. Months are abbreviated: A = April, AU = August, D = December, F = February, J = June, JL = July, M = May, N = November, O = October, S = September.*

Acknowledgments This presentation was made possible by the data collection of various investigators. In addition to data collected by R.E. DeWreede and K. Milligan, the following investigators collected and prepared data: L. Druehl, Simon Fraser University & Bamfield Marine Station; C.T.J. Elliott, Bamfield Marine Station; and C. Peters, University of British Columbia

All data were collected with logistical support from Bamfield Marine Station and financial support from the Department of Fisheries and Oceans, Canada (for May 1998 sample date and data compilation), NSERC (for R. DeWreede, K. Milligan, and C. Peters), and Parks Canada (for L. Druehl and C.T.J. Elliott). Field assistants in May 1998 were Sophie Boizard and Bob Cheema.

References

Deysher, L.E. and Dean, T.A. 1986. *In situ* recruitment of sporophytes of the giant kelp, *Macrocystis pyrifera* (L.) C.A. Agardh: effects of physical factors. *J. Exp. Mar. Biol. Ecol., 103,* 410150–63.

Druehl, L.D. and Elliott, C.T.J. 1996. *Parks Canada Barkley Sound Kelp Distribution*. Parks Canada Contract #K3489-3-0006.

Widdowson, T.B. 1965. A taxonomic study of the genus *Hedophyllum* Setchell. *Can J. Bot., 43,* 1409–1420.

Zimmerman, R.C. and Kremer, J.N. 1984. Episodic nutrient supply to a kelp forest ecosystem in southern California. *J. Mar. Res., 42,* 591–604.

Reviewing the Evidence that Adult Sockeye Salmon Strayed from the Fraser River and Spawned in Other Rivers in 1997

S.M. McKinnell,[1] C.C. Wood,[1] M. Lapointe,[1] J.C. Woodey,[1]
K.E. Kostow,[2] J. Nelson[3] and K.D. Hyatt[1]

[1] *Pacific Biological Station*
Hammond Bay Rd.
Nanaimo, B.C. V9R 5K6, Canada
e-mail: mckinnells@dfo-mpo.gc.ca

[2] *Oregon Department of Fish and Wildlife*
2501 SW First Ave.
P.O. Box 59, Portland, OR 97207
U.S.A.

[3] *Seastar Biotech Inc.*
32056–3749 Shelbourne St.
Victoria, B.C. V8P 5S2, Canada

During the summer and autumn of 1997, sea surface temperatures (SSTs) along the British Columbia coast and in the Gulf of Alaska were the warmest on record, and the return migration of sockeye salmon to the Fraser River was unusually protracted (McKinnell, 1997). Some sockeye salmon had developed secondary sexual characteristics in the sea. From northern California (Smith River) to northern Vancouver Island, sockeye salmon were observed in unusual abundance in rivers and streams where they are not normally seen. Two hypotheses were developed to explain these observations: (1) there had been good survival of small local sea- and river-type populations that had largely gone unnoticed by biologists, and/or (2) an unusually high number of the abundant Fraser River sockeye salmon had strayed. Samples of sockeye salmon (whole fish and/or tissues) were collected from 30 locations on Vancouver Island (~450 fish) and 4 locations in Oregon (45 fish) to investigate their origin. Of the whole fish collected on Vancouver Island, most were spawned out.

Mitochondrial DNA (mtDNA) variation in sockeye salmon has been surveyed throughout the species' range and baseline haplotype frequencies were available from all major populations (36 sample sites) spanning the region of interest from Queen Charlotte Sound to the Columbia River (Wood, unpublished data). Genetically similar populations were pooled to form 11 "stocks", the maximum number that could be resolved with the 11 haplotypes observed in this region. Simulations with mixtures of sockeye salmon of known origin were conducted to determine the reliability of stock composition estimates based on mtDNA variation among the 11 stocks. Haplotype frequencies in samples collected from rivers on the west coast of Vancouver Island (WCVI), the east coast of Vancouver Island (ECVI), and Oregon were compared with corresponding frequencies in the baseline to determine first, whether non-Fraser sockeye salmon haplotypes were present, and second, to estimate the most likely contributions by each of the 11 stocks using Statistical Program for Analyzing Mixtures (SPAM). Where haplotype frequencies were consistent with significant contributions from Fraser River fish, scale patterns were used to estimate contributions by individual populations within the Fraser River using the baseline developed by the Pacific Salmon Commission. Estimates of stock composition from mtDNA and scale patterns were then assessed for consistency with information on age composition, run timing and parasites carried by the sockeye.

Analyses of mtDNA (Figure 1) and scale patterns (Figure 2) of sockeye salmon sampled from rivers

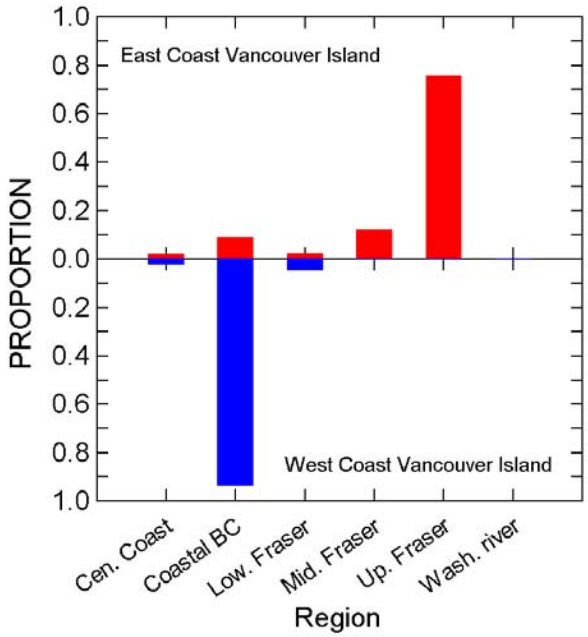

Figure 1. *Maximum likelihood estimates of sockeye salmon population origin based on mtDNA haplotypes for samples taken on the east and west coasts of Vancouver Island, B.C.*

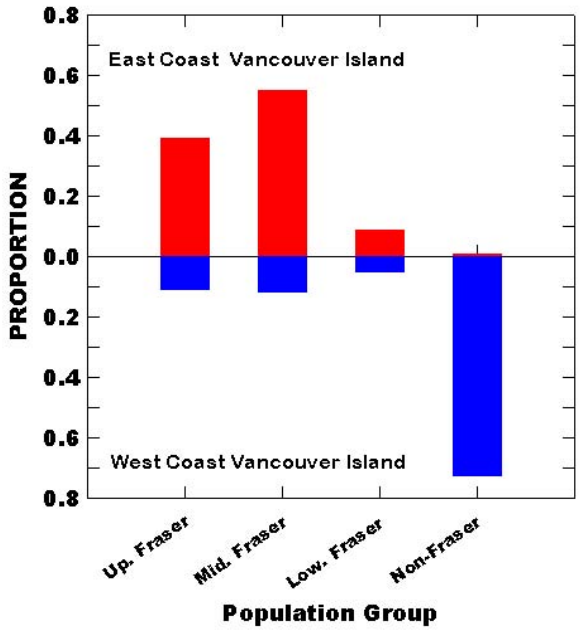

Figure 2. *Maximum likelihood estimates of sockeye salmon population origin based on scale patterns for samples taken on the east and west coasts of Vancouver Island, B.C.*

along the ECVI are consistent with the hypothesis of straying Fraser River sockeye salmon; however, there was also evidence of non-Fraser haplotypes in these samples suggesting that a small fraction of the sockeye salmon were of local origin. Age composition (mostly age 1.2) and *Myxobolus* and *Philonema* parasite incidence were consistent with sockeye of Fraser River origin. On the other hand, analyses of mtDNA haplotypes and scale patterns of sockeye salmon sampled from rivers on the WCVI are not consistent with the hypothesis of straying Fraser River fish, suggesting an unusual recruitment to local populations. Age composition data were similar to Fraser River and other southern sockeye populations. Parasite data were not available for these samples.

The mtDNA haplotypes sampled from the Deschutes River, Oregon (n = 33) were those typically found in many southern sockeye salmon populations such as the Columbia and Fraser rivers. The haplotype frequencies, however, were not typical of populations sampled to date from either of these rivers, with the possible exception of some small populations in the lower Fraser River. The date of sample collection in the Deschutes River (mid-August) was earlier than would be expected for sockeye salmon from the lower Fraser River. Of two sockeye salmon sampled from the Rogue River, Oregon, one contained a haplotype that is not found in the Fraser River but is common in river-type populations on the west coast of North America and north of central British Columbia Four fish from the Clackamas and two from the Klaskanine rivers had haplotypes that are common in southern populations and little can be said of their origin.

At least some Fraser River sockeye strayed. These fish may have (1) begun their migration from a location that was more distant than normal, or (2) started their migration from a normal location but took a longer route homeward, or (3) encountered anomalous ocean currents that made their migration more arduous, or (4) some combination of the above. Homeward migration was likely abandoned in favour of a more convenient river due to advancing sexual maturation.

References

McKinnell, S. 1997. An unusual ocean climate in the Gulf of Alaska during the spring of 1997 and its effect on coastal migration of Fraser River sockeye. (*NPAFC Doc. 282*) 10 pp. Fisheries and Oceans Canada, Ocean Science and Productivity Division, Pacific Biological Station, Nanaimo, B.C. V9R 5K6.

Sardines Return to British Columbia Waters

G.A. McFarlane and R.J. Beamish
Pacific Biological Station
Hammond Bay Rd.
Nanaimo, B.C. V9R 5K6
Canada
e-mail: mcfarlanes@dfo-mpo.gc.ca

"The Indians have told of catching pilchards in years long forgotten. None were around when white men first set their nets; then they came back, and nobody knows why. They crowded the waters along the West Coast of Vancouver Island in ever larger numbers after 1916. The late twenties brought the big catches, and pilchard reduction plants sprang up between Kyuquot and Barkley Sound."

Forester and Forester, 1975

Sardines (*Sardinops sagax*) constituted the largest fishery in British Columbia from the mid-1920s to the mid-1940s. During this period catches averaged 40,000 t annually (Figure 1). The fishery off British Columbia collapsed in 1947 and sardines disappeared totally from British Columbia waters. The collapse of this fishery has been described as a classic example of over-fishing (Hilbourn and Walters, 1992). The complete absence of sardines in Canadian and northern U.S. waters was never recognized as a consequence of changes in species distribution. Instead it was believed that overfishing in some way eliminated every single fish. It was also generally believed that there was little prospect for the recovery of the fishery off the British Columbia coast because supposedly it was the genetically distinct northern migratory stock that had been overfished (Murphy, 1966; MacCall, 1979). The remaining biomass of this genetically distinct stock was considered to be too small to rebuild.

Another explanation for the changes in abundance of sardines was proposed by Kawasaki and Omori (1988). They recognized that there was a synchrony in the trends of abundance of sardine populations off Japan, California and Chile (Figure 2).The collapse of sardine stocks off Canada and the United States in the late 1940s corresponded with the collapse off Japan. Beginning in the late 1970s the stocks off Japan, California and Chile increased dramatically. The synchrony persisted when stocks declined off Chile and Japan in the late 1980s and early 1990s, while off California the stocks have not yet declined. The results of Kawasaki's studies indicate that large fluctuations in sardine populations are a consequence of changes in ocean habitat. Shifts in climate/ocean regimes are now recognized as important factors affecting the abundance trends of a variety of fishes (Beamish et al., 1998; Mantua et al., 1997; Minobe, 1997).

Historically, sardines entered British Columbia waters in mid-June and returned to southern spawning grounds (California) in mid-October. Most spawning occurred from April to June in the southern California Bight. It was primarily the older, larger sardines, which migrated north to feed off

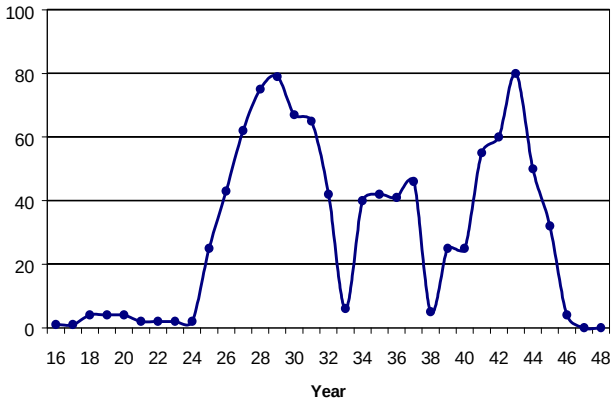

Figure 1. *Catches (tonnes) of Pacific sardine from Canadian waters, 1917 to 1947.*

British Columbia. Hart (1943) noted that in a few years, some sardines remained in the inlets off the west coast of Vancouver Island throughout the winter.

In 1992, sardines reappeared in British Columbia waters (Figure 3, Hargreaves et al., 1994) after a total absence of over 40 years. Sardines were first reported in 1992 in both commercial and research catches of Pacific hake (*Merluccius productus*). The catches in the hake fishery have continued through to 1998, but are not an indication of sardine abundance as hake are fished at depths greater than 80 m, well below the concentrations of sardines in the surface waters (Figure 4). The sardines probably were captured in the hake fishery when the nets were pulled through the surface waters. In our research surveys that began in 1997 we caught large numbers of sardines in the surface waters relative to the catches in the hake fishery (Figure 3). This may indicate that sardines were abundant in the surface waters prior to 1997 and this is supported by the initiation of an experimental commercial fishery in 1995 (Figure 3). Movement into the Canadian zone may be continuing because sardines continue to move farther north each year (Figure 5).

The abundance off British Columbia appears to be increasing. During July 1997, we estimated abundance using large surface trawls (Beamish and Folkes, 1997) from the Columbia River to the tip of Vancouver Island at 135,000t, of which approximately 60,000 t was present off the west coast of Vancouver Island. The 60,000 t represent approximately 250,000,000 sardines. For comparison, a catch of 1,800,000 coho salmon in the same area was considered to satisfy conservation needs and meet fishery expectations (DFO, 1985). This would be equivalent to approximately 9,000,000 sardines (the weight of 1 coho = the weight of 5 sardines). The numbers of sardines present in 1997 indicated that the abundance of fishes in the surface waters had not only changed, but had increased.

The large abundance of sardines in the Canadian zone in 1997 was observed prior to the major increase in temperature (August, September) of the surface waters as a result of the 1997 El Niño. The large abundance persisted off British Columbia through 1998. At the same time as large numbers of sardines appeared off British Columbia, the total abundance off California was considered to be unchanged (400,000 t). Catches off California have been maintained although there are indications that catches have decreased in 1998. This indicates that

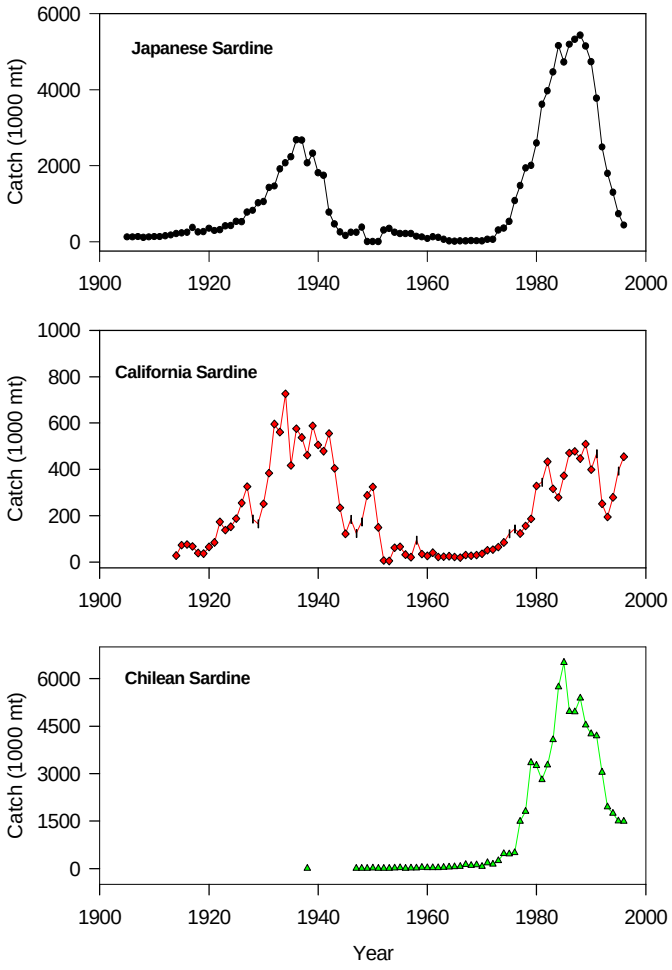

Figure 2. *Catch of sardines (1000 tonnes) from the three major stocks in the Pacific ocean (updated from Kawasaki). Note the synchrony in catch trends.*

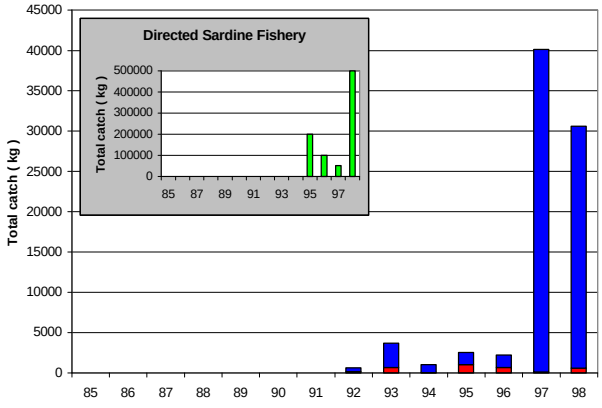

Figure 3. *Recent catches (kg) of Pacific sardine in the Pacific hake fishery (red) (x = 0 catch), research surveys (blue), and an experimental sardine fishery off the west coast of Vancouver Island (green). The experimental fishery was initiated in 1995 in response to fishers' comments of large schools of sardine in inlets off the west coast of Vancouver Island.*

the distribution of sardines may have shifted northward in 1997 and 1998. Sardines moved into the Strait of Georgia late in 1998. Additionally, large numbers of other species (Pacific hake and Pacific mackeral) have moved into the Canadian zone in larger numbers and are also moving farther north each year (Figure 6) and spawning.

Another change in behaviour was the documented spawning of sardines off the west coast of Vancouver Island (Figure 7). Sardines in spawning condition were sampled off southern Vancouver Island in July 1997, and large numbers of young of the year were captured in the same area in February, March and April of 1998. In February 1998, 31 sets were made in the top 30 m off the west coast of Vancouver Island. The catches of sardines from the 1997 year class were twice that of catches of the 1997 year class of herring (*Clupea harengus*) in the same sets indicating that these juvenile sardines were a common component of the fish community in the surface waters off Vancouver Island. The young fish have remained off the coast and have been captured throughout British Columbia waters including the Strait of Georgia, northern Hecate Strait and Alaska. Sardines remained abundant and spawned off the west coast of Vancouver Island in 1998 even though El Niño conditions did not persist. Two prior instances of sardine spawning near the British Columbia coast have been recorded (Williamson, PBS unpublished report, 1929; Hart, 1943). In both instances, 1929 and 1939, the authors reported one-year-old sardines in the catch, but the presence of young-of-the-year sardines was always considered to be rare.

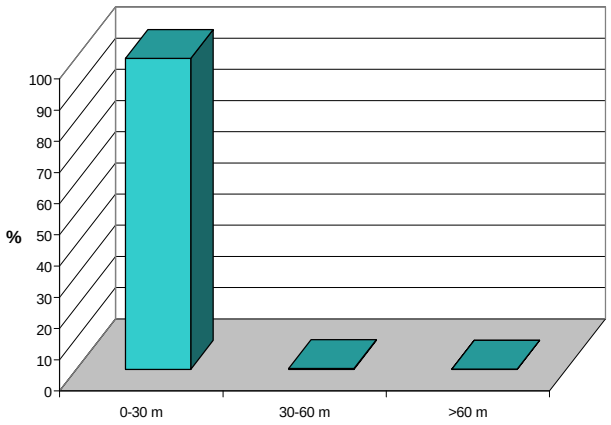

Figure 4. *Percentage of the catch by fishing depth during research surveys conducted during 1997.*

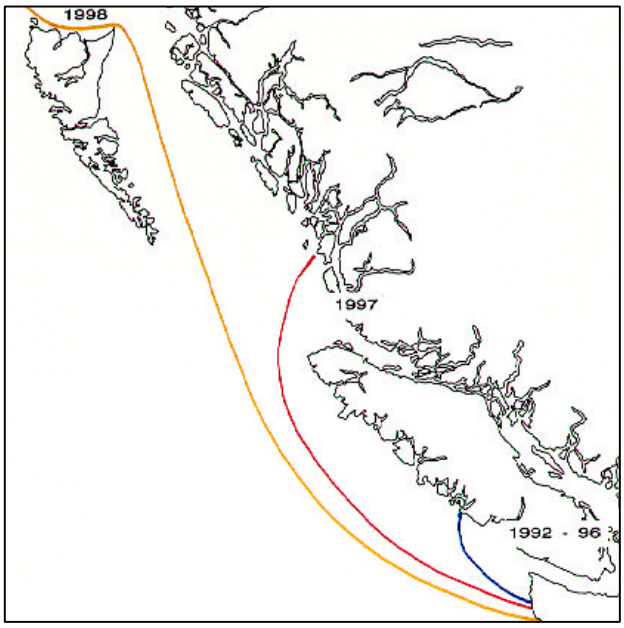

Figure 5. *Distribution of sardines in Canadian waters in 1992–1996, 1997 and 1998.*

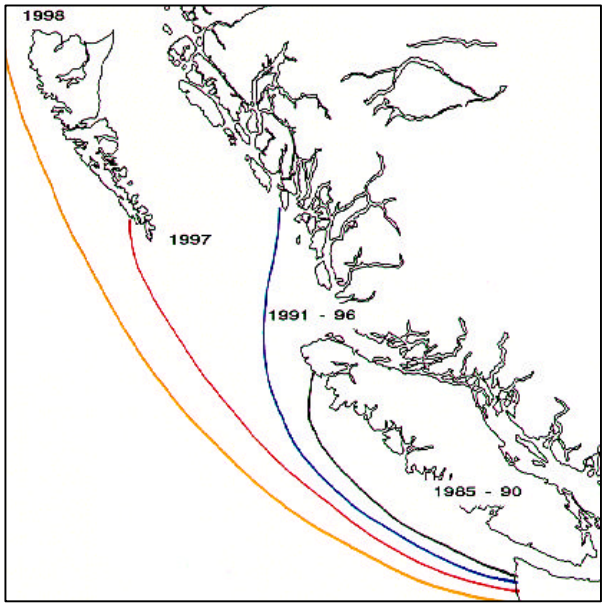

Figure 6. *Distribution of Pacific hake in Canadian waters in 1985–1990, 1991–1996, 1997 and 1998.*

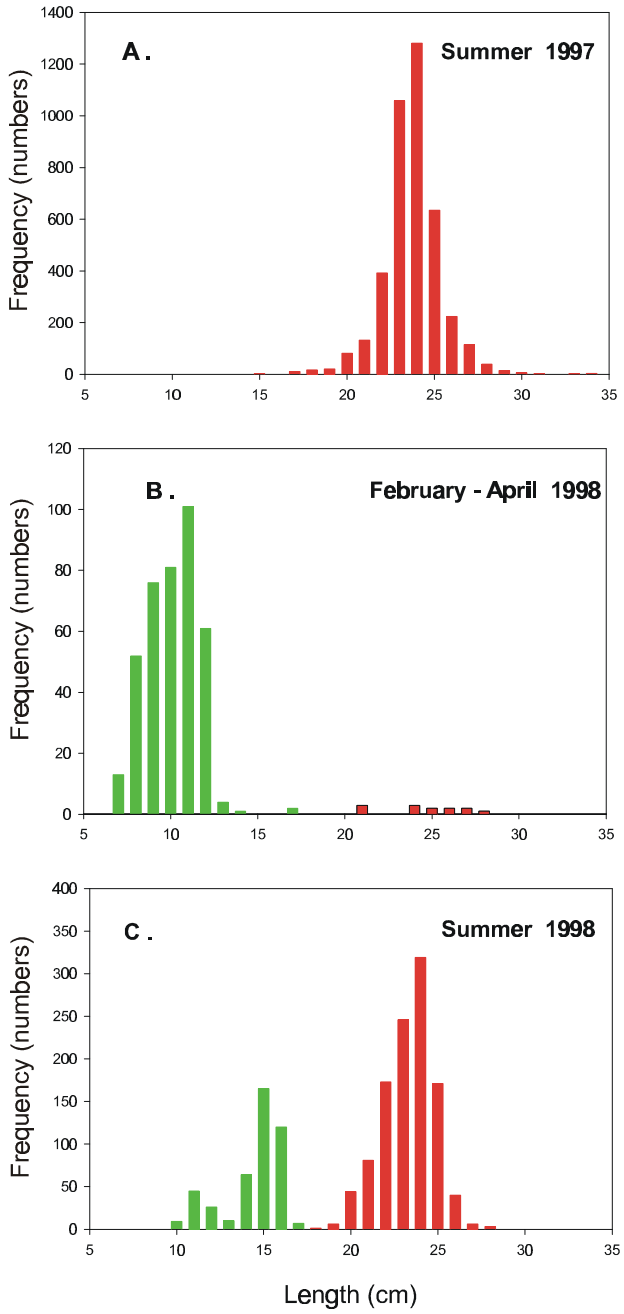

Figure 7. *Length frequency of Pacific sardine (A) summer 1997, (B) February–April 1998, (C) summer 1998. Note the abundance of 7- and 8-month-old sardine in the winter.*

Sardines were feeding mainly on phytoplankton (diatoms) and zooplankton (copepods and euphausiids) (Figure 8). In 1997, all fish examined (140) were feeding. In 1998, about 28% had empty stomachs (97 out of 347). In addition, during February

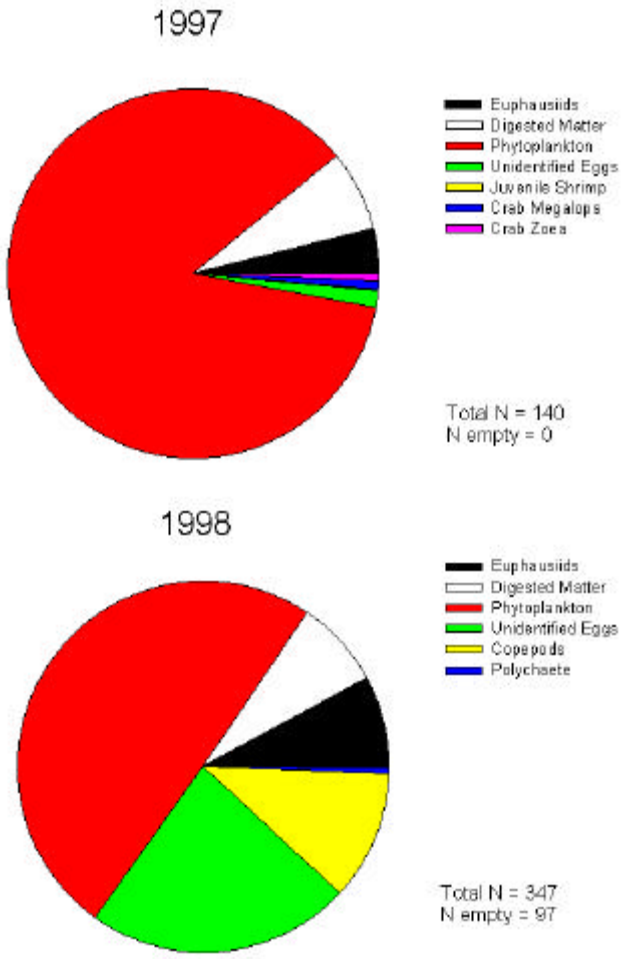

Figure 8. *Stomach contents of Pacific sardine, captured off the west coast of Vancouver Island in 1997 and 1998.*

to April 1998, juvenile sardines were a common prey of salmon captured off the west coast of Vancouver Island.

Conclusions

Sardines have increased in abundance in waters off British Columbia and are a dominant species in the surface waters. The unexpected large abundance of sardines has changed our thinking with respect to the cause of the collapse of sardines in the 1940s. The traditional explanation of overfishing as the principal cause for the collapse needs to be reexamined as it is clear that ocean conditions affected both distribution and survival. Also, it is illogical that overfishing would eliminate every single fish for over 40 years. The spawning of sardines in 1997

and 1998 also represents a change in their behavior. This change may be related to El Niño, but is also likely to be related to other changes in the ecosystem, as the El Niño events in the 1950s through to the 1980s were not associated with sardine movement and biology. It is worth remembering that the California Cooperative Oceanic Fisheries Investigations (CalCOFI) studies were initiated in an attempt to explain the collapse of the sardine stocks in the late 1940s. A lot of information has been collected about the ocean ecosystem since, but we still do not understand the mechanisms that are responsible for the fluctuations in sardine abundance. We propose that, in order to understand how to manage sardine stocks, we must understand how they are regulated naturally. These animals are an excellent indicator of ecosystem change. This means that the population dynamics of other species, such as coho (*Oncorhynchus kisutch*) and chinook (*O. tshawytscha*) salmon could also change for natural reasons. We believe that the changes we have seen in sardine distribution, abundance and spawning (and the same changes in other fish) indicates a major shift in the dynamics of the ecosystem that occurred in waters off British Columbia in the early 1990s. A key to understanding why large fluctuations in sardine abundance occur may be by understanding why they have shifted their range northward. Thus it may be as important to study the impact of the upcoming La Niña on sardines as it was to study the impact of the 1997 El Niño.

References

Beamish, R.J. and Folkes, M. 1998. Recent changes in the marine distribution of juvenile chum salmon off Canada. *N. Pac. Anadr. Fish. Comm Bull No.1,* 443–453.

Beamish, R., Noakes, D., McFarlane, G.F., Klyahtorin, L., Ivanov, V.V. and Kurashov, V. 1998. The regime concept and natural trends in the production of pacific salmon. *Can. J. Fish. Aquat. Sci.* (in press).

Forester, J.E. and Forester, A.D. 1975. *Fishing: British Columbia's Commercial Fishing History.* Hancock House Publishers Ltd. Saanichton, B.C. 224 pp.

Hargreaves, N.B., Ware, D.M. and McFarlane, G.A. 1994. Return of the Pacific sardine (*Sardinops sagax*) to the British Columbia coast in 1992. *Can. J. Aquat. Sci. 51,* 460–463.

Hart, J.L 1943. The pilchard (*Sardinops caerulea*) on Canadian fishing grounds with special reference to an unusual abundance of young fish. *Trans. R. Soc. San. Ser 3(37),* 55–73.

Hilbourn, R. and Walters, C.J. 1992. *Quantitative Fisheries Stock Assessment: Choice, Dynamics and Uncertainty.* Chapman and Hull, New York. 570 pp.

Kawasaki, T. and Omori, M. 1988. Fluctuations in the three major sardine stocks in the Pacific and the global temperature. *In* Long Term Changes in Marine Fish Populations. A Symposium held in Vigo. T. Wyatt and G. Larranenta (eds). pp. 37–53.

MacCall,A.D. 1979. Population estimates for the waning years of the Pacific sardine fishery. *Calif. Coop. Oceanic Fish. Invest. Rep. 20,* 72–82.

Mantua, N.J., Hare, S.R., Zhang, Y., Wallace, J.M. and Francis, R.C. 1997. A Pacific interdecadal climate oscillation with impacts on salmon production. *Bull. Am. Met. Soc. 78,* 1069–1079.

Minobe, S. 1997. A 50–70 year climatic oscillation over the North Pacific and North America. *Geophys. Res. Lett. 24(6),* 683–686.

Murphy, G.I. 1996. Population biology of the Pacific sardine (*Sardiniops caerulea). Proc. Calif. Acad. Sci. Fourth Ser. 34(1),* 1–84.

D.F.O., Canada. 1985. *Pacific Salmon Treaty: A treaty between the government of Canada and the government of the United States of America concerning Pacific Salmon.* 56 pp.

Impact of the 1997/98 El Niño on Seabirds of the North East Pacific

Ken H. Morgan
Canadian Wildlife Service, Environment Canada
c/o Institute of Ocean Sciences
P.O. Box 6000, Sidney, B.C., V8L 4B2
Canada
e-mail: morgank@dfo-mpo.gc.ca

To a large extent, seabirds are constrained to specific parts of the ocean on the basis of the characteristics of the marine climate. Large water masses or groups of similar, adjacent water masses often have characteristic assemblages of seabirds. Large-scale events that alter marine climates should produce changes in the seabird community characteristics that are consistent with the water mass alterations. However, because the factors that constrain seabirds to particular water masses are poorly understood, it is difficult to predict their response to large-scale perturbations.

Wahl et al. (1993) noted that during the 1982/83 El Niño, Fork-tailed Storm-Petrels *Oceanodroma furcata* were observed to feed atypically on the larvae of Dungeness crab *Cancer magister* in coastal Washington. During that same summer, widespread abandonment and failure of Brandt's *Phalacrocorax pencillatus* and Pelagic *P. pelagicus* cormorants occurred in Oregon (Graybill and Hodder, 1985). It was assumed that the elevated surface water temperatures had affected the distribution and recruitment of prey fish, which in turn had impacted the feeding (and reproductive) ability of these species. Off California, Briggs et al. (1987) observed (during 1982/83) lower overall at-sea seabird densities; higher relative percentages of warm-water species; and reduced numbers and southward dispersal of northern nesting species. Common Murres *Uria aalge* were 60% less numerous at sea during the 1982/83 winter and they foraged unusually far from land. In marked contrast, off Washington passage migrants and resident species fed nearer to the coast during that same event. Wahl et al. (1993) suggested that detritus-based estuarine systems (such as off Washington), were less affected by El Niño events than upwelling systems (off California).

In an effort to better understand the impacts of large-scale variations in oceanographic conditions on seabirds off the British Columbia coast, I began monitoring seabirds along a repeated 1500-km cruise track (Line P) to Ocean Station Papa (50°N by 145°W) in May 1996. To date, six surveys have been completed (May and August '96, February and June '97, and February and June '98). Surveys were conducted only while the ship was steaming at more than 5 knots (9.25 km h^{-1}) during daylight hours. During the surveys, the sea and sky were continuously scanned in a 180° field centred on the ship's bow. Transects were a running series of 5-min counts; the start and end position and time of each transect series were noted. Within each 5-min count period, all birds seen within 250 m of the ship were identified and tallied. Numbers of birds observed in each transect were transformed into densities (no./km^2) by species and by total birds. Mean densities were calculated for five segments of the route (Table 1), as well as for the entire survey line.

It was predicted that the warming of the coastal surface waters, the depression of the thermocline, and the northward displacement of the Subarctic Boundary would significantly influence the composition, abundance and distribution of the pelagic seabird community. Preliminary examination of the data only partially supported this hypothesis. The following observations suggested that 97/98 El Niño impacted the seabird community.

- Comparing only the early summer cruises (May '96, June '97 and June '98), the overall total density of birds and the diversity of species, were lowest in June '97 (see Table 2). Of the three early summer cruises, June '97 had the highest near-surface temperatures (Figure 1).
- Species of birds that are usually associated with the continental shelf, such as Common Murre, Cassin's Auklet *Ptychoramphus aleuticus*, and

Rhinoceros Auklet *Cerorhinca monocerata* (Morgan et al. 1991) were entirely absent from the June '97 survey.

- Fork-tailed Storm-Petrels, a species that typically is most abundant along the outer edge of the shelf and over the slope, ranged considerably farther offshore in June '97 (see Figure 2); indicating that they were travelling greater distances in search of food, and were most likely working harder to find sufficient energy for themselves and/or for their young.

Table 1. *Line P segments, station numbers, locations and water depths (on station). Segments refer to all bird survey transects conducted between the station pairs noted.*

Line P Segment	Line P Station No.	Latitude (° ′ N)	Longitude (° ′ W)	Water Depth Range (m)
	P1	48 34.5	125 30.0	120
A	↓↑			
	P4	48 39.0	126 40.0	1300
	P4	48 39.0	126 40.0	1300
B	↓↑			
	P12	48 58.2	130 40.0	3300
	P12	48 58.2	130 40.0	3300
C	↓↑			
	P16	49 17.0	134 40.0	3550
	P16	49 17.0	134 40.0	3550
D	↓↑			
	P20	49 34.0	138 40.0	3890
	P20	49 34.0	138 40.0	3890
E	↓↑			
	P26	50 00.0	145 00.0	4200

Table 2. *Average densities (no./km^2) of the 8 most common species of birds along the entire survey route. Elevated sea surface temperatures were most pronounced during the June 1997 survey.*

	May '96	Aug '96	Feb '97	June '97	Feb '98	June '98
Black-footed Albatross	0.13	0.09	0.03	0.12	0.05	0.04
Northern Fulmar	0.04	0.01	0.44	0.02	0.41	0.15
Dark shearwaters *	1.03	0.02	0.01	0.31	0.002	11.05
Fork-tailed Storm-Petrel	0.34	0.02	0.06	0.16	0.10	0.14
Leach's Storm-petrel	1.47	0.42	–	0.40	–	0.84
Common Murre	0.09	0.002	0.31	–	0.14	0.01
Cassin's Auklet	0.05	0.27	0.18	–	–	0.03
Rhinoceros Auklet	0.07	0.01	0.01	–	0.02	0.02
Total Birds	3.60	1.09	2.48	1.19	1.47	12.77
Number of Species	22	23	20	16	20	21
Area Surveyed (km^2)	474.6	460.2	204.9	286.6	489.9	294.9

* Dark shearwaters = Sooty and Short-tailed Shearwaters, plus unidentified dark shearwaters.

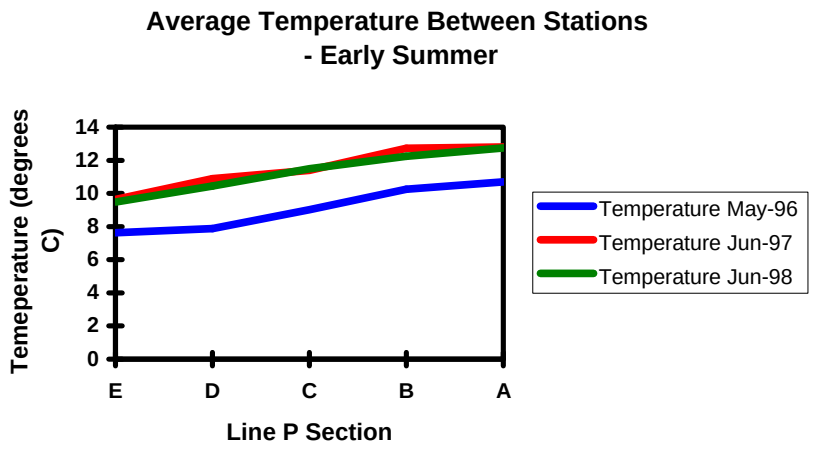

Figure 1. *Near surface (5m depth) temperatures averaged between stations during the three early summer cruises (May '96, June '97, June '98).*

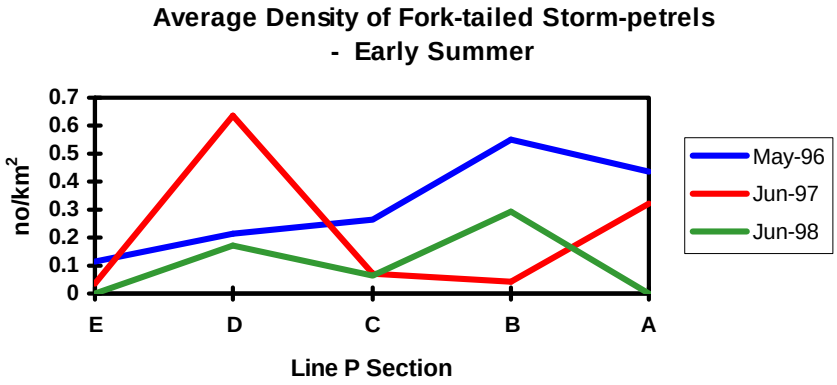

Figure 2. *Average density of Fork-tailed Storm-petrels within each line segment during the May '96, June '97 and June 98 surveys. Refer to Table 1 for location of each segment.*

Results that tended to contradict the hypothesis are as follows.

- Despite the continued persistence of warm near-surface waters (to at least June '98) the densities of dark shearwaters (Sooty *Puffinus griseus* and Short-tailed shearwaters *P. tenuirostris*, Figure 3) and Leach's Storm-petrel *Oceanodroma leucorhoa* surpassed the long-term average summer densities (derived for pelagic waters off the BC coast, see Table 3). The apparent "re-bounding" of dark shearwaters suggests that the decline was due to distributional shifts rather than due to population declines as suggested by Veit et al. (1996).
- In contrast to the previous year, the diversity of species in June '98 returned to pre-El Niño levels.
- Preliminary statistical analyses failed to demonstrate any significant relationships between species densities and the water characteristics tested (surface temperature, salinity, chlorophyll-*a* and nitrate levels).

Speculations on the results observed:

- Over the duration of the study, changes in the climatic/oceanographic conditions outside of the route covered by these surveys may have altered the normal migration routes, resulting in a depressed abundance of seabirds and an altered species mix.
- A time lag of unknown length (12 months or more?) may have existed between the changing oceanographic conditions and the response of the local seabird assemblage. Such a time lag would likely negate simple correlation tests between seabirds and water characteristics (that had been measured concurrently).

- The seabird community of the North East Pacific may have been dramatically altered long before this study commenced, from either a "regime shift" step-change or because of inter-decadal fluctuations (e.g., Francis and Hare, 1993; Mackas, 1995).

Figure 3. *Short-tailed Shearwater (Puffinus tenuirostris). Photograph by T. Palliser*

Table 3. *Long-term average seasonal densities (no./km^2, plus Standard Deviation) of common seabird species in pelagic waters off the coast of British Columbia[1], 1981–1998.*

	Spring		Summer		Winter	
	Density	SD	Density	SD	Density	SD
Black-footed Albatross	0.29	1.35	0.39	3.79	0.02	0.27
Northern Fulmar	0.16	2.08	1.14	18.36	0.29	2.56
Dark shearwaters	24.40	397.22	8.72	52.36	0.05	0.21
Fork-tailed Storm-petrel	0.86	4.15	1.01	9.29	0.11	0.57
Leach's Storm-petrel	0.55	2.18	0.50	2.13	0.003	0.04
Common Murre	0.65	9.17	0.84	5.48	1.21	3.34
Cassin's Auklet	1.68	19.16	2.26	27.73	0.67	2.76
Rhinoceros Auklet	0.47	1.45	0.58	3.45	0.05	0.31
Total Birds	32.36	398.93	23.67	172.90	6.85	21.72
Total Area Surveyed (km^2)	4369		7614		940	

[1] Data are from seabird surveys conducted anywhere within pelagic waters off the west coast of Canada, not just along Line P.

References

Briggs, K.T., Tyler, W.B., Lewis, D.B. and Carlson, D.R. 1987. Bird communities at sea off California: 1975 to 1983. *Stud. Avian Biol., 11.*

Francis, R.C. and Hare, S.R. 1993. Decadal-scale regime shifts in the large marine ecosystems of the Northeast Pacific: a case for historical science. *Fish. Oceanogr., 3,* 279–291.

Graybill, M.R. and Hodder, J. 1985. Effects of the 1982–83 El Niño on reproduction of six species of seabirds in Oregon. pp. 205–210 *in* W.S. Wooster and D.L. Fluharty (eds.), El Niño North, Washington Sea Grant Program, Univ. Washington, Seattle.

Mackas, D.L. 1995. Interannual variability of the zooplankton community off southern Vancouver Island. pp. 603–615 *in* R.J. Beamish (ed.), *Can. Spec. Publ. Fish. Aquat. Sci., 121.*

Morgan, K.H., Vermeer, K., and McKelvey, R.W. 1991. Atlas of pelagic birds of western Canada. *Occas. Pap. No. 72,* Can. Wildl. Serv., Ottawa.

Veit, R.R., Pyle, P. and McGowan, J.A. 1996. Ocean warming and long-term change in pelagic bird abundance within the California current system. *Mar. Ecol. Prog. Ser. 139,*11–18.

Wahl, T.R., Morgan, K.H. and Vermeer, K. 1993. Seabird distribution off British Columbia and Washington. pp. 39–47 *in* K. Vermeer, K.T. Briggs, K.H. Morgan, and D. Siegel-Causey (eds.). The status, ecology, and conservation of marine birds of the North Pacific. *Can. Wildl. Serv. Spec. Publ.*, Ottawa, Ont.

Coastal Hydrographic Responses in the Northern Gulf of Alaska to the 1997–98 ENSO Event

Thomas C. Royer[1] and Thomas Weingartner[2]

[1] *Center for Coastal Physical Oceanography*
Old Dominion University
Norfolk, VA 23529, U.S.A.
e-mail: royer@ccpo.odu.edu

[2] *Institute of Marine Science*
University of Alaska
Fairbanks, AK 99709, U.S.A.

Abstract

The El Niño–Southern Oscillation events for the past 22 years including the 1997–98 event have been captured by a long time series hydrographic station in the northern Gulf of Alaska. These events appear as positive subsurface temperature anomalies with the 1997–98 event being nearly 3 standard deviations above normal at 250 m. The mechanism for this heat transport is uncertain but an enhanced California Undercurrent or Kelvin wave propagation are likely candidates. This connection with tropical events could have implications on biological production in the Gulf of Alaska.

Background

Temperature and salinity versus depth at the mouth of Resurrection Bay, Alaska (60°N, 149°W) in 263 m of water have been measured since 1970 with sampling intervals ranging from hours to months. Since 1990, the sampling has been more regular, approximately monthly. The location was originally selected for its proximity to research vessel berthing facilities in Seward for logistical reasons. However, the station is also located in the Alaska Coastal Current, ensuring good connection with the regional coastal circulation.

The atmospheric forcing for this site includes seasonal heating, wind stress and buoyancy forcing in the form of freshwater discharges. The region is dominated by the Aleutian Low in winter and has a slight influence from the North Pacific High in summer. Intense winter downwelling is followed by weak summer upwelling. The freshwater discharge is greatest in autumn and least in early spring. The maximum discharge leads the maximum winds by about 3 months, and this enables to winds to force a coastal convergence of the low density surface water in the winter, which should intensify the Alaska Coastal Current at this time.

The monthly means of salinity and temperature at standard depths have been determined (Figures 1–3). The monthly mean temperatures (Figure 1) from 0–50 m are minima in March increasing a maximum at the surface of more than 13°C in August followed by lessor maxima at depth up to 3 months later. This seasonal temperature cycle is similar for the upper 100 m. Below 150 m the temperature cycle peaks in January with amplitudes of less than 0.5°C. The mean temperature at 250 m is slightly greater than that at 200 m. The monthly mean salinity (Figure 2) and density (Figure 3) are very similar since salinity here controls the water density. The minimum surface salinity is in August with the minima at increasing depths taking place later in the year. The minimum salinity at 100 m is in February, 6 months out of phase with the surface salinity minimum. The minimum vertical stratification is in March with the maximum in August. The minimum surface salinity leads the maximum in runoff by about two months. This could be a consequence of the autumn increase in winds, mixing the upper layers. Such mixing is evident in the autumn temperature inversions. The salinity and density

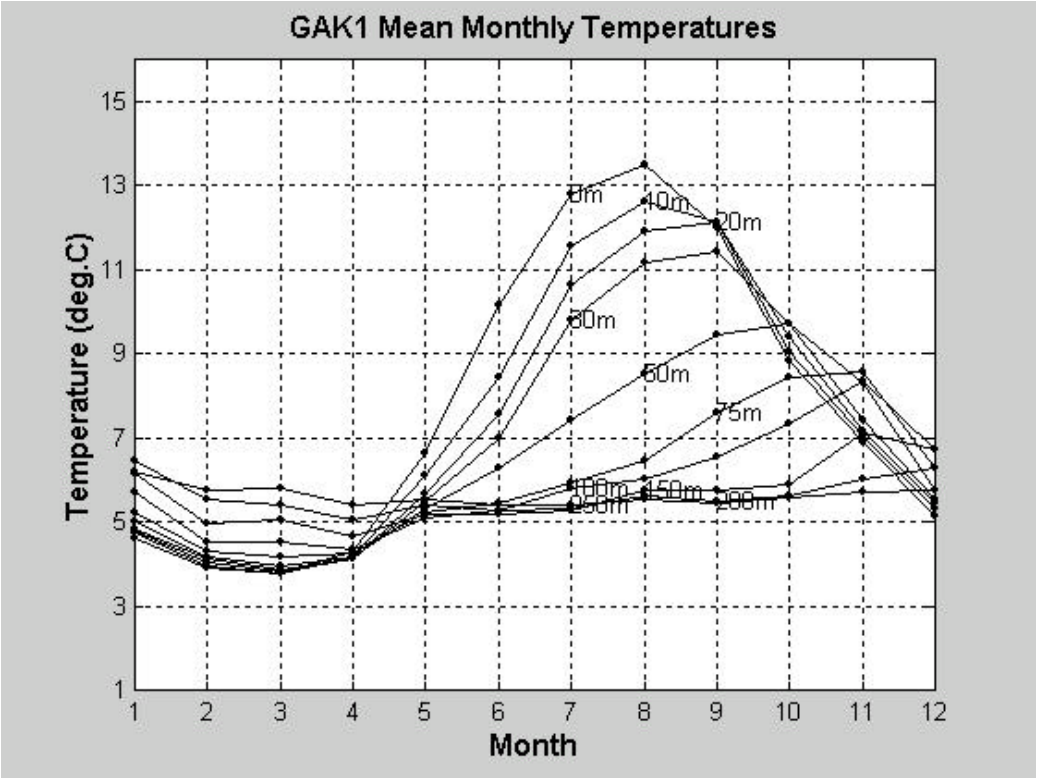

Figure 1. *Seasonal cycle in temperature at GAK 1.*

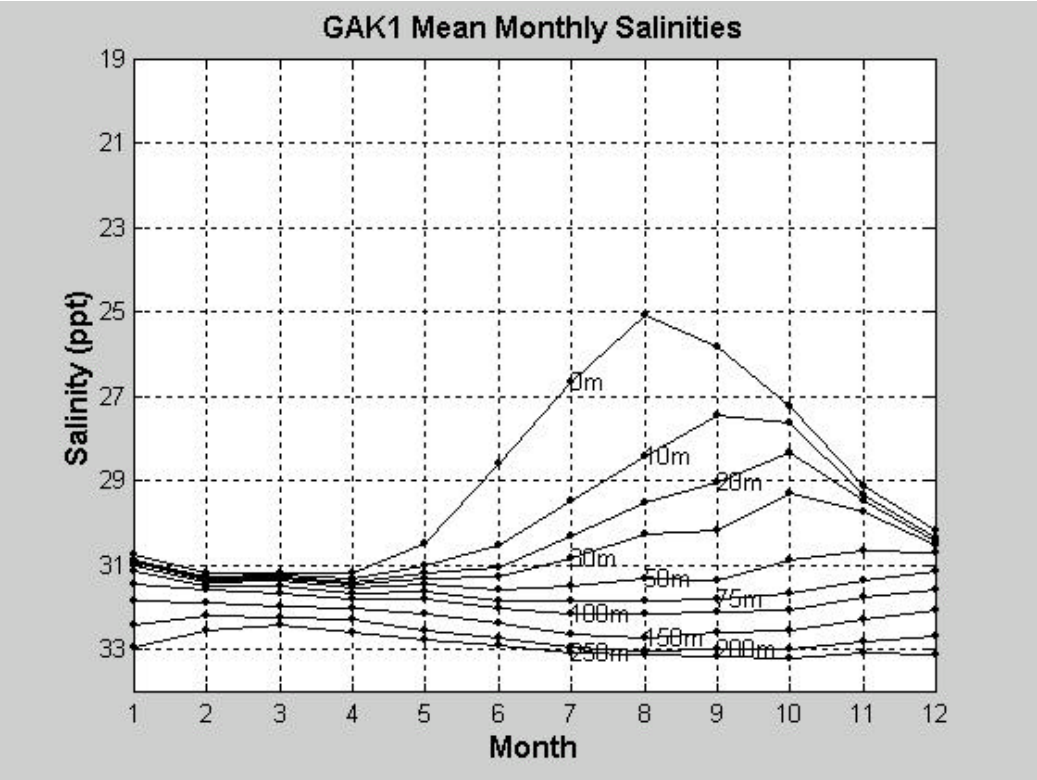

Figure 2. *Seasonal cycle in salinity at GAK 1.*

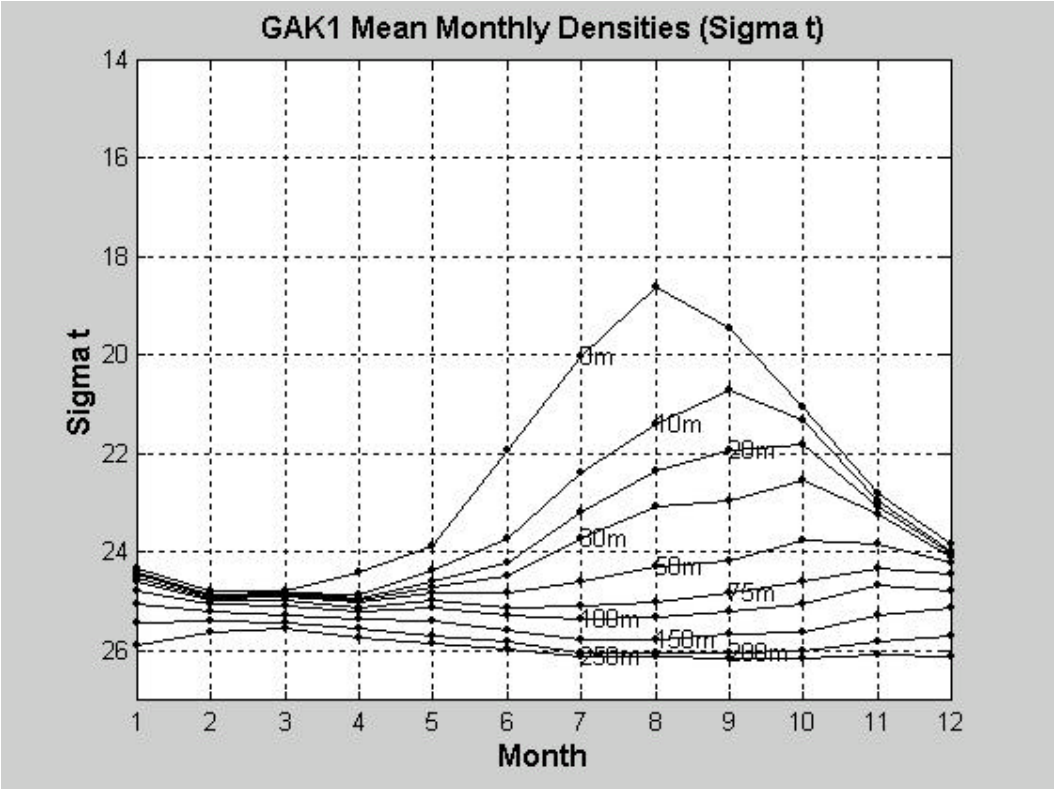

Figure 3. *Seasonal cycle in water density at GAK 1.*

variations at 150 and deeper are out of phase with those at the surface suggesting a different mechanism for their control. The upper 100 m of this water column appear to fluctuate on a seasonal basis under the influence of vertical mixing.

The monthly means of temperature and salinity are subtracted to yield anomalies of salinity and temperature over the water depth of 263 m. The anomalies of salinity and temperature are coherent with depth, suggesting that they are advected into the region rather than being induced by local surface evaporation, runoff, heating and cooling.

Salinity Anomalies

The salinity anomaly (Figure 4) was greatest in the early 1970s followed by a pattern of positive and negative values. The major periodicities of salinity at the surface are 4 and 9 years but only about 5 and 3%, respectively, of the variance is explained by fluctuations at these periods. ENSO is associated with the 4-year period and the 9-year periodicity of the surface salinity is consistent with decadal atmospheric variations found in the Arctic. Near bottom at 250 m, the 4-year period accounts for more than 8% of the variance while the fluctuations at 14–15 years can explain more than 10%. Coastal freshwater discharge is a potential driving force and has dominate periodicities of 4 and 16 years, but this can only explain 2 and 3% of the variability, respectively. The relatively small amount of salinity variance explained by ENSO suggests that it is not a major factor in interannual salinity variability at any depth. The relatively coherent salinity anomaly signal with depth suggests that the horizontal advection of these anomalies is important rather than local surface forcing by atmospheric processes.

Temperature Anomalies

The temperature anomalies (Figure 5) were below normal in the early 1970s, increasing to above normal in 1977–98. The 1980s brought anomalies with broad temporal scales while shorter duration events were found in the 1990s, punctuated by the 1997 upper layer warming, then a mid-depth and deep warming in 1998. The dominate periods of the surface temperature anomalies are 5 (<3%) and 9 (3%) years with the majority of the variance contained in the interdecadal periods. In the lower layers (150–200 m) a 5-year period (10%) fluctuation is accompanied by interdecadal fluctuations with a period of

19–20 years that accounts for about 30% of the variance. Thus, the temperature and salinity anomalies differ in their dominate time scales. Using an increase of one standard deviation as an indicator of ENSO (Figure 6) all prior ENSO events (1977, 1982–93, 1987, 1992–93 and 1997–98) can be seen in the 250-m temperature anomaly record with the exception of the 1972 ENSO that did not propagate to high latitudes. The 1997–98 event has produced an anomaly that exceeds 3 standard deviations. It reached its maximum in February 1998 and was back below the ENSO threshold by May. It must be noted that in comparing these measurements with prior ENSO events, since September 1990, sampling has been approximately monthly rather than irregularly as was the case with the "ship of opportunity" sampling. It is uncertain as to whether the ENSO signal propagates only in the subsurface layers only or whether it propagates throughout the water column but is masked by other forcing in the upper layers.

What are the possible causes for this ENSO signal? The lack of a salinity signal with this temperature elevation suggests that the baroclinic flow in the region is not altered. However, a barotropic forcing such as the change in the California and Alaska Currents could bring warmer water into the region. The alongshore gradient of bottom temperature at 250 m is uncertain but might be about half that in the surface layers that is about 1°C/ 200 km. A poleward excursion of about 600 km would cause the observed temperature elevation of about 1.4°C. Since the salinity gradients are parallel to the coast, there would be no salinity change. To accomplish this shift, there would have to be an increase in the coastal current of about 8 cm/s over 3 months. In either case, the ENSO signal is superimposed on a decadal deep temperature signal and its effect on biological productivity depends on both the amplitudes and phases of these cycles.

Hydrographic sampling at GAK 1 will continue and the suite of parameters will be expanded to include nutrients as part of the Northeast Pacific GLOBEC program. These hydrographic data are available on-line at http://www.ims.alaska.edu:8000/GAK1/GAK1.dat.

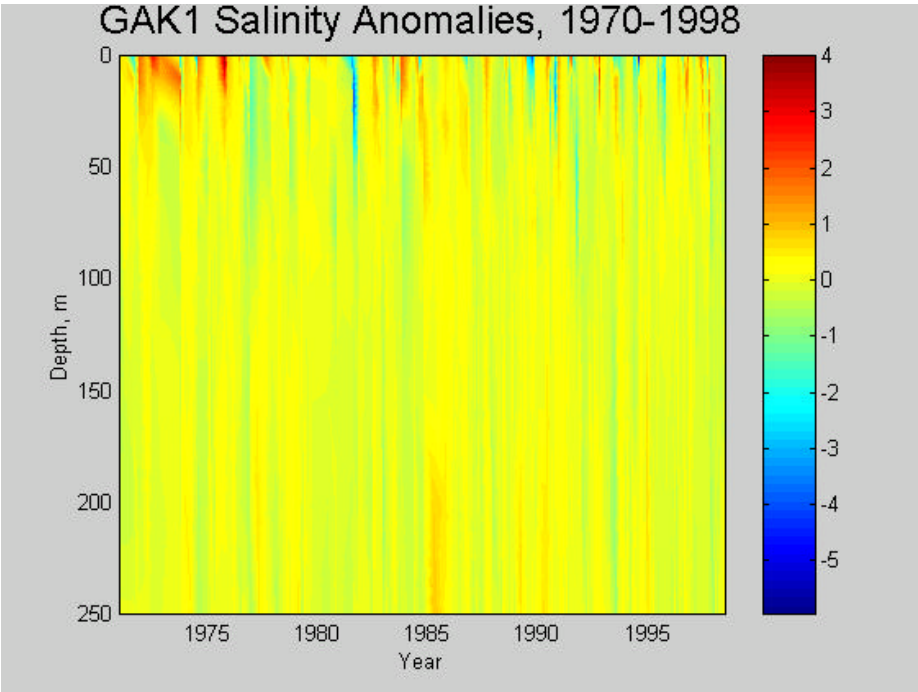

Figure 4. *Salinity Anomalies at GAK 1.*

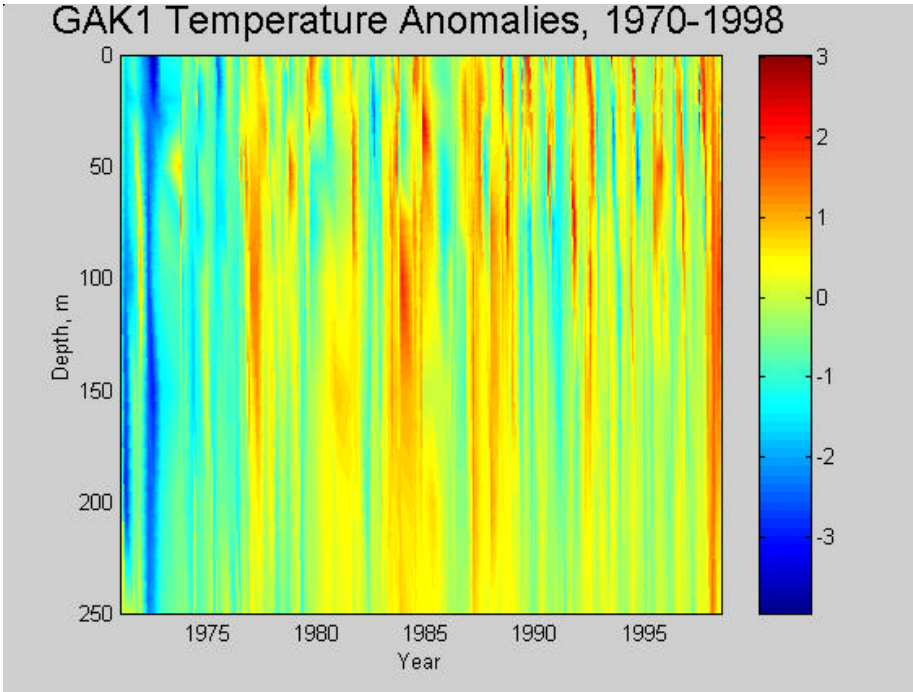

Figure 5. *Temperature Anomalies at GAK 1.*

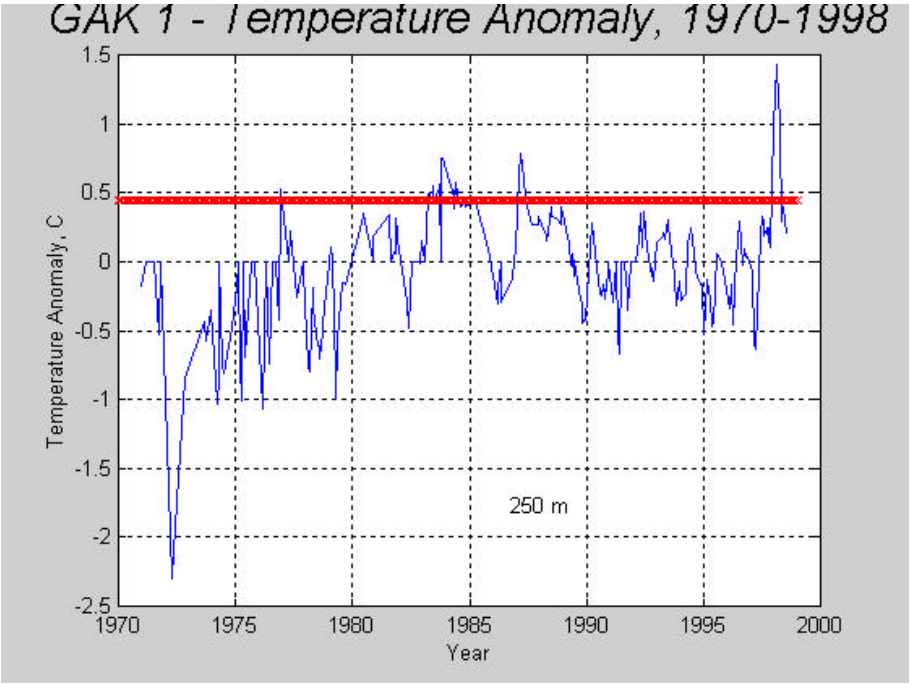

Figure 6. *Temperature Anomalies at 250 m depth at GAK 1 with + one standard deviation (red) used as the threshold for ENSO events.*

References

Proshutinsky, A. and M. A. Johnson. 1997. Two circulation regimes of the wind-driven Arctic Ocean *J. Geophys. Res., 102*, 12493–12514.

Royer, T. C. 1993. High latitude oceanic variability associated with the 18.6 year lunar nodal tide. J. Geophys. Res., 98, 4639–4644.

Biological Effects of the 1997/98 ENSO in Cook Inlet, Alaska

John F. Piatt, Gary Drew, Thomas Van Pelt, Alisa Abookire,
April Nielsen, Mike Shultz, and Alexander Kitaysky
USGS, Alaska Biological Science Center
1011 East Tudor Road Anchorage, AK 99503
U.S.A.
e-mail: john_piatt@usgs.gov

Abstract

We have been conducting detailed studies of the biology of seabirds in relation to oceanography and forage fish ecology in lower Cook Inlet, Alaska, since 1995. This fortuitously allowed us to document biological effects of the 1997/98 ENSO in this region. Anomalously warm sea surface temperatures (SSTs) were observed in the Gulf of Alaska (GOA) beginning in June of 1997, but not in Cook Inlet until September, 1997. Warm temperature anomalies at the surface and at depth persisted until May of 1998, when temperatures returned to average in the GOA and Cook Inlet. Thus, temperature anomalies occurred outside the core window of productivity (June–August) for forage fish and seabirds in both 1997 and 1998. Abundance or production of phytoplankton, zooplankton, fish, and seabirds in lower Cook Inlet varied among years, and overall appeared to be depressed in 1998. We observed a few biological anomalies that might be attributed to ENSO effects: (1) a significant die-off of Common Murres occurred in March–May of 1998, (2) murres and Black-legged Kittiwakes were physiologically stressed during the 1998 breeding season, (3) murres failed to reproduce at one colony in 1998, (4) kittiwake breeding success was lower than usual at colonies in 1998, and (5) phenology of breeding was later in 1998 for both murres and kittiwakes. We presume that seabird die-offs, reduced productivity and delayed phenology were linked to a reduction or delay in food availability, but the mechanism by which anomalously warm water temperatures in winter reduce forage fish availability during the summer breeding season for seabirds is not known.

Oceanography

The 1997/98 ENSO was well developed at the equator by July of 1997. Anomalously warm sea surface temperatures (SSTs) developed rapidly during June in the GOA and Bering Sea, presumably via atmospheric tele-connection with the tropics. SST positive anomalies of 2°C in the GOA persisted throughout summer of 1997 (Figure 1), diminished to ~1°C in October; and persisted until May/June of 1998. Water temperatures at depth (0–250 m) differed markedly from surface temperatures during summer of 1997. Warming of deeper waters started much later (September) and peaked in February/March of 1998. In lower Cook Inlet, effects of the 1997/98 ENSO were ameliorated by upwelling and tidal mixing at the entrance to Cook Inlet. Whereas the northern GOA was well stratified during summer of 1997 and capped by warm surface layers, strong upwelling occurs around the Kodiak Archipelago and at the entrance to Cook Inlet, leading to complete mixing of the water column and reduced surface temperatures in these areas (Figure 2). Cold, mixed waters are carried north by prevailing currents far into Cook Inlet. Strong tidal mixing limits stratification to protected areas such as Kachemak Bay where river outflows create shallow lenses of warm, low-salinity water at the surface. On the west side of Cook Inlet, currents flow south and

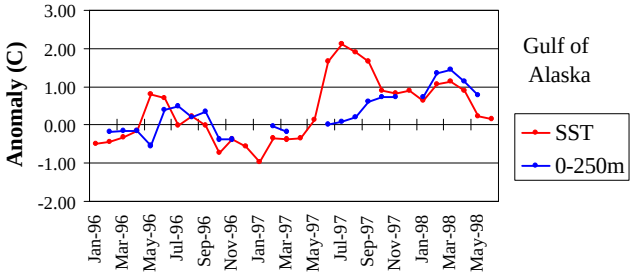

Figure 1. *Temperature anomalies at the surface and over the entire water column in the Gulf of Alaska from January 1996 to May 1998.*

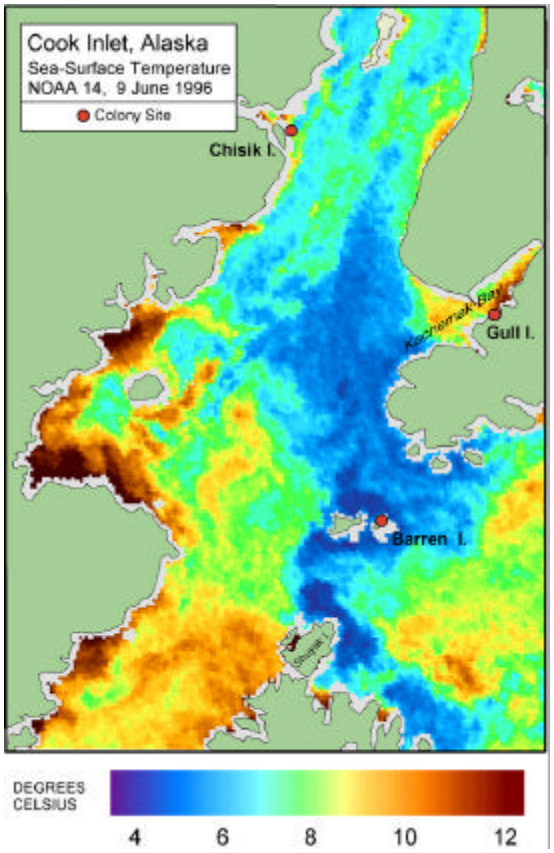

Figure 2. *AVHRR image showing sea surface temperatures in Cook Inlet and seabird colonies under investigation.*

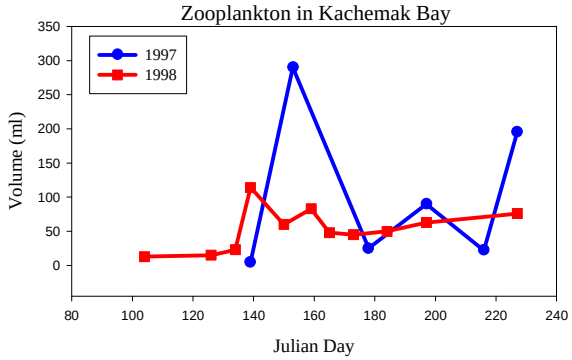

Figure 3. *Sea surface temperatures (5 m below low-low tide) in Kachemak Bay, Cook Inlet, Feb. 1996 to Aug. 1998. Mean daily temperatures smoothed with 7-day running average.*

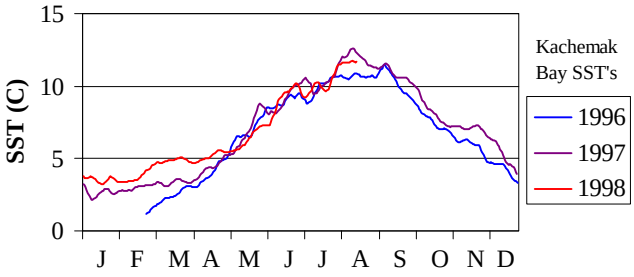

waters are weakly stratified, warmer and less saline. Although they differ slightly in absolute temperature, SSTs from Kachemak Bay, Chisik (on the west side, Figure 2) and the Barren Islands (entrance to Cook Inlet) show similar seasonal and annual SST trends. As a consequence of this oceanographic regime, SSTs in Kachemak Bay (Figure 3) do not reflect SSTs in the outer GOA; instead they reflect temperature fluctuations of the entire GOA water column (Figure 1). SSTs in Kachemak Bay and the GOA during 1996 were about average most of the year. The large SST anomaly observed in the GOA during June–August of 1997 (Figure 1) was not observed in Kachemak Bay (Figure 3) or at Chisik and Barren islands. SSTs in Kachemak Bay began to increase in August 1997 and were 1–2°C higher than average throughout fall and winter; returning to average in May of 1998. As for GOA temperatures at 0–250 m depth, SSTs in Kachemak diverged most from average values during February and March of 1998 (Figure 3).

Biological Effects

Plankton

We began monitoring phytoplankton and zooplankton abundance in 1997. Phytoplankton concentrations were measured using a CTD with attached fluorometer. Zooplankton were collected seasonally at a single station in Kachemak Bay, and we measured settled volumes to estimate abundance (Figure 4). Primary and secondary production in Kachemak Bay varied among and between seasons, but with only two years of data we can only conclude that there was no indication of any dramatic ENSO effects (e.g., total production failure) in either year. However, maximum zooplankton volumes in 1998 were about a third of those observed in 1997.

Fish

Fish were sampled in both Kachemak Bay and around Chisik Island using a modified herring midwater trawl (July) and beach seines (June–Aug.), and in Kachemak Bay using a small bottom trawl (Aug.). The same gear and methods were used in all years of study. We targeted small forage fishes consumed by seabirds. More than 300,000 fish comprising over 60 species have been caught on these surveys. Dominant taxa include juvenile pollock, sand lance, osmerids, and herring. In general, fish

Figure 4. *Seasonal variation in zooplankton volume in Kachemak Bay during 1997 and 1998. Zooplankton were collected using a 1-m ring net with 505 micron mesh.*

catches are much higher in Kachemak Bay (Figure 5a) than around Chisik Island (Figure 5b) owing to regional differences in productivity. Catches of forage fish increased in Kachemak Bay, but decreased around Chisik Island, between 1997 and 1998. Catches in both areas in 1997/98 were higher or similar to those observed in 1996. However, trawl catches are highly variable and biased because we conduct trawls only where hydroacoustic signals indicate the presence of fish. Analyses of hydroacoustic data (in prep.) suggest that biomass of fish was reduced in most areas of Cook Inlet in 1998. Beach seines suggest that fish were delayed in arriving nearshore in 1998.

Seabird Productivity

Here we consider two species (Common Murres and Black-legged Kittiwakes) from colonies at Chisik Island and Gull Island. Murres maintained relatively high productivity among all years of study at Gull Island in Kachemak Bay (Figure 6). Diets were similar among years, and analyses of time budgets (foraging trip duration, "loafing time") suggest that murres had no difficulty finding food in 1997 or 1998. At Chisik Island, however, murres experienced a complete breeding failure in 1998 (Figure 6). They started breeding later than usual (Figure 7), displayed erratic attendance, and had significantly higher levels of stress hormones in their blood plasma in 1998 than in 1997 (Figure 8). Complete breeding failure is rare in murres because they can compensate for wide fluctuations in food supply by

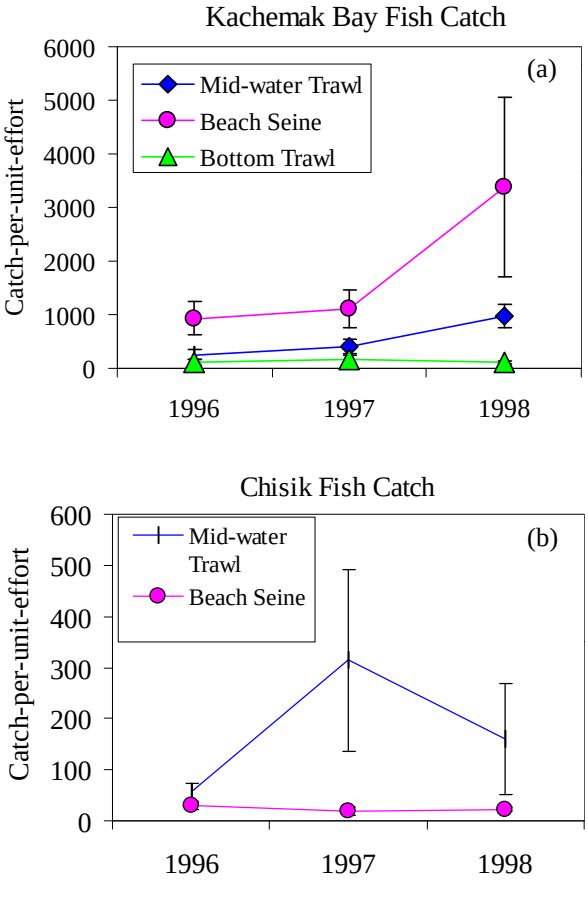

Figure 5. *Catches of fish in mid-water trawls, beach seines and bottom trawls: (a) in Kachemak Bay and (b) around Chisik Island, 1996–1998.*

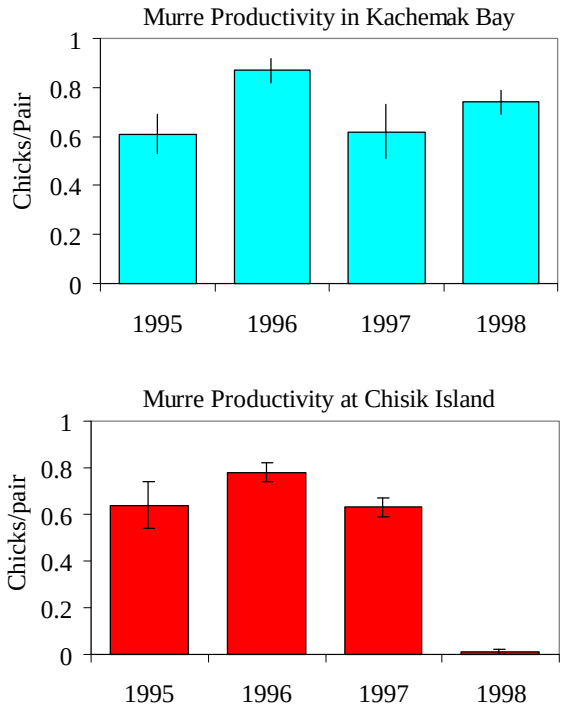

Figure 6. *Breeding success of Common Murres in 1995–1998.*

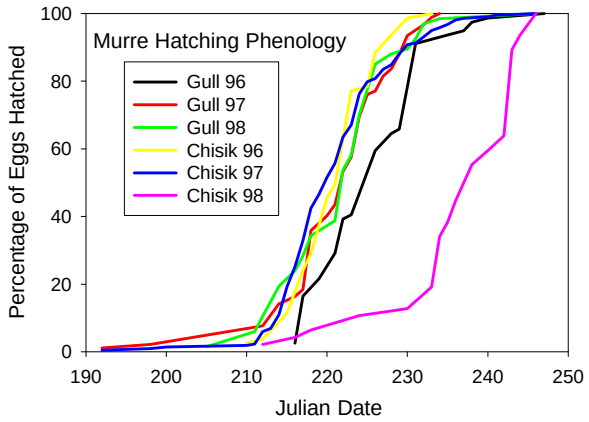

Figure 7. *Phenology of egg hatching in murres at Gull and Chisik islands, 1996–1998.*

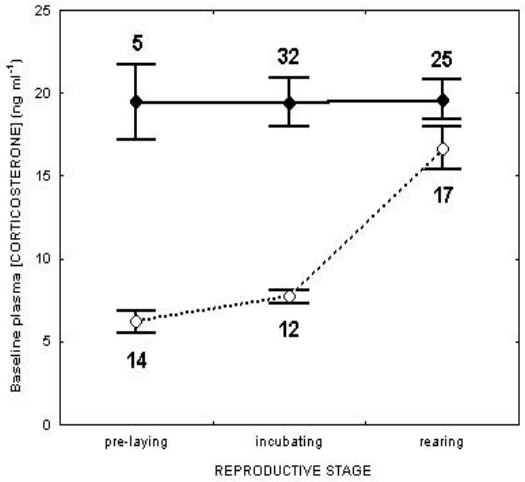

Figure 8. *Stress hormone levels in murres at Chisik during a 'normal' year (1997, open circles) with seasonal increase in food stress, and ENSO year (1998, closed circles) with high stress load at beginning of the breeding season.*

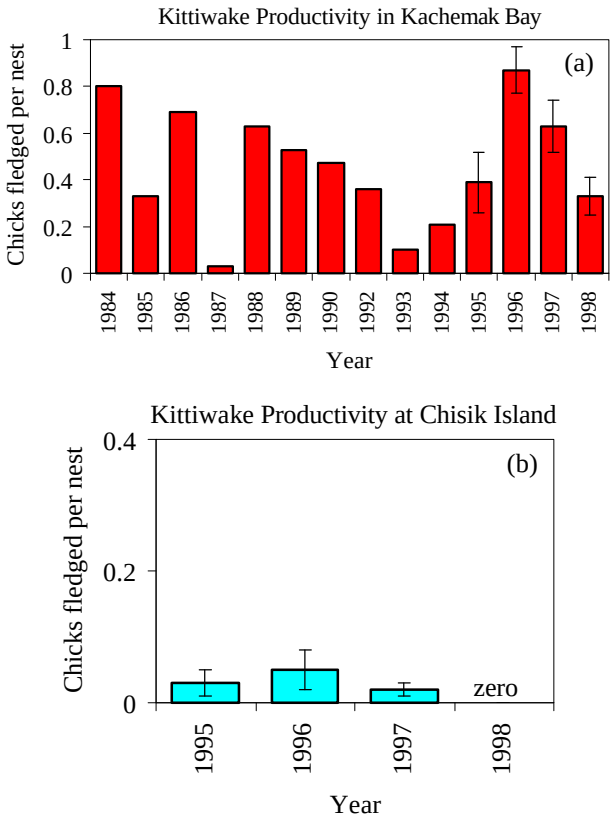

Figure 9. *Breeding success of Black-legged Kittiwakes at (a) Gull Island, Kachemak Bay and (b) Chisik Island.*

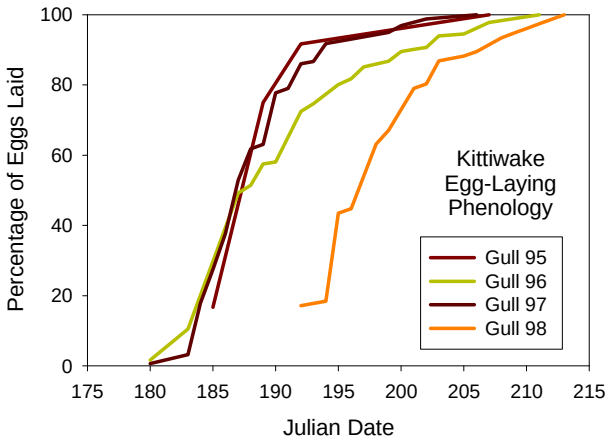

Figure 10. *Phenology of kittiwake egg-laying on Gull Is., 1995–1998.*

adjusting their time budgets – which is why they usually manage to produce chicks at Chisik despite poor food supplies. We therefore view the delayed phenology and subsequent breeding failure of murres at Chisik in 1998 as particularly significant.

In contrast, kittiwake breeding success is typically more variable and sensitive to fluctuations in food supply. In Kachemak Bay, kittiwake breeding success was much reduced in 1998 compared to 1996/1997 – but fell within range of variability observed in previous years of study (Figure 9a). However, notable low production events in the past also correspond to years with moderate ENSO warming of winter water temperatures in Alaska (1987, 1993, 1994). Low production in 1998 was largely due to low laying and hatching success, which was about 3 weeks later than usual (Figure 10). Once hatched, chick survival was high. At Chisik Island, kittiwakes have always done poorly in recent years (Figure 9b). Evidence suggests this is because of generally poor food supplies around Chisik and because, in contrast to murres, kittiwakes cannot adjust their time budgets to deal with fluctuations in food supply, nor can they range as far to find food. The 1998 breeding season at Chisik was notable because birds failed much earlier than usual (during incubation), phenology of egg laying was about 2–3 weeks later than usual, and adults produced absolutely zero chicks.

Seabird die-offs

A large and extensive seabird die-off was observed in Alaska during summer 1997; largely confined to the southern Bering Sea and Aleutians. Surface-feeding species such as shearwaters (and much lesser numbers of kittiwakes) died *en masse* from apparent starvation. Some hundreds of thousands of birds were probably affected, and peak mortality occurred in August when SST anomalies were highest. Smaller die-offs of murres were also reported from the northern Bering Sea, mostly in May and June. Although SST anomalies were also high in the GOA during the summer of 1997, no die-offs were reported there. In 1998, however, a moderate die-off of Common Murres was observed in the northern GOA. Dead murres were reported over a wide area (Figure 11) from about March through May, with peak mortality occurring in mid-April. This followed a long period of anomalously warm water temperatures in the GOA (Figure 1). Most murres were apparently subadult (non-breeders) and died of starvation. A preliminary tally indicates that at least 1300 dead murres were observed on beaches in the GOA. Previous studies indicate this would be a small fraction of the total mortality, which probably numbered in the tens of thousands. The most recent large seabird die-off observed in the GOA occurred during late winter of 1993 following a prolonged period of anomalously warm SSTs associated with the 1992/93 ENSO. In that die-off, about 120,000 murres died from starvation in the northern GOA.

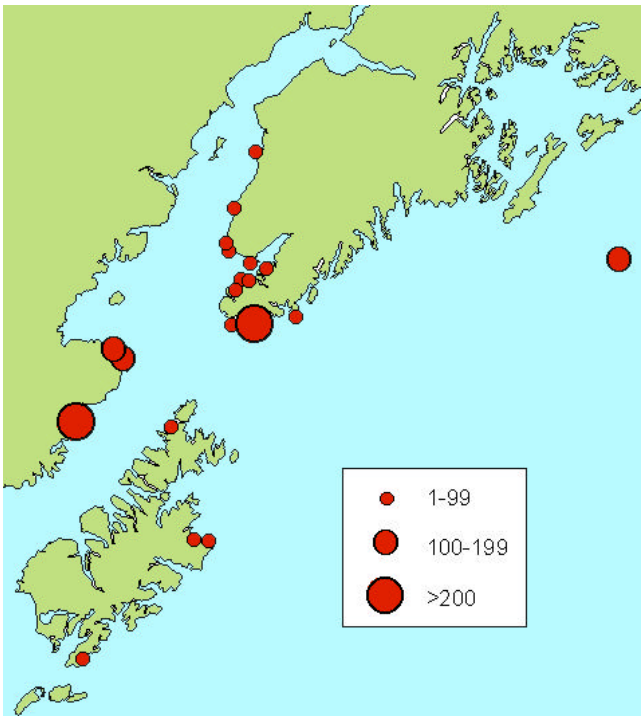

Figure 11. *Distribution of dead murres recovered from beaches in the northern Gulf of Alaska during March–May, 1998.*

The 1997–98 EL Niño in the Bering Sea as Compared with Previous ENSO Events and the "Regime Shift" of the Late 1970's

H.J. Niebauer
Atmospheric and Oceanic Science
Univ. Wisconsin-Madison, Madison
WI 53706-1695
U.S.A.
e-mail: niebauer@sunset.mateor.wise.edu

The Bering Sea undergoes exceptional seasonal as well as extreme interannual variability. In the mean, winter sea ice advance exceeds 1000 km while in summer the Bering Sea is ice free. However, interannual ice variability is as great as 400 km.

The interannual variability of the Bering Sea depends in large part on the winter variability of the Aleutian low. Results of analyses (e.g., Niebauer, 1988) of the Aleutian low, monthly mean ice cover from the Bering Sea, and the Southern Oscillation Index (SOI), show that before a regime shift in the late 1970s, below normal ice cover in the Bering Sea was typically associated with El Niño. That is, El Niño conditions caused the Aleutian low to move eastward of normal carrying warm Pacific air from the south over the Bering Sea. Sea and air temperatures were above normal under winds from the south or less strongly from the north. Conversely, above normal ice cover was associated with La Niña conditions which caused the Aleutian low to move westward of normal allowing higher pressure to move over the Bering Sea. Sea and air temperatures were below normal under stronger winds from the north.

In the late 1970's, a "regime shift" or "step" occurred in the climate of the north Pacific causing, among many other effects, a 5% reduction in the ice cover in the eastern Bering Sea (Figure 1) as well as shifts in the position of the Aleutian low. The overall reduction in ice cover can be traced to an overall increase in El Niño conditions which has resulted in an increase in the influence of the Aleutian low over the eastern Bering Sea (Niebauer, 1998). However, during El Niños since the regime shift, the Aleutian low has been moving even farther to the east causing winds to blowfrom the east and north off Alaska instead of from the south. This has caused ice advance during El Niños (as during this last El Niño of 1997–98) whereas before the regime shift, the ice retreated during El Niño (Niebauer, 1998).

This shift in the organization of ENSO (El Niño–Southern Oscillation) events has had a strong effect on the statistical correlation between the Southern Oscillation Index and Bering Sea ice cover. This Aleutian low movement has caused the correlation

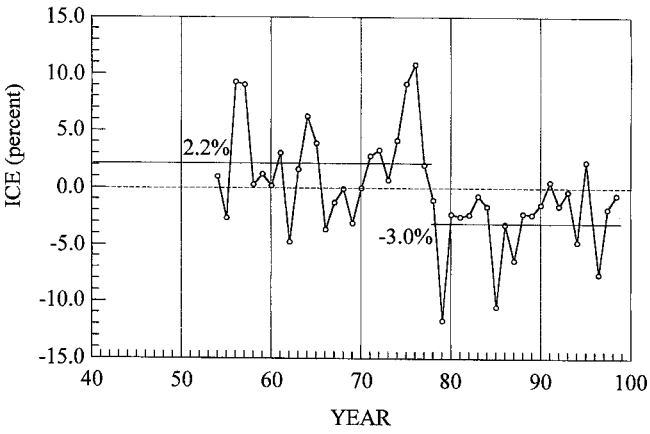

Figure 1. *Winter averaged (NDJFM) percent ice cover anomalies for the Bering–Chukchi Seas for the period 1954–98. Average anomalies for the periods 1954–77 and 1977–98 are also shown. The difference in the means is statistically significant at the 0.005 level. For comparison, standard deviations of ~6.6% and ~4.8% were obtained for the 44-year long monthly mean and winter mean sea ice anomalies time series respectively (After Niebauer, 1998).*

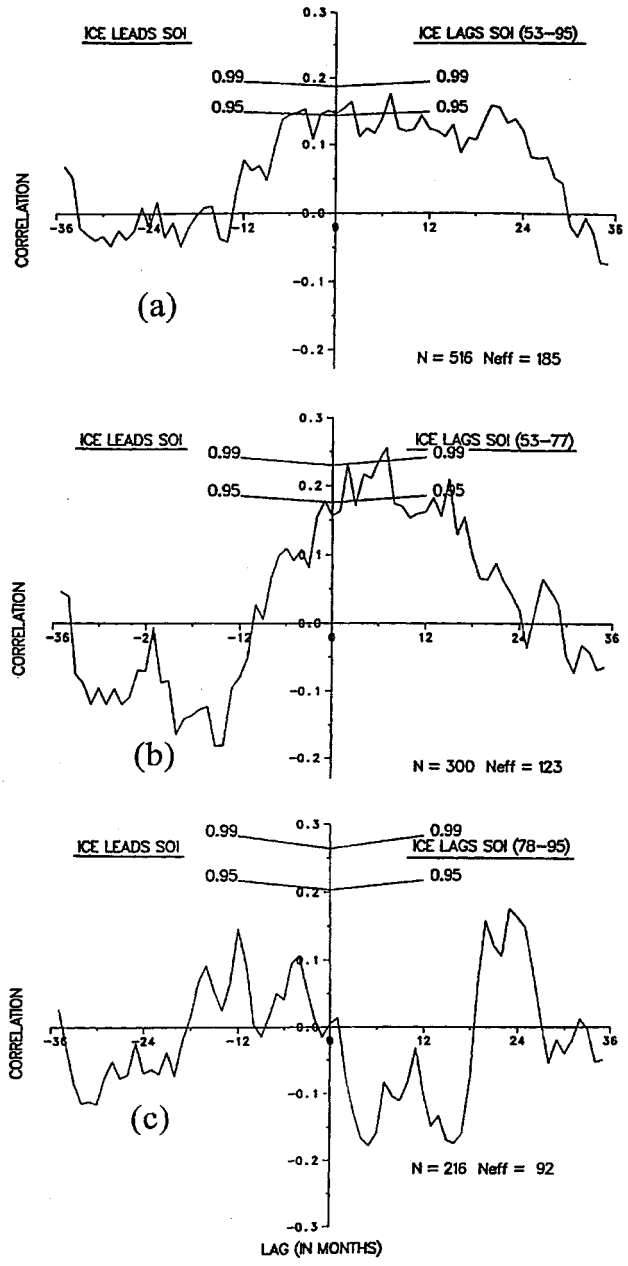

Figure 2. *Cross-correlation plots of monthly mean Bering Sea time series SOI = southern oscillation index vs. ICE = sea ice. Panel (a) is for 1953–95, panel (b) is for 1953–77, and panel (c) is for 1978–95. The x-axis is the lag in months between data sets. N is the number of data points while, Neff is the number of effective or independent data points available for use in calculating the significance levels shown on each plot as calculated via Trenberth (1984) and Zar (1984) (From Niebauer, 1998).*

of ice with the SOI to change sign compared to before the "regime shift" (Niebauer, 1998). For the period 1953–78 (i.e., before the regime shift), the correlation coefficient was positive (less ice during and following El Niño, and more ice during and following La Niña) with ice lagging the SOI by ~7 months (Figure 2).

In strong contrast, after the regime shift, for the period 1978–95, the correlation coefficient changes sign (Figure 2). The change in sign of the correlation means that since the regime shift, **decreases** in ice are now associated with El Niño events. An important point (as outlined above) is that this is consistent with El Niño-associated Aleutian lows becoming even more intense and moving even farther east following the regime shift. These more easterly Aleutian low pressure patterns are forcing winds northward off the Pacific into interior Yukon/Alaska where the winds turn westward carrying continental air out over the Bering Sea. Before the regime shift, during El Niño, the Aleutian low was not so far east so that the northward winds carried warm north Pacific air over the Bering Sea.

In considering the specific example of this latest El Niño of 1997–98, in the mean, during the winter the Aleutian low was more intense and eastward of normal in teleconnection with the Southern Oscillation. However, in November and again in March, the Aleutian low was directly over the Bering Sea causing strong below normal ice conditions in November and slightly below normal ice conditions in March and April (Figure 3). But in December, January and February, the Aleutian low moved so far to the east that winds over the Bering Sea were from the northeast resulting in above normal ice conditions as well as colder than normal air and sea temperatures under abnormally cool winds (Figure 3).

This relationship between SOI and ice provides the possibility of predicting ice conditions because of this long duration lag of statistically significant correlation (Figure 2), and because of (or perhaps in spite of) the change in sign of correlation between ice and SOI through the climate shift.

Before the regime shift, the occurrence of El Niño and La Niña conditions was about even. Since the regime shift, El Niño conditions are about 3 times more prevalent (Niebauer, 1998). The result is a general warming of the Bering Sea associated with the 5% decrease in ice cover. There is evidence (Mantua et al., 1997; Minobe, 1997) that this regime

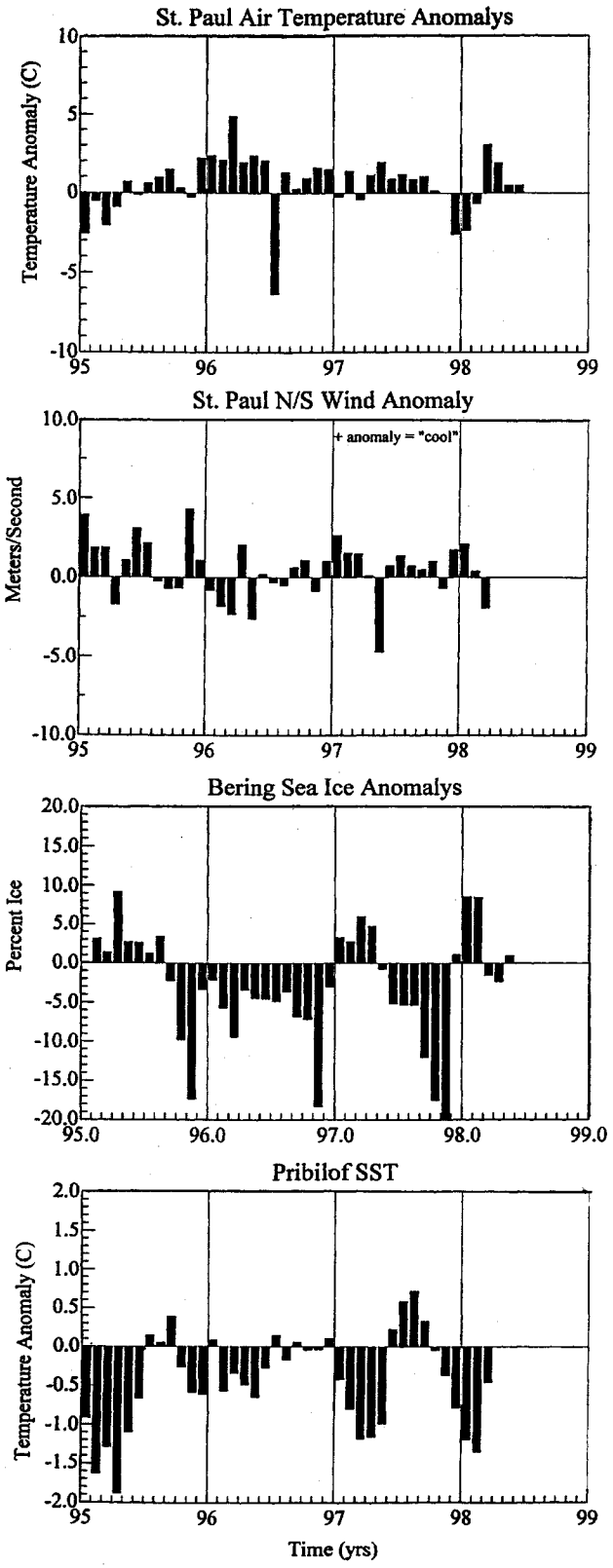

Figure 3. *Monthly anomalies of Bering Sea air temperatures (top panel), surface winds (second panel), sea ice (third panel) and sea surface temperature (bottom panel) for the period 1995 to ~mid-1998.*

shift is the latest in a series of climate shifts going back to at least the late 1800's, and may be due to a 50–70 year oscillation in a north Pacific atmospheric–ocean coupled system.

ENSO events are probably not the only phenomena causing interannual variability in the Bering Sea. In addition to ENSO events, the atmospheric circulation over the North Pacific is probably also sensitive to local SST anomalies. In some winters, the atmospheric teleconnection mode called the Pacific-North American pattern (PNA), and/or the Western Pacific oscillation (WPO or WP), a north–south dipole over the western north Pacific, are prominent, with substantial effects on the Aleutian low.

Acknowledgements This research was sponsored by NOAA Coastal Ocean Program through Southeast Bering Sea Carrying Capacity. Support was also provided by the University of Alaska-Fairbanks Cooperative Institute for Arctic Research (CIFAR/NOAA) grant CIFAR 97-102R (Arctic Research Initiative). The support of the Department of Atmospheric and Ocean Science, University of Wisconsin-Madison is gratefully acknowledged.

References

Mantua, N.J., S.R. Hare, Y. Zhang, J.M. Wallace and Francis, R.C. 1997. A Pacific interdecadal climate oscillation with impacts on salmon production. *Bull. Amer. Meteor. Soc., 78,* 1069–1079.

Minobe, S. 1997. A 50–70 year oscillation over the north Pacific and north America. *Geophys. Res. Lett., 24,* 683–686.

Niebauer, H.J. 1988. Effects of El Niño–Southern Oscillation and North Pacific weather patterns on interannual variability in the subarctic Bering Sea. *J. Geophys. Res., 93,* 5051–5068.

Niebauer, H.J. 1998. Variability in Bering Sea ice cover as affected by a "regime shift" in the north Pacific in the period 1947–96. *J. Geophys. Res., 103(C12),* 27,717–27,737.

Trenberth, K.E. 1984. Signal versus noise in the southern oscillation. *Mon. Weather Rev. 112,* 326–332.

Zar, J.H. 1984. *Biostatistical Analysis*. 2nd ed., Prentice Hall, Englewood Cliffs, N.J., 718 pp.

The State of the Far East Seas during the 1997/98 El Niño Event

A.S. Krovnin,[1] G. P. Vanyushin,[1] M. Yu. Kruzhalov,[1] G.V. Khen,[2]
M.A. Bogdanov,[1] E.I. Ustinova,[2] V.V. Maslennikov,[1] A.M. Orlov [1]
B.N. Kotenev,[1] V.V. Bulanov[1] and G.P. Muriy[1]

[1] *Russian Federal Research Institute of Fishery and Oceanography (VNIRO)*
17 V. Krasnoselskaya, Moscow 107140, Russia
e-mail: akrovnin@mx.iki.rssi.ru

[2] *Pacific Research Fisheries Centre (TINRO-Centre)*
4, Shevchenko Alley, Vladivostok 690600, Russia

Oceanographic conditions, mainly temperature fields, in the Bering and Okhotsk Seas in 1997/98 are compared with those in previous, non-El Niño years (1995–1996). The study is based on monthly sea surface temperature (SST) maps constructed at the Russian Federal Research Institute of Fishery and Oceanography (VNIRO) as part of the program on the use of satellite and ship data to monitor the dynamics of SST in various fishing areas of the world ocean. The main purpose of the program is to provide the Russian fishery community with operative and monthly information on the state of environment in regions where the Russian fleet operates. Also, data of several oceanographic surveys conducted in the western Bering Sea in 1995–1997 are used. Figure 1 demonstrates the variability in mean monthly SST anomalies in the Northwest Pacific for 1997.

As is seen, the El Niño signal appeared in April, 1997 and reached it maximum in October, when positive SST anomalies in the central Sea of Okhotsk and northwestern Bering Sea exceeded 3°C. Figure 2 shows differences in mean winter (left panel) and mean summer (right panel) SST and sea level pressure (SLP) values between 1996 and 1995, 1997 and 1996, 1998 and 1997.

The maps allow one to identify some features of climatic variability in the region for 1996–1998. The warming started in winter, 1996 and was observed on most of the investigated region. The only exception was the area off Kamchatka, at the northwestern part of the Bering Sea, and the eastern

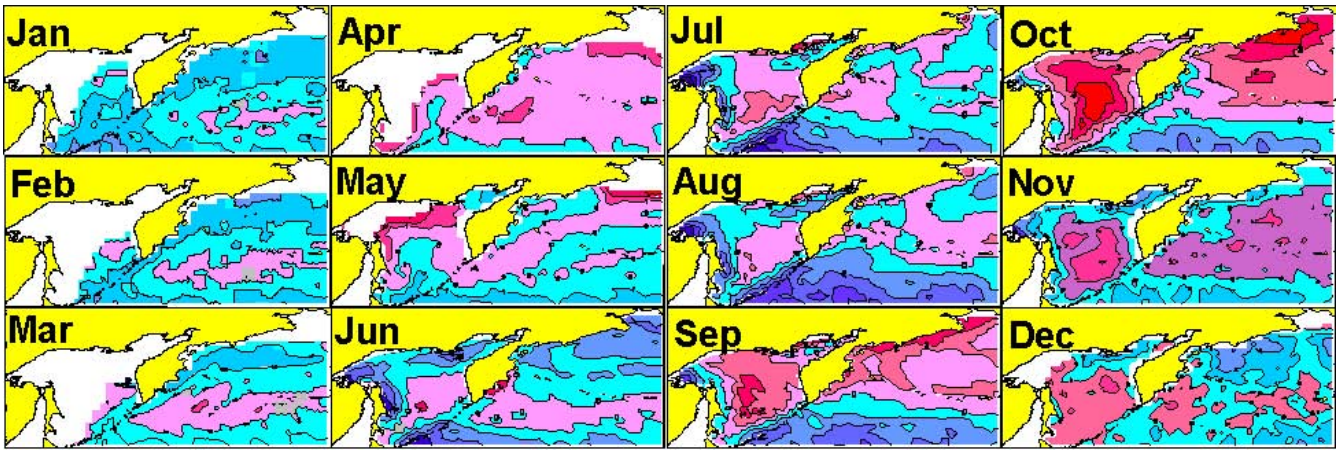

Figure 1. *Variability of SST anomalies in the Northwest Pacific during 1997 (by satellite data).*

Sea of Okhotsk. In 1997 warming was observed in the whole Northwest Pacific, including the Bering and Okhotsk Seas. Positive differences between 1996 and 1997 exceeded 1.0–1.5°C. Quite the opposite situation was noted between the cold seasons of 1998 and 1997. In fact, SST decreased over the whole Northwest Pacific (about 1–2°C), and ice cover area increased.

These changes in SST patterns corresponded to changes in the character of the atmospheric circulation. Thus, if in 1996 the northwestern Bering Sea was affected by the northeastern periphery of the Siberian High with a prevalence of the northern winds and corresponding decrease in SST, in 1997 this part of the sea was under influence of the eastern periphery of a large cyclonic formation with predominately southern winds. In 1998 the atmospheric situation was very similar to that of 1996 (Figure 2, left panel).

The development of atmospheric and oceanic processes in the summer seasons of 1996–1998 was somewhat different from that in winter (Figure 2, right panel). The clear lessening of the East Kamchatka Current was observed in 1996. Compared with 1995, 1996 showed positive SST differences of 1–2°C in its core. The same situation was observed in summer, 1997. Differences in mean summer SST between 1997 and 1996 in the western Bering Sea exceeded 3°C. However, cooling that started in the Northwest Pacific in 1998 was more pronounced in summer than in winter. A decrease in SST in Anadyr Bay and off Navarin Cape in the Bering Sea exceeded 3°C

Changes in ice conditions during 1996–1998 were also considered which allowed one to identify some anomalous events occurring in the Bering and Okhotsk Seas during the El Niño in 1997 (Figures 3 and 4).

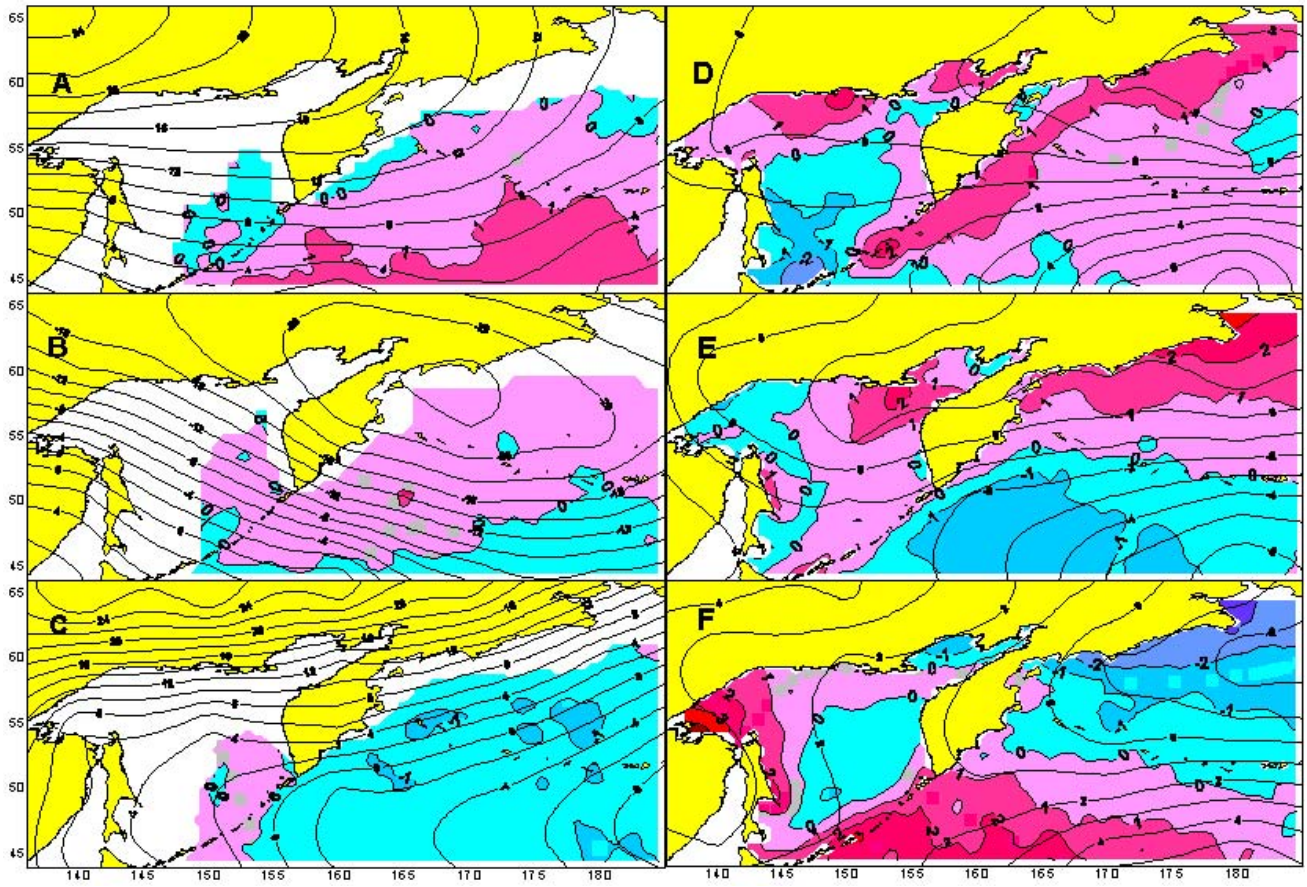

Figure 2. *Differences in mean winter (left panel) and mean summer (right panel) SST and SLP values between (A, D) 1996 and 1995, (B, E), 1997 and 1996, and (C, F) 1998 and 1997.*

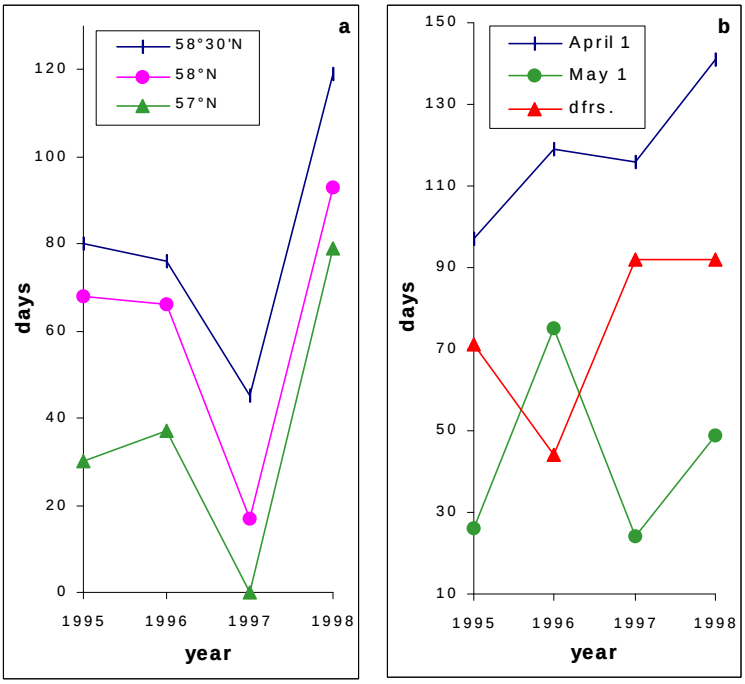

Figure 3. *Duration of the ice period in the eastern Sea of Okhotsk ("eastern channel") at (a) different latitudes and (b) numbers of 1° ´ 1° squares covered by ice on April 1 and May 1 and their differences for 1995–1998.*

For example, in 1997 the northern boundary of the so called "eastern channel" (aquatory permanently free of ice during the cold season in the eastern Sea of Okhotsk) did not cross 57°N, while in 1998 the boundary was located south of this latitude for 80 days (Figure 3a). The rate of decreasing ice area in the sea was highest in 1997–1998 compared with 1995–1996, as is demonstrated by differences in the number of 1° × 1° squares covered by ice between April 1 and May 1 (Figure 3b).

Duration of the ice period around St. Matthew Island in the Bering Sea decreased beginning in 1996, and in 1998 it equaled 48 days compared with 138 days in 1996 (Figure 4a). 1997 was also characterized by the early retreat of the ice boundary to the north of 63°N in both the western and eastern Bering Sea. If, in 1996, ice boundary crossed the western Bering Sea at 63°N in mid-June, in 1998 this occurred in the third ten-day period of April (Figure 4b). Thus, the difference was about 55 days. Also, in the western region of the sea a decrease in the ice cover area in 1997 started on February 17, while in 1996 it began on April 15, and in 1998, on March 15 (Figure 4c).

Results of joint Russian–Japanese surveys conducted in June and September, 1997 onboard of Japanese trawler *Tenyo Maru 78* in the northwestern Bering Sea showed some significant anomalies in the development of oceanographic conditions. First, the core of Warm Intermediate Layer (WIL), in both June and September, was located at depths of 320–370 m which was by 30–100 m shallower than that found from Arsenyev's data (1967) and by 50–100 m shallower compared with values given in the atlas prepared by Sayles et al. (1978). Along with the rising of the core, an increase in WIL temperature and a decrease in its salinity were observed. The values of sea water temperature in the WIL core along the 180° meridian were 3.80–4.00°C, while in previous years the temperatures did not exceed 3.70–3.75°C. Salinity decreased by 0.05 psu and greater. The mean long-term salinity in the region is 33.80 psu. In 1997 its mean values were only 33.72 psu. Such a decrease in salinity is possibly associated with the change in the character of WIL transformation in the Olutorsky-Navarinsky region. Oceanographic parameters in this region are similar to those for the Pribyloff-Matthew continental slope.

In all, positive sea water temperature anomalies in 1997 were about 1.0–1.5°C in the surface layer, 0.5–0.7°C in the core of Cold Intermediate Layer, and 0.1–0.3°C in the Warm Intermediate Layer.

El Niño effects were apparently observed in the western Bering Sea in 1998 as well. Despite the sur-

face thermal conditions in this region being close to normal, temperature values in WIL remained high. Along the continental slope off the Koryaksky coast and Navarin area values exceeded 3.80°C. As in 1997, the location of the WIL core was exclusively shallow, 230–280 m (cruise of *R/V Professor Kaganovsky*, August–November, 1998). In 1998 the significant lessening of the Kamchatka Current was also observed. There was a negative water exchange balance via the Kamchatka Strait between the Bering Sea and North Pacific: in the 0–1000 m layer outflow equaled 0.97 Sv, while inflow was 1.52 Sv, and the resulting flow was –0.55 Sv. Even taking into account the seasonal lessening of the Kamchatka Current, the result is amazing.

We consider that one of the 1997/98 El Niño effects was an appearance of a typically American fish species to the Asian coast. In 1997, rex sole (*Errex zachirus*) which was recorded there only once (Kulikov, 1964) spread over almost the entire basin (Figure 5a). Compared with previous years, large-sized (mean length 54.8 cm) arrowtooth flounder (*Aterestes stomias*) also became a widely common species in the western Bering Sea (Figure 5c). According to similarity of the size composition of both the species with that in the eastern Bering Sea, we could assume that the warming associated with the El Niño event led to an extension of these species westwards.

In 1997–1998, a large record number of northern rockfish (*Sebastes polyspinis*) (Figure 5b) and dusky rockfish (*Sebastes ciliatus*) (Sheiko and Trabenkova, 1998) occurred in Pacific waters off the northern Kurils; these waters also revealed juvenile arrowtooth flounder (Figure 5d) and sablefish. Earlier, all the four species were never registered, or were accidentally caught there. Because these species have pelagic larvae and juveniles, one can suppose their larvae or juveniles were transported from the Aleutian area to the North Kurils by currents in previous years. However, they were not recorded off the Kurils earlier. The similarity in size composition of captured fish with those off the Aleutian Islands may indicate their Aleutian genesis.

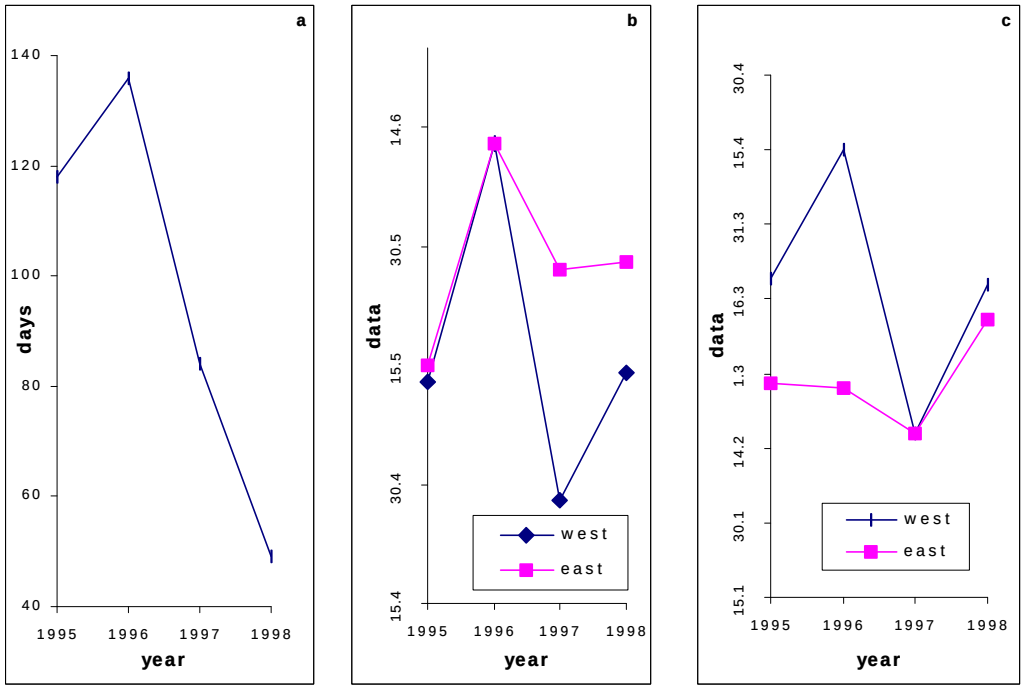

Figure 4. *(a) Duration of the ice period around St. Matthew Island; (b) dates when the ice boundary crossed 63°N; (c) dates when the ice cover started to decrease, in the Bering Sea.*

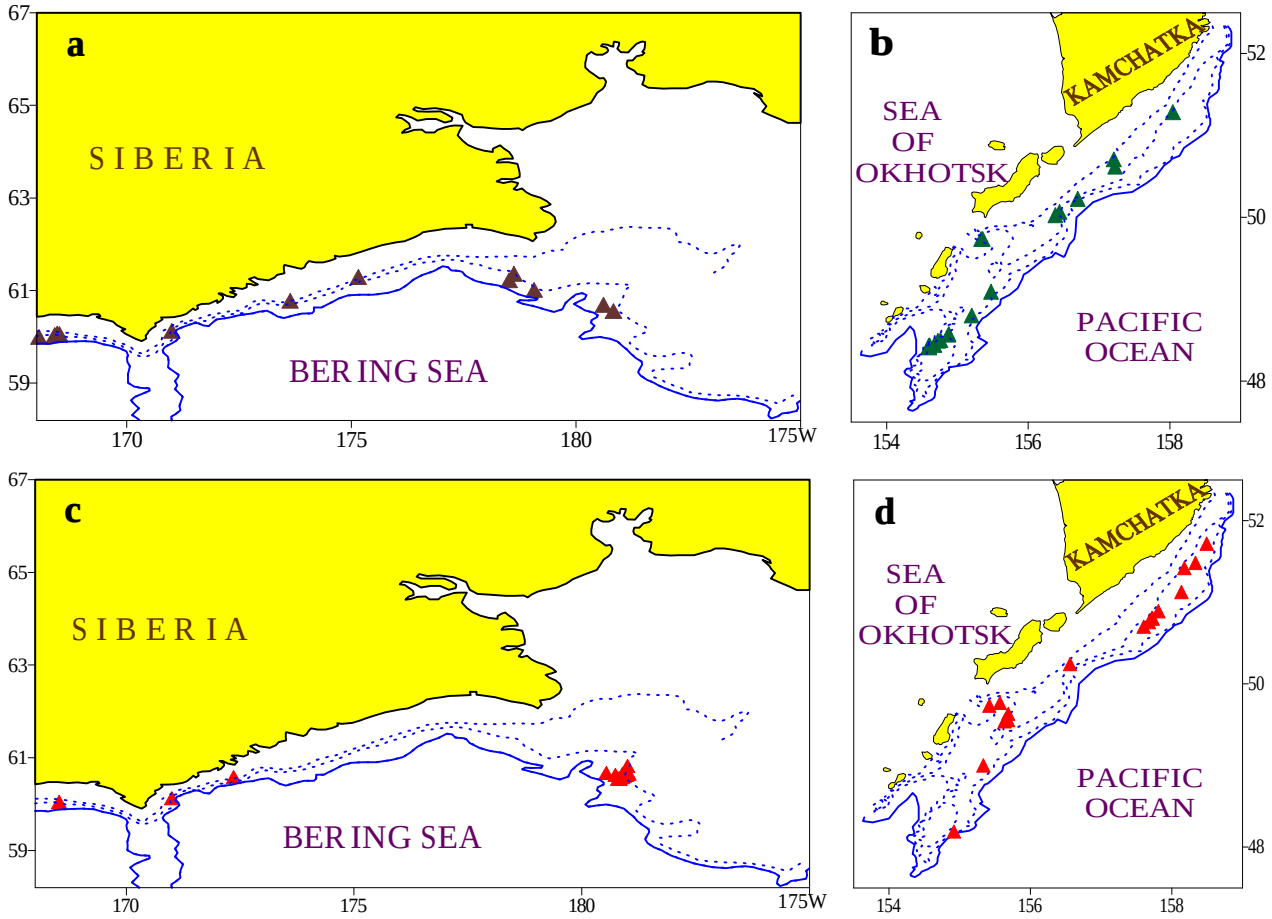

Figure 5. *Records sites (triangles) of (a) rex sole and (c) arrowtooth flounder in the western Bering Sea in 1997, and (b) northern rockfish and (d) arrowtooth flounder in Pacific waters off the North Kurils and southeast Kamchatka in 1998. The continuous line shows the 1000-m isobath.*

References

Arsenyev, V.S. 1967. *Currents and Water Masses*. Nauka, Moscow, 133 pp. (in Russian)

Kulikov, M.Yu. 1964. The First Record of Rex Sole *Errex zachirus* (Lock) off the Asian Coast of the Bering Sea. Izvestiya TINRO, vol. *55*, p. 245. (in Russian)

Sayles, M.A., Aagaard, K. and Coachman, L.A. 1978. *Oceanographic Atlas of the Bering Sea Basin*. Univ. of Washington, 158 pp.

Sheiko, B.A., and Trabenkova, A.G. 1998. New for Russian fauna and rare marine fishes from Kamchatka, Kuril and Commander Islands. pp 62–63 *in* Actual problems of fish taxonomy. Abstracts of conference St. Petersburg, Zoological Institute of Russian Academy of Science.

Phytoplankton Collected by a Time-Series Sediment Trap Deployed in the Southeast Bering Sea during 1997

Stacy Smith and Susan Henrichs
University of Alaska Fairbanks
Alaska, U.S.A.
e-mail: sstacy33@ims.uaf.edu

Introduction

The Bering Sea shelf, over 500 km wide, is separated into three distinct biological regimes (inner, middle and outer shelf areas) by density fronts. Its middle shelf (located between the 50- and 100-m isobaths) averages 30–50 g C m^{-2} $year^{-1}$ in new production, derived mainly from the annual spring bloom in April and May. Two unusual events occurred over the middle shelf in 1997: The first was an intense though short-lived midsummer bloom of mainly small diatoms; the second was the first-ever-recorded coccolithophorid bloom. Anomalous sea surface temperatures - possibly due to El Niño and a relatively storm-free summer – could be the cause of these events.

Methods

We deployed a time-series sediment trap at 35 m depth from April 1997 through February 1998. The deployment site was Mooring 2 (Figure 1) on the southeast Bering Sea middle shelf region where the bottom depth was 70 m. The trap was outfitted with a rotating carousel containing 12 sample tubes for sub-sampling. Trap sub-sample intervals lasted either one or two weeks. The number of phytoplankton in each sample was counted (Figure 2). The $\delta^{15}N$ and $\delta^{13}C$ of each sub-sample were measured. Also, a scanning electron microscope was used to identify the coccolithophorid, *Emiliania huxleyi* (Figure 2).

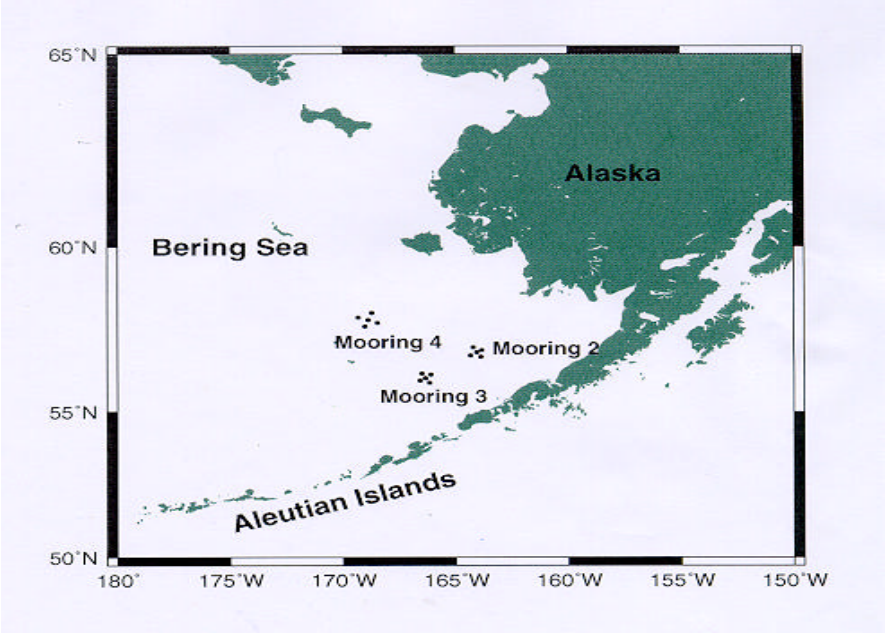

Figure 1. *Location of mooring site 2 in the southeast Bering Sea.*

(a)

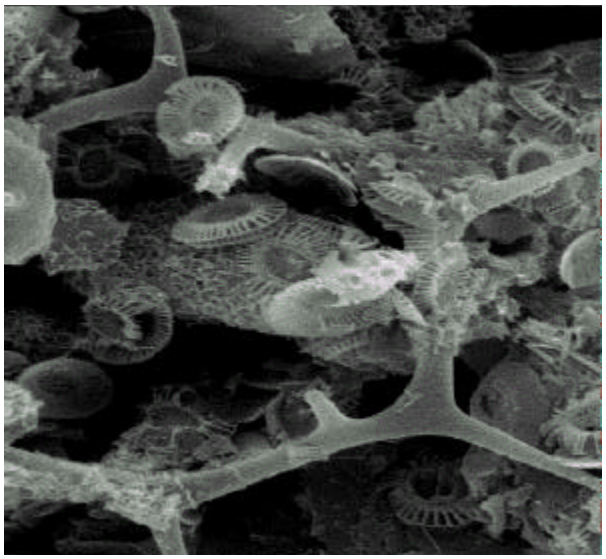

(b)

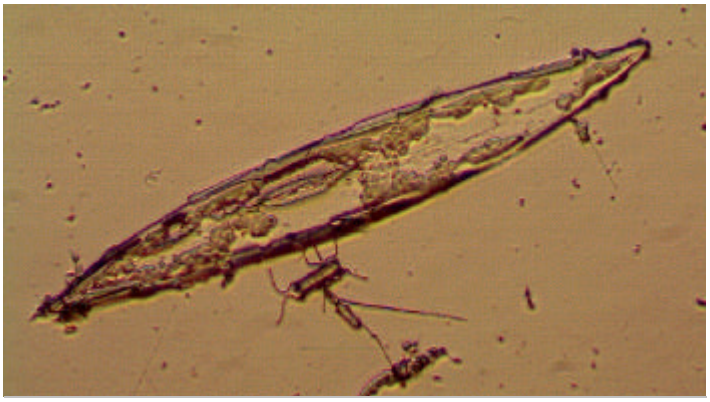

Figure 2. *Phytoplankton derived from the spring, summer and fall blooms over the Bering Sea middle shelf included diatoms, flagellates and coccolithophores. (a) A silicoflagellate is surrounded by scores of 2-mm Emiliania huxleyi coccoliths. (b) A 400-mm diatom Pleurosigma simonsenii overshadows a Chaetoceros spp.*

A high relative number of diatoms in the sediment trap sub-samples (Figure 3) corresponds to phytoplankton blooms over the middle shelf. The late April to mid-May sub-samples represent the end of the spring bloom, comprised mainly of large diatoms (50–600 μm) such as *Coscinodiscus spp.* and *Pleurosigma simonsenii*. Our sediment trap recorded an unusual mid-July bloom, which consisted of a greater number of small diatoms (20–50 μm) such as *Odontella aurita*.

In Figure 3 the $\delta^{15}N$ of each sample reflects bloom dynamics. The initial $\delta^{15}N$ value of 12.2‰ represents plankton utilizing relatively more new NO_3^-. As the nutrient is depleted, the $\delta^{15}N$ of the sub-samples increases, eventually to a maximum of 15.5‰ at nitrate depletion. Over the next two months, fixed nitrogen is returned to the euphotic zone through microbial breakdown of particulate organic matter and wind mixing of the water column. As the midsummer bloom resumes, nutrients are quickly depleted and the $\delta^{15}N$ increases until algae growth slows.

The 9/22–10/13 sub-samples contain the coccolithophorid bloom. Although the bloom was observed over the middle shelf in July (Napp et al., 1998), the trap did not collect numerous coccoliths until autumn. The isotopic signal during these inter-

vals changes less dramatically. The plankton are most likely using more new nitrogen supplied to the euphotic zone, as mixing due to wind events increases in autumn.

In Figure 4 the $\delta^{13}C$ tracks phytoplankton growth rates. As diatoms grow faster they discriminate less between the heavy isotope, ^{13}C, and the lighter one they prefer during CO_2 uptake. The $\delta^{13}C$ increases as diatom biomass increases in the sub-samples and decreases as the number of diatoms decreases.

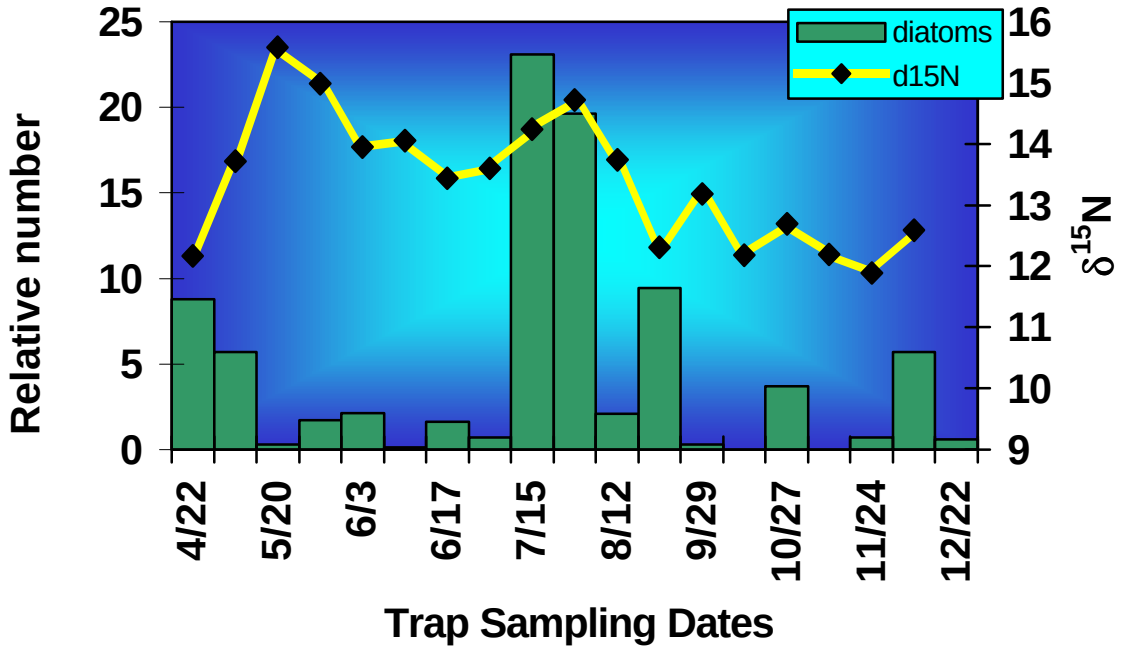

Figure 3. *Temporal change in diatom numbers and d^{15}N of sediment trap samples.*

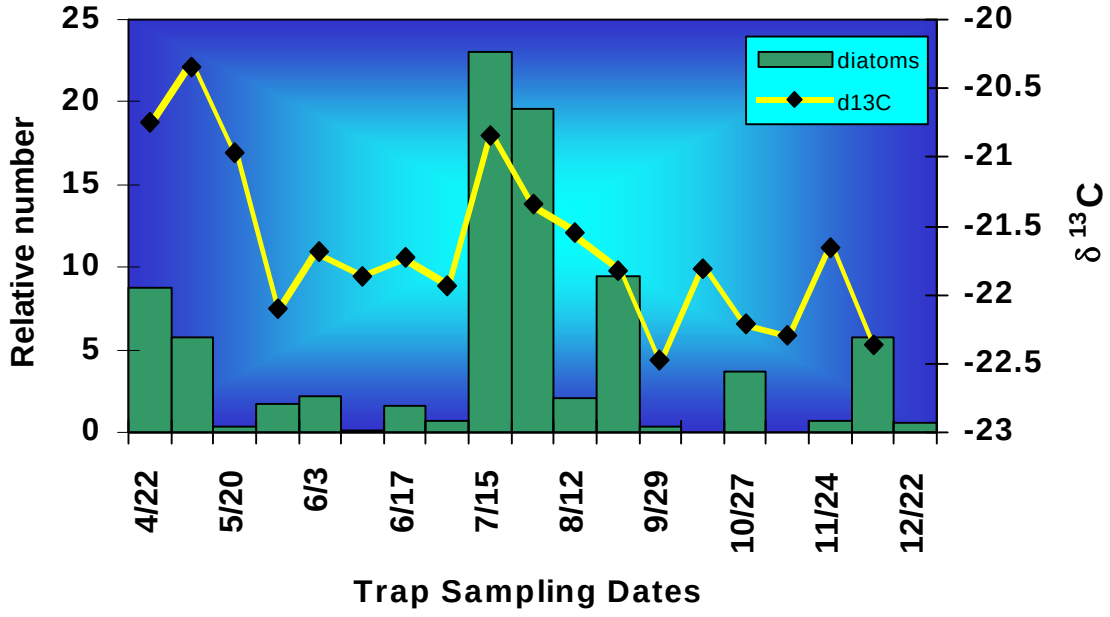

Figure 4. *Temporal change in diatom numbers and d^{13}C of sediment trap samples.*

Conclusions

During 1997, the composition of material collected by the sediment trap over the middle shelf primarily reflected events affecting primary producers. These included spring and summer diatom blooms and the late autumn sinking of the coccolithophorid bloom. The stable C and N isotopic composition of trapped organic matter also apparently reflected phytoplankton growth rates. Heavier $\delta^{15}N$ and $\delta^{13}C$ were associated with nutrient depletion.

References

Napp, J.M., Baier, C.T., Brodeur, R.T., Cullen, J.J., Davis, R.F., Becker, M.B., Goering, J.J., Mills, C.E., Schumacher, J.D., Smith, S.L., Stabeno, P.J., Vance, T.C. and Whitledge, T.E. 1998. The 1997 eastern Bering Sea shelf-wide coccolithophorid bloom: Ecosystem observations and hypothesis. AGU/ASLO Ocean Sciences Meeting,

Redistributions of Cetaceans in the Southeast Bering Sea Relative to Anomalous Oceanographic Conditions during the 1997 El Niño

Cynthia T. Tynan
Joint Institute for the Study of the Atmosphere and Ocean
University of Washington
NOAA, Alaskan Fisheries Science Center
7600 Sand Point Way NE, Seattle WA 98115-0070
U.S.A.
e-mail: tynan@afsc.noaa.gov

The distributions of foraging whales typically reflect the productivity of their pelagic and coastal environments (Tynan, 1998; Croll et al., 1998). Whales can therefore serve as important integrators of the regional biomass of their principal prey: euphausiids, copepods and schooling fish. Redistributions of whales can also serve as important indicators of change in the ecosystem. In order to consider how the distribution of whales in the southeast Bering Sea may have changed relative to the anomalous oceanographic conditions of 1997 and 1998, it is first necessary to review the historical distributions of whales relative to the mean circulation.

The general circulation consists of a cyclonic gyre over the deep basin, with the Kamchatka Current forming the western boundary and the Bering Slope Current forming the eastern boundary of the gyre. A 0.5 m sea-level difference between the Bering Sea and the Arctic Ocean drives the mean northward transport through Bering Strait (Coachman, 1993). The circulation and hydrographic structure of the Bering Sea is highly variable on interannual and decadal time scales. Transport in the gyre can vary by as much as 50% due to changes in the Alaskan Stream inflow or alteration in the wind-driven circulation (Schumacher and Stabeno, 1998). The Bering Slope Current is primarily an extension of the Alaskan Stream water which enters through the passes along the Aleutian Chain. This flow turns eastward along the northern side of the Aleutian Chain as the North Aleutian Slope Flow and then continues to the northwest over the slope at mean speeds of 3–15 cm s^{-1} as the Bering Slope Current (Schumacher and Reed, 1992). The nutrient-rich waters of the Bering Slope Current help to create one of the most productive ecosystems in the world.

Approximately half of the Bering Sea consists of the broad continental shelf, which is more than 500 km wide in the eastern portion (Coachman, 1986). The circulation over the eastern shelf is sluggish, with current speeds on the order of 1–5 cm s^{-1} (Schumacher and Kinder, 1983; Coachman, 1986). Three frontal zones divide the shelf into distinct hydrographic domains: an Inner Front at approximately the 50 m isobath separates the Coastal Domain from the Middle Shelf Domain; a Middle Front at approximately the 100 m isobath separates the Middle and Outer Shelf Domains; and a salinity front at the shelf-break separates the Outer Shelf and slope domains (Coachman, 1986).

The region of the Bering Slope Current has been called the 'green belt' (Springer et al., 1996) due to its high primary production linked to nutrient availability. Not surprisingly, this region also had high historical catches of fin whales (Nasu, 1974). The historical distribution of right whales (Omura et al., 1969) also suggests that this species tracked the Bering Slope Current and the movement of Alaskan Stream waters in the southeast Bering Sea. It has been decades however since any large-scale synoptic surveys of cetaceans have been conducted in the eastern Bering Sea shelf and slope regions.

In order to quantify the modern distributions of cetaceans in the Southeast Bering Sea, I conducted line-transect surveys of whales from July 17 to August 5, 1997, across the southeastern shelf from outer Bristol Bay to 10 km west of St. Paul Island. Survey effort covered the middle and outer shelf domains as well as the shelf-edge and slope regions.

We completed a total of 2021 km of survey effort. Multiplying this distance by an effective strip width of 6 km produces a survey area of approximately 12,000 km^2.

During the summer of 1997, anomalous oceanographic conditions occurred in the Southeast Bering Sea (Vance et al., 1998). By mid-July, sea surface temperatures were 2–4°C warmer than in 1996 and an extensive coccolithophore bloom of *Emiliania huxleyi* developed over the middle shelf. Our survey found that the coccolithophore bloom was restricted to the middle shelf domain during July and early August. By September, when the first SeaWiFS (Sea-viewing Wide Field-of-view Sensor) satellite images of ocean color were available, the bloom was approximately 700 km wide and extended over most of the southeastern Bering Sea shelf. Both the occurrence of the bloom and the unusually warm temperatures have the potential to alter the trophic dynamics and prey availability in the region.

Results of this cetacean survey suggest that redistributions of some species may have occurred. Five species of large whales occurred in or near the coccolithophore bloom: fin whale *Balaenoptera physalus*, humpback whale *Megaptera novaeangliae*, minke whale *Balaenoptera acutorostrata*, sei whale Balaenoptera borealis, and the northern right whale *Eubalaena glacialis*. The relatively high abundance of large whales south of the Inner Front (50 m isobath) and near the coccolithophore bloom, suggests that conditions on the middle shelf in 1997 provided productive foraging for cetaceans and their principal prey: euphausiids and copepods. This distribution contradicts the historical pattern of higher whale biomass associated with the "green belt" of the shelf edge. This redistribution is consistent with either a shift in foraging ecology linked to anomalous oceanographic conditions during an El Niño year, or is indicative of a longer-term change in the regional productivity and trophic structure of the Bering Sea ecosystem.

It is important to determine how zooplankton production, biomass, and species composition may have shifted in the shelf system. The zooplankton communities of the southeast Bering Sea shelf are separated by distinct hydrographic domains. The Middle Front (100 m isobath) is a hydrographic boundary which also separates two major zooplankton communities: an outer shelf community of large species of calanoid copepods, such as *Calanus plumchrus*, *Calanus cristatus*, and *Eucalanus bungii*; and a zooplankton community inshore of 100 m composed of smaller species such as *Calanus marshallae*, *Pseudocalanus* spp., and *Acartia* spp. (Cooney and Coyle, 1982; Smith and Vidal, 1986). During 1997 and 1998, trophic dynamics may have altered, depending on whether diatom production became limiting and if so, whether zooplankton could efficiently graze the coccolithophores. Some copepods, such as *Calanus*, are able to feed on coccolithophores (Marshall and Orr, 1972). Diet studies and SEM (Scanning Electron Microscopy) analyses of gut contents from zooplankton, collected from the bloom water, may help definechanges in the trophic structure.

During July 1997, I collected two zooplankton samples from the coccolithophore bloom on the middle shelf (58 m depth). Samples were collected with bongo nets (333 μm mesh size) in the vicinity of right whales, a species which forages specifically on calanoid copepods. The species collected were typical of the middle shelf species assemblage: *Calanus marshallae*, *Pseudocalanus newmani*, and *Acartia longiremis*. Historically however right whales fed on *Calanus plumchrus* and *C. cristatus* in deeper water along the shelf break (Nemoto, 1963). Therefore, this population of right whales, which is the world's most depleted population of large whale (National Marine Fisheries Service, 1991), appears to have shifted both its foraging ground and prey species in the Southeast Bering Sea. The higher densities of other species of baleen whales on the middle shelf suggests that this region now supports among the highest zooplankton biomass in the Southeast Bering Sea. It is important to continue to define the effects of interannual and longer-term climatic variability on the productivity, structure, and function of the Bering Sea ecosystem.

References

Coachman, L.K. 1986. Circulation, water masses, and fluxes on the southeastern Bering Sea shelf. *Cont. Shelf Res., 5*, 23–108.

Coachman, L.K. 1993. On the flow field in the Chirikov Basin. *Cont. Shelf Res., 13*, 481–508.

Cooney, R.T. and Coyle, K.O. 1982. Trophic implications of cross-shelf copepod distributions in the Southeastern Bering Sea. *Mar. Biol., 70*, 187–196.

Croll, D.A., Tershy, B.R., Hewitt, R.P., Demer, D.A., Fiedler, P.C., Smith, S.E., Armstrong, W., Popp, J.M., Kiekhefer, T., Lopez, V.R., Urban, J. and Gendron, D. 1998. An integrated approach to the foraging ecology of marine birds and mammals. *Deep-Sea Res. II, 45*, 1353–1371.

Marshall, S.M. and Orr, A.P. 1972. The Biology of a Marine Copepod *Calanus finmarchicus* (Gunnerus). Oliver and Boyd, Edinburgh, 195 pp.

Nasu, K. 1974. Movement of baleen whales in relation to hydrographic conditions in the northern part of the North Pacific Ocean and the Bering Sea. *in* D.W. Hood and E.J. Kelley (eds.), *Oceanography of the-Bering Sea with Emphasis on Renewable Resources.*

Institute of Marine Science, University of Alaska, Fairbanks, pp. 345-361.
National Marine Fisheries Service. 1991. Recovery Plan for the Northern Right Whale (*Eubalaena glacialis*). Prepared by the Right Whale Recovery Team for the National Marine Fisheries Service, Silver Spring, Maryland, 86 pp.
Nemoto, T. 1963. Some aspects of the distribution of *Calanus cristatus* and *Calanus plumchrus* in the Bering and its neighboring waters, with reference to the feeding of baleen whales. *Sci. Rep. Whales Res. Inst., 17,* 157–170.
Omura, H., Ohsumi, S., Nemoto, T., Nasu, K. and Kasuya, T.. 1969. Black right whales in the North Pacific. *Sci. Rep. Whales Res. Inst., 21,* 1–78.
Schumacher, J.D. and Kinder, T.H. 1983. Low-frequency current regimes over the Bering Sea Shelf. *J. Phys. Oceanogr., 13,* 607–623.
Schumacher, J.D. and Reed, R.K. 1992. Characteristics of currents over the continental slope of the eastern Bering Sea. *J. Geophys. Res., 97,* 9423–9433.
Schumacher, J.D. and Stabeno, P.J. 1998. The continental shelf of the Bering Sea. *in* K.H. Brink and A.R. Robinson (eds.), *The Sea*, Vol. XI. The Global Coastal Ocean: Regional Studies and Synthesis (John Wiley, Inc., New York, pp. 759–788.
Smith, S.L. and Vidal, J. 1986. Variations in the distribution, abundance, and development of copepods in the southeastern Bering Sea in 1980 and 1981. *Cont. Shelf Res., 5,* 215–239.
Springer, A.M., McRoy, C.P. and Flint, M.V. 1996. The Bering Sea Green Belt: Shelf-edge processes and ecosystem production. *Fish. Oceanogr., 5,* 205–223.
Tynan, C.T. 1998. Ecological importance of the Southern Boundary of the Antarctic Circumpolar Current. *Nature, 392,* 708–710.
Vance, T.C., Baier, C.T. Brodeur, R.D., Coyle, K.O., Decker, M.B., Hunt, G.L., Napp, J.M., Schumacher, J.D., Stabeno, P.J., Stockwell, D., Tynan, C.T., Whitledge, T.E., Wyllie-Echeverria, T. and Zeeman, S. 1998. Aquamarine waters recorded for first time in the Eastern Bering Sea. *Eos, 79(10),* 122, 126.

Stock Abundance and Size Compositions of the Neon Flying Squid in the Central North Pacific Ocean during 1979–1998

Akihiko Yatsu[1], Junta Mori[1], Hiroyuki Tanaka[1], Tomowo Watanabe[1], Kazuya Nagasawa[1], Yukimasa Ishida[2], Toshimi Meguro[3], Yoshihiko Kamei[3] and Yasunori Sakurai[3]

[1] *National Research Institute of Far Seas Fisheries*
Shimizu 424-8633, Japan
e-mail: yatsu@enyo.affrc.go.jp

[2] *Hokkaido National Fisheries Research Institute*
Kushiro 085, Japan

[3] *Faculty of Fisheries, Hokkaido University,*
Hakodate 041-8611, Japan

Introduction

The neon flying squid, *Ommastrephes bartrami*, is one of the most dominant nekton in the epipelagic subtropical and subpolar waters of the world oceans, and it undertakes extensive seasonal north–south migration (Seki, 1993). In the North Pacific Ocean, this species is composed of an autumn cohort and a winter–spring cohort, both having a one-year life span (Yatsu et al., 1997).

O. bartrami has been harvested in the North Pacific Ocean since 1974 until the present with an intensive fishing period by the international squid driftnet fishery during 1978–92, when the annual commercial catch fluctuated between 152,505 and 356,882 metric tons (Gong et al., 1993). The autumn cohort is abundant in the Central North Pacific and was the major target of driftnet fishery since 1979 (Yatsu et al., 1993).

The closure of the large-scale high seas driftnet fisheries was in effect by the end of 1992 according to the bycatch problem. Since 1993, fishing mortality of the autumn cohort has been derived only by jig fishing, whose annual catch has been estimated to be less than 10,000 tons for this cohort.

Since 1979, Hokkaido University (HU) and National Research Institute of Far Seas Fisheries (NRIFSF) have been conducting monitoring surveys for oceanographic and biological conditions by using research driftnets in the western and central North Pacific Ocean. Yatsu and Watanabe (1996) indicated that these monitoring data would reveal stock abundance of *O. bartrami* since catch-per-unit-effort (CPUE) of this fishery was significantly correlated with that of the research driftnet surveys along 175°30´E in July, which coincided with the peak of the commercial fishery.

The purpose of this study is to examine interannual variability in research net CPUE, size compositions and growth of the autumn cohort until 1998 in relation to pronounced El Niño Events during 1997.

Materials and Methods

1. Sea surface temperature (SST)

SST anomalies over the North Pacific Ocean were determined on the basis of Comprehensive Ocean Atmosphere Data Set (COADS) during 1978–97, which was supplied by the Japan Meteorological Agency as monthly means in two-degree latitude and longitude blocks.

Interannual variability in SST around the western feeding grounds of *O. bartrami* (both along 175°30´E and area of 40°–44°N, 170°E–180°) and around spawning grounds (30°–36°N, 150°–170°W) was also examined from COADS and HU monitoring data.

Table 1. *Location and period of driftnet survey.*

Vessel	Longitude	Year	Date	Latitude	Interval (nautical mile)
Hokusei Maru	155°E	1982–98	June 4–July 7	35°00′N–44°00′N	90
Hokusei Maru	170°E	1981–97	July 15–24	38°30′N–47°30′N	90
Hokusei Maru	175°30′E	1979–98	July 22–August 1	38°30′N–47°30′N	90
Osyoro Maru	180°	1979–98	June 8–19	36°00′N–47°00′N	90
Wakatake Maru	179°W/180°	1991–98	June 12–28	38°30′N–47°30′N	90

2. Driftnet monitoring

Monitoring operations by HU and NRIFSF have been carried out at almost fixed sites and dates along five transects, 155°E, 170°E, 175°30´E, 180° (HU) and 179°W (NRIFSF), from June to early August over the Subarctic Domain, Transitional Domain and Subtropical region. (Table 1, Figure 1). At 155°E, monitoring was repeated two times in early June and from late June to early July for each year.

The driftnets were composed of non-size-selective nets (Takagi, 1975) and commercial nets for squid and salmon (mesh sizes 112–130 mm). Each net panel was 50 m long and 6 m deep. A total of 49–134 net panels were connected to form a long net section and soaked over night.

CPUE is the number of animals caught per a 50-m net panel. We separated catch of *O. bartrami* into a autumn cohort with mantle length (ML) 30 cm and larger, and a winter–spring cohort with less than 30 cm ML according to Yatsu et al. (1997).

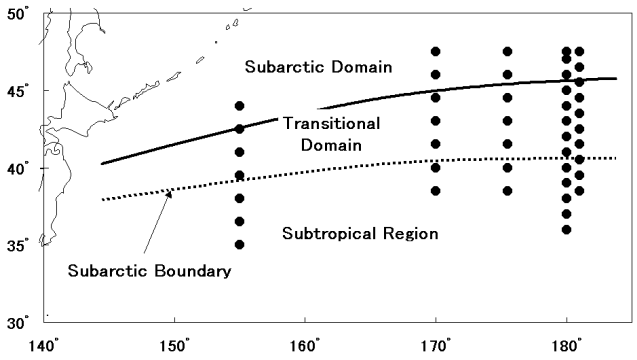

Figure 1. *Oceanographic regions and location of monitoring sites.*

3. Size composition and age estimation

ML composition data were derived from these monitoring surveys and from jigging surveys during 1994–97. Ages of selected autumn cohort specimens obtained from 180° longitude during June, 1995–97, were determined with statolith microstructure, following the methods of Yatsu et al. (1997).

Results and Discussion

1. SST conditions

In the feeding grounds of *O. bartrami* around the Transitional Domain in summer, strong negative

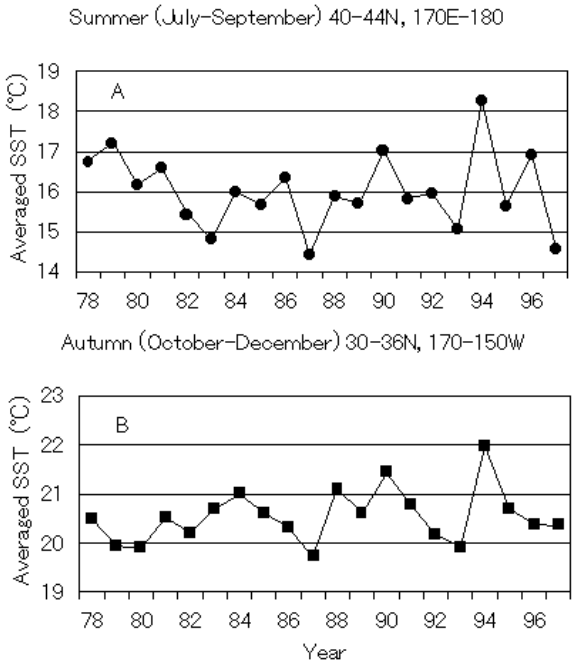

Figure 2. *Averaged sea surface temperatures (SST) during 1978-97 around feeding grounds (A) and spawning grounds (B) of the autumn cohort of Ommastrephes bartrami in the North Pacific Ocean.*

SST anomalies were detected in 1983, 1987, 1993, and 1997 (Figures 2A and 3), corresponding to El Niño years. In the spawning ground mainly located north of the Hawaiian Islands (30°–36°N) in autumn, low SSTs were also found in 1987 and 1993 (Figure 2B).

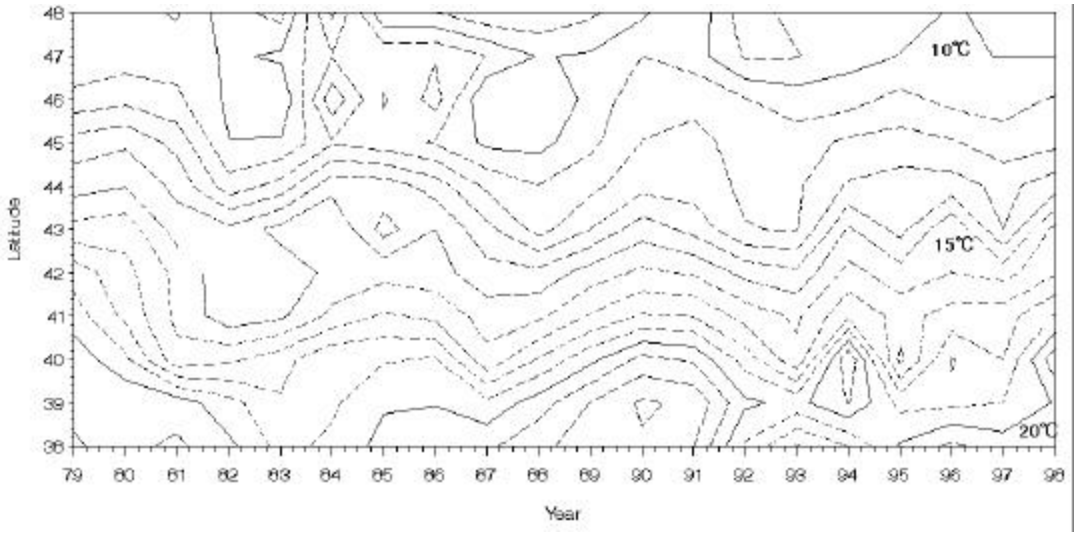

Figure 3. *Interannual variation in sea surface temperatures during 197998 a t 175°30' E longitude*

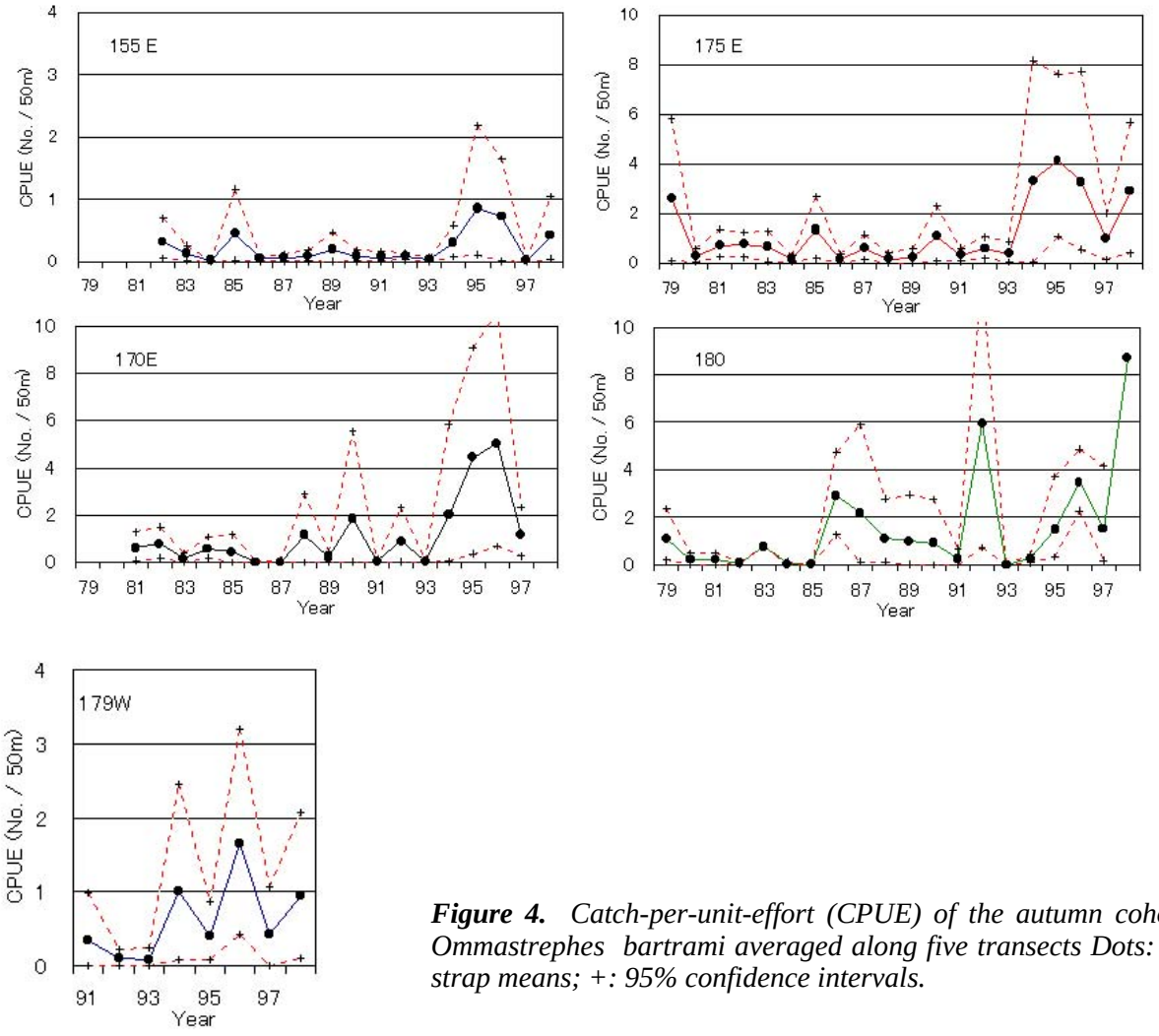

Figure 4. *Catch-per-unit-effort (CPUE) of the autumn cohort of Ommastrephes bartrami averaged along five transects Dots: bootstrap means; +: 95% confidence intervals.*

2. Distribution and CPUE

The autumn cohort was mainly distributed in the southern area of the Subarctic Domain and in the Transitional Domain, contrasting with the winter–spring cohort, which occupied subtropical waters, as in Yatsu and Watanabe (1996).

Averaged CPUE of the autumn cohort at each 5° longitude were generally low during 1980–93 and in 1997 and were high during 1994–96 and in 1998 (Figure 4). Low CPUE during 1980–93 could be attributed to high fishing rates derived from driftnet fisheries. After the moratorium of the fishery, *O. bartrami* stock seemed to quickly recover.

Stock abundance of the autumn cohort was extremely low in 1993 and in 1997, the most prominent El Niño year in this century. For these year-cohorts, spawning ground SST (autumn, 1992 and 1996) were also low (Figure 2).

3. Size compositions, age and growth

ML ranges and modes of the autumn cohort in July indicate that squid were considerably larger in 1997, and smaller in 1996 compared to other years (Figure 5).

The ML-age relationship (Figure 6A) indicates that squid collected in 1997 were larger than in 1995 and 1996, yet estimated hatching months were mostly between November and December of previous years with slight year-to-year variation (Table 2). ML-statolith length relationships did not seem to depend on sampling years (Figure 6B).

On the basis of statolith daily increment width, Yatsu et al. (1996, 1998) postulated that the most distal part of the broader increment area (increment width >3 μm) correspond to the end of juvenile stage. In the present samples, these ages were slightly younger in 1997 (Table 3)

Statolith growth rates during the juvenile stage seemed to be related to neither ML at capture nor year (Figure 6C). In contrast, statolith growth rates seemed to decrease with ML at capture and were slightly higher in 1997 samples (Figure 6D). Although sample sizes are very limited, this may indicate that higher somatic growth rates in the 1997 samples were derived mainly in the subadult stage.

Provisional Conclusions

In El Niño years, summer SST around the Transitional Domain in the central North Pacific Ocean (40°–44°N, 170°E–180°) had negative anomalies. Extremely low stock abundance in 1993 and 1997 might have been derived from negative SST anomalies around the feeding and nursery grounds (40°–44°N, 170°E–180°). An observed lower CPUE in 1993 than in 1997 can be explained by a lower abundance of spawning biomass in 1992 due to intensive driftnet fishing. Higher somatic growth rates in the 1997 samples may have been achieved during their subadult stage rather than juvenile stage.

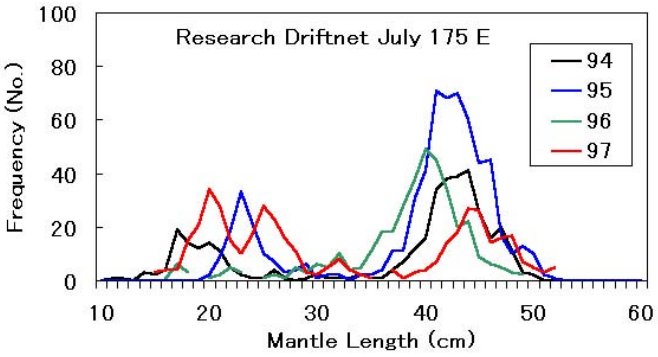

Figure 5. *Mantle length compositions of Ommatrepehs bartrami caught with non-size-selective-driftnet along 175° 30'E during July, 1994 97.*

Table 2. *Estimated hatching month by sampling year.*

	Sep	Oct	Nov	Dec	Jan
1995	1	4	4	4	1
1996	–	1	7	8	–
1997	–	1	6	7	3

Table 3. *Estimated age at the end of the juvenile stage by sampling year.*

	N	Min	Mean	Max
1995	13	79	90.3	113
1996	13	76	92.9	107
1997	16	70	87.4	111

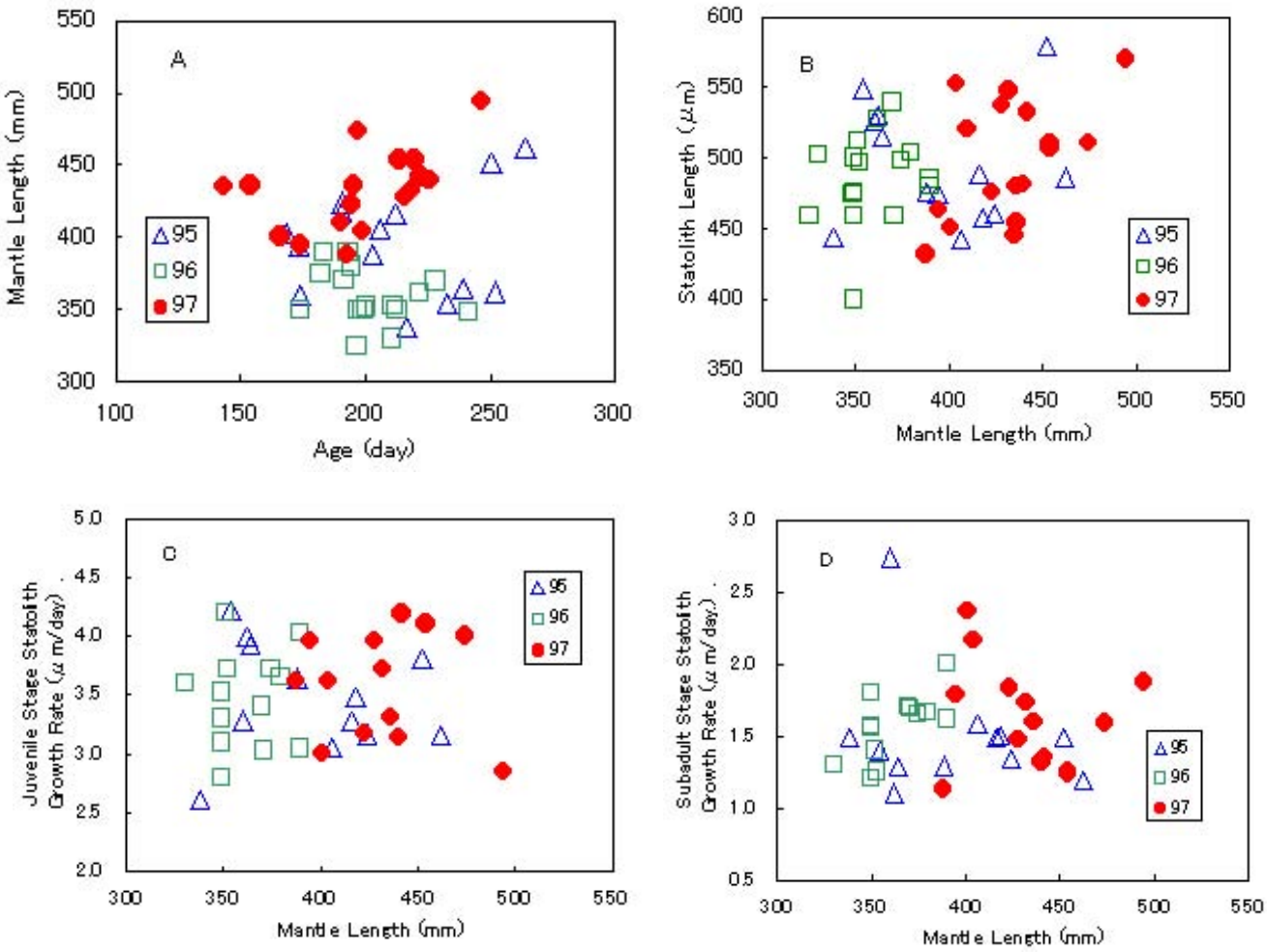

Figure 6. *Relationships between mantle length (ML) and age (A), ML and statolith length (B), ML and juveniule statolith growth rates (C) and ML and subadult statolith growth rates (D) in the autumn cohort Ommatrepehs bartrami collected during June, 1995–97 at 180° longitude.*

Acknowledgments We thank the captains and crews of *Oshoro Maru*, *Hokusei Maru* and *Wakatake Maru*, who supported these monitoring surveys. We also thank Ms. Kozue Wakabayashi for her assistance in statolith preparation and age estimation.

References

Gong, Y., Kim, Y.S. and Hwang, S.J. 1993. Outline of the Korean squid gillnet fishery in the North Pacific. *Bull. Int. Nat. North Pacific Fish. Comm., 53,* 45–69.

Seki, M.P. 1993. The role of neon flying squid, *Ommastrephes bartrami*, in the North Pacific pelagic food web. *Bull. Int. Nat. North Pacific Fish. Comm., 53,* 207–215.

Takagi, K. 1975. A non-selective salmon gillnet for research operations. *Bull. Int. Nat. North Pacific Fish. Comm., 32,* 13–33.

Yatsu, A., Hiramatsu, K. and Hayase, S. 1993. Outline of the Japanese squid driftnet fishery with notes on the bycatch. *Bull. Int. Nat. North Pacific Fish. Comm., 53,* 5–24.

Yatsu, A. and Watanabe, T. 1996. Interannual variability in neon flying squid abundance and oceanographic conditions in the central North Pacific, 1982–1992. *Bull. Nat. Res. Inst. Far Seas Fish., 33,* 123–138.

Yatsu, A., Midorikawa, S., Shimada, T. and Uozumi, Y. 1997. Age and growth of the neon flying squid, *Ommastrephes bartrami*, in the North Pacific Ocean. *Fish. Res., 291,* 257–270.

Yatsu, A., Mochioka, N. Morishita, K. and Toh, H. 1998. Strontium:Calcium Ratios in Statoliths of the Neon Flying Squid, *Ommastrephes bartrami* (Cephalopoda), in the North Pacific Ocean. *Mar. Biol., 131,* 275–282.

A New Point of View Concerning the El Niño Mechanism

O.B. Feschenko
Pacific Research Fisheries Center (TINRO)
4 Shevchenko Alley
Vladivostok, Russia 690600
e-mail: root@tinro.marine.su

It is generally believed that the lack of progress towards successful forecasting of El Niños is because of an incorrect interpretation of the mechanisms. On the largest scale, the ocean and atmosphere interact as water is moved from east to west by the trade winds. Wind fields are determined by four pressure centres: the Hawaiian and Tahitian centres are stationary anticyclones, whereas the Asian and Australian centres are seasonal. When there is a cyclone above Asia, there is an anticyclone above Australia and *vice versa*. Theory suggests that the water warming in the east (the El Niño phenomenon) can arise in two ways:

1) under simultaneous abnormally weak development of a seasonal anticyclone and abnormally strong development of a seasonal cyclone (the trade winds in the winter hemisphere become substantially weaker and the monsoons in the summer hemisphere become stronger in the Western Pacific);
2) under asynchronous seasonal alternation in Asia and Australia that lead the development of cyclones (trade winds do not reach the Western Pacific; monsoons can be seen in northern and southern hemispheres). Opposite situations will induce the La Niña phenomenon.

The strength of development and the continuation of naturally synoptical seasons in Asia and Australia are analyzed. The input was daily atmospheric pressure in Hong Kong and Darwin from 1984 through 1987. During this period one La Niña and one El Niño were observed. Analysis confirmed the reliability of the theory. Statistical testing, with a larger database, of the stability of the discovered connection is presented.

97/98 Ocean Climate Variability in the Northeast Pacific: How Much Blame does El Niño Deserve

Nathan Mantua
JISAO, University of Washington
Seattle, WA 98195-4235
U.S.A.
e-mail: mantua@atmos.washington.edu

The rapid warming of the coastal NE Pacific in the spring and summer of 1997 is viewed in relation to local and remote atmospheric anomalies in the Pacific Basin. North Pacific climate anomalies observed in 1997/98 are compared with those observed in past warm episodes in the Northeast and tropical Pacific, respectively.

Of particular interest is the extent to which the tropical ENSO is reliably teleconnected to the ocean climate of the Northeast Pacific. This issue is addressed by tabulating atmospheric circulation anomalies for events showing coherent and incoherent temperature anomalies between the tropical and Northeast Pacific.

Sharp Changes of Hydrometeorological Conditions in The Northwestern Pacific during the 1997/1998 El Niño Event

Vadim P. Pavlychev
Pacific Research Fisheries Centre (TINRO)
4, Shevchenko Alley
Vladivostok, 690600
Russia
e-mail: root@tinro.marine.su

The unusual development of the last El Niño (for the first time the event appeared in April 1997, instead of November or December as usual) was reflected on natural conditions of remote regions of the northern North Pacific Ocean. In the present work, observations of anomalous changes of hydrometeorological conditions in the northwestern Pacific, including the far-eastern seas, are summarized:

- A significant weakening of cyclonic activity was observed at the region 30–70°N and 130–180°E in January–March, 1997. The number of cyclone-days for the Earth, counted on 5° squares, was low (247) compared to the previous three years (337 in 1994, 335 in 1995, 296 in 1996). It was especially expressed for the western part of the circulation and corresponded to a minimum solar activity (based on data from V.F. Chistyakov, Ussuriskaya Observatory).
- Less ice was seen in the Sea of Okhotsk and Bering Sea.
- The summer was unusually warm in Primorye. Positive temperature anomalies were registered in the north Okhotsk Sea, western Kamchatka and in the northwestern part of the Bering Sea.
- Data collected by TINRO-Centre specialists show an unusual distribution of marine hydrobionts: the appearance *of Eumicrotremus soldativi*, low abundant year-class (Melnicov, 1997), displacement of *Paralithodes camstehatica* to the south (Myasoedov, 1997), spreading of *Chionocetes opilio* to the north near the cape Navarin and even in the Anadir Bay (Slizkin, 1997).

In January–March 1998, the meteorological situation changed abruptly.

- The number of cyclone days increased relatively (319 in 1997). In February 1998, not one cyclone reached the Sea of Okhotsk.
- The ice coverage for the Sea of Okhotsk (84% for 9 March) was significantly higher than in previous years with low ice conditions.
- The ice edge in the Bering Sea was 90–100 miles farther south than in 1997.

All the above-mentioned facts reflect indirectly the impacts of the 1997/98 El Niño event on the N. Pacific Ocean and its marginal seas.

Predictability and Forecast Verification of El Niño Events

Jingyi Wang
National Research Center for Marine Environment Forecasts
Da Hui Si No. 8
Haidian District, Beijing
People's Republic of China 100081
e-mail: ltj@mx.cei.gov.cn

The 1997/98 El Niño prediction and natural disasters over the coastal areas for China (the strongest storm surge in this century, the lighter than normal sea ice cover in the Bohai Sea, and so on) are reviewed. In fact, the prediction of El Niño has improved world wide. The 1997/98 El Niño prediction of the National Research Center for Marine Environment Forecasts was very successful.

Methods to make the El Niño prediction more reliable are discussed. A method of forecast verification was developed. For each test parameter, the following factors were tabulated: average deviation, mean absolute error, tendency correlation, anomaly correlation, absolute correlation, skill index, and ability index. The most successful El Niño predictions (correlation coefficients were 0.5–0.7 with six or more months lead) were those using statistical–dynamic methods, but they still exhibited the spring predictability barrier in February to April.

The primary objective of El Niño prediction is to improve the ability to predict sea surface temperature anomalies (SSTA). The analyses indicate that the correlation of SST between two or three continuous months is strong, and it shows that the regions with the strongest SST persistence are concentrated in specific areas. This demands more attention.

It is possible that operational El Niño predictions in the next few years should continue to be based on the statistical–dynamic methods rather than on the dynamic models.